

Development and exploration of nitrogen heterocycle methodologies : experimental and theoretical investigations
by Thomas Nicholas Jones

A dissertation submitted in the partial fulfillment of the requirements for the degree of Doctor of Philosophy in Chemistry
Montana State University
© Copyright by Thomas Nicholas Jones (2003)

Abstract:
The first room temperature stable 4-ethoxy-2,3-dihydropyridines derived from 2,3-dihydropyridones were prepared. Additionally, 2,3-dihydropyridinium salts derived from N-substituted-2,3-dihydropyrid-4-ones have also been prepared. These compounds were screened under a variety of different Diels-Alder conditions and found to be unreactive.

The C3-substituent effect on the oxa-di-φ-methane photoisomerization was explored using the DFT method B3LYP. No barrier height variation was observed with respect to the electronic character of the C3-substituent. An inductive effect model has been proposed to explain the observed reactivates.

Bisphosphonates represent an important class of medicinal agents. Herein we describe the preparation of two new bisphosphonomethyl-pyrimidinediones. These bisphosphonates were prepared utilizing oxaphospholene methodology.

DEVELOPMENT AND EXPLORATION OF NITROGEN HETEROCYCLE METHODOLOGIES: EXPERIMENTAL AND THEORETICAL INVESTIGATIONS

by

Thomas Nicholas Jones

A dissertation submitted in the partial fulfillment
of the requirements for the degree

of

Doctor of Philosophy

in

Chemistry

MONTANA STATE UNIVERSITY
Bozeman, MT

December 2003

©COPYRIGHT

by

Thomas Nicholas Jones

2003

All Rights Reserved

D378
J7265

APPROVAL

of a dissertation submitted by

Thomas Nicholas Jones

This dissertation has been read by each member of the dissertation committee and has been found to be satisfactory regarding content, English usage, format citations, bibliographic style, and consistency, and is ready for submission to the College of Graduate Studies.

Dr. Cynthia K. McClure _____ (Signature) 12/1/03 (Date)

Approved for the Department of Chemistry and Biochemistry

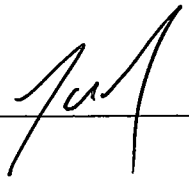
Dr. Paul A. Grieco _____ (Signature) 12/1/03 (Date)

Approved for the College of Graduate Studies

Dr. Bruce McLeod _____ (Signature) 12-8-03 (Date)

STATEMENT OF PERMISSION TO USE

In presenting this dissertation in partial fulfillment of the requirements for a doctoral degree at Montana State University, I agree that the Library shall make available to the borrowers under the rules of the Library. I further agree that copying of this dissertation is allowable only for scholarly purposes, consistent with "fair use" as prescribed in the U.S. Copyright Law. Requests for extensive copying or reproduction of this dissertation should be referred to Bell & Howell Information and Learning, 300 North Zeeb Road, Ann Arbor, Michigan 48106, to whom I have granted "the exclusive right to reproduce and distribute my dissertation in and from microform along with the non-exclusive right to reproduce and distribute my abstract in any format in whole or in part."

Signature 

Date 12-1-2003

ACKNOWLEDGEMENTS

I would like to thank everyone who has supported me on this journey, without their kindness and encouragement this would not have been possible. To begin with I would like to thank my advisor Professor Cynthia McClure for providing the opportunity and environment to produce this work. I would also like to thank the members of my graduate committee: Professor Paul Grieco, Professor Charles Spangler, Professor Patrik Callis, Professor Lee Spangler, and Professor Johan Jonsson.

Special thanks go to past and present members of the McClure research group, especially: Dr. Holly Heath, Dr. Jeffrey Link, Dr. Royce Wilkenson, Dr. Baozhong Cai, and Todd Madsen. Additionally, I would like to thank departmental faculty and fellow graduate students with whom I have had many useful conversations; particularly Dr. Christopher Markworth, and Professor Robert Szilagyi. Dr. Scott Busse and Dr. Joe Sears have been instrumental in helping to run and interpret NMR and mass spec data. I would also like to thank the departmental staff.

Last, but certainly not least, I give the greatest thanks to my family! Thank you for your understanding and support. I could not have gotten through this without you.

TABLE OF CONTENTS

1. INTRODUCTION 1

2,3-Dihydropyridines 2
C3 Substituent Effects on the Oxa-Di-π-Methane Photoisomerization 3
Bisphosphonomethyl-pyrimidindiones 5

2. SYNTHESIS AND CHARACTERIZATION OF 2,3-DIHYDROPYRIDINES 6

Introduction 6
Review of 2,3-Dihydropyridines 7
Review of 2,3-Dihydropyridinium salts 9
Review of 2,3-Dihydropyridones. 13
Aza-Diels-Alder Reactions 15
Results and Discussion 17
Preparation of 2,3-Dihydropyridones 17
Preparation of 2,3-Dihydropyridines 21
Preparation of 2,3-Dihydrppyridinium Salts 23
Attempted Diels-Alder Cyclizations Using 2,3-Dihydropyridines and 2,3-Dihydropyridinium salts 26
Experimental 30
General 30
Experimental 31

3. INVESTIGATION OF THE REACTIVITY EFFECTS OF C3 SUBSTITUENTS ON THE OXA-DI-π-METHANE PHOTOISOMERIZATION 45

Introduction 45
Computational Investigations of the Oxa-Di-π-Methane Mechanism 50
Project Aim 54
Computational Methods 54
Results and Discussion 57
Calibration of B3LYP/BS3 Level of Theory Using Acetone 57
Examination of VE Energies 58
Examination of I1 to I2 Barrier Heights 70
Examination of I2 to I3 Barrier Heights 75
Mapping of the Starting Material Singlet Potential Energy Surface (S_0 PES) 79
Inductive Effect Model 81
Conclusions 84

TABLE OF CONTENTS - CONTINUED

4. SYNTHESIS OF BISPHOSPHONOMETHYL-PYRIMIDINDIONES 86

Introduction 86
Historical Background 86
Oxaphospholene Methodology 89
Project Scope 90
Results and Discussion 92
Retrosynthetic Analysis 92
Preparation of Monophosphonates 93
Phosphorylation of Monophosphonates 95
Preparation and Use of a Phosphono-Oxaphospholene 96
Deprotection of the PMP-Phosphonates 97
Deprotection of Benzyl-Phosphonates 98
Conclusion 99
Experimental 100

REFERENCES CITED 107

APPENDICIES 114

APPENDIX A: NMR Spectra 2,3-Dihydropyridine **1** 115
APPENDIX B: NMR Spectra 2,3-Dihydropyridone **49** 118
APPENDIX C: NMR Spectra 2,3-Dihydropyridone **55** 121
APPENDIX D: NMR Spectra 2,3-Dihydropyridone **57** 123
APPENDIX E: ^{1}H-NMR Spectrum 2,3-Dihydropyridinium salt **58** 126
APPENDIX F: NMR Spectra 2,3-Dihydropyridone **60** 128
APPENDIX G: NMR Spectra 2,3-Dihydropyridone **61** 131
APPENDIX H: NMR Spectra 2,3-Dihydropyridone **62** 134
APPENDIX I: NMR Spectra 2,3-Dihydropyridone **63** 137
APPENDIX J: NMR Spectra 2,3-Dihydropyridine **64** 140
APPENDIX K: NMR Spectra 2,3-Dihydropyridine **65** 143
APPENDIX L: ^{1}H-NMR Spectrum 2,3-Dihydropyridinium salt **66** 146
APPENDIX M: ^{1}H-NMR Spectrum 2,3-Dihydropyridinium salt **67** 148

LIST OF ABBREVIATIONS

ADPM	Aza-di-π-methane
B3LYP	Becke 3-parameter exchange and Lee-Yang-Parr correlation
BS1	6-31G*
BS2	6-311G**
BS3	6-311G**
CAN	Ceric ammonium nitrate
CAS-SCF	Complete Active Space – Self Consistent Field
CNDO/S	Complete Neglect of Differential Overlap with Spectroscopic extention
ΔSCF	Difference between two Self Consistent Field optimized states
DFT	Density Functional Theory
DPM	Di-π-methane
ED_{50}	Effective Dosage
FVP	Flash Vacuum Pyrolysis
HF	Hartree-Fock
HOMO	Highest Occupied Molecular Orbita
hυ	light
I1	Intermediate 1
I1co	Intermediate 1co
I1cc	Intermediate 1cc
I2	Intermediate 2
I3	intermediate 3

INDO-MO	Intermediate Neglect of Differential Overlap – Molecular Orbitals
ISC	Intersystem Crossing
KTPBH	Potassium tert-isopropoxyborohydride
KVP	Keto Vinyl Phosphonate
LUMO	Lowest Unoccupied Molecular Orbital
MC-SCF	Multi Configuration - Self Consistent Field
MO	Molecular Orbital
MP	Moller Plessett pertubative methods
NPA	Natural Population Analysis
ODPM	Oxa-di-π-methane
P	Product
PES	Potential Energy Surface
PMP	4-Methoxyphenyl
QCISD	Quadratic Configuration Interaction of Singles and Doubles
S_0	Singlet ground state
S_1	First excited singlet state
sens	Triplet sensitizer
SM	Starting Material
SOMO	Singly Occupied Molecular Orbital
SPE	Single Point Energy
TD-DFT	Time Dependant – Density Functional Theory
TIPS	Triisopyropylsilyl

TS0	Transition State between I1 (exo) and I1 (endo)
TS1	Transition State between I1 and I2
TS2	Transition State between I2 and I3

ABSTRACT

The first room temperature stable 4-ethoxy-2,3-dihydropyridines derived from 2,3-dihydropyridones were prepared. Additionally, 2,3-dihydropyridinium salts derived from N-substituted-2,3-dihydropyrid-4-ones have also been prepared. These compounds were screened under a variety of different Diels-Alder conditions and found to be unreactive.

The C3-substituent effect on the oxa-di-π-methane photoisomerization was explored using the DFT method B3LYP. No barrier height variation was observed with respect to the electronic character of the C3-substituent. An inductive effect model has been proposed to explain the observed reactivates.

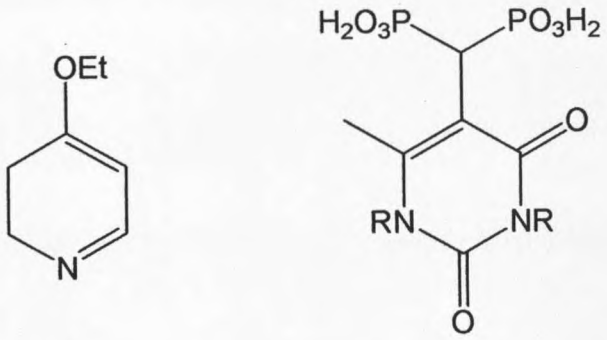
Bisphosphonates represent an important class of medicinal agents. Herein we describe the preparation of two new bisphosphonomethyl-pyrimidinediones. These bisphosphonates were prepared utilizing oxaphospholene methodology.

CHAPTER 1

INTRODUCTION

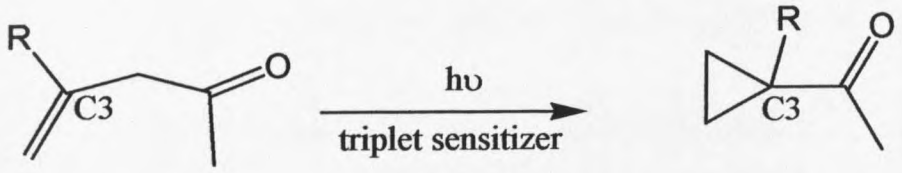
The development and exploration of synthetic methodologies are central to organic chemistry. Often chemists are faced with unexpected or undesirable results. Understanding and possibly utilizing these results can lead to new and interesting chemistries.

The objectives of this work are three fold: (1) development of methodology to access new 2,3-dihydropyridines such as 4-ethoxy-2,3-dihydropyridine, **1**, (Figure 1); (2) understanding the role of C3-substituents in the oxa-di-π-methane photoisomerization (Scheme 1); and (3) development of methodology toward the preparation of bisphosphonomethyl-pyrimidinediones **2** (Figure 1). Herein these methodologies will be explored, and new insights into their chemistries will be presented.



1 **2**

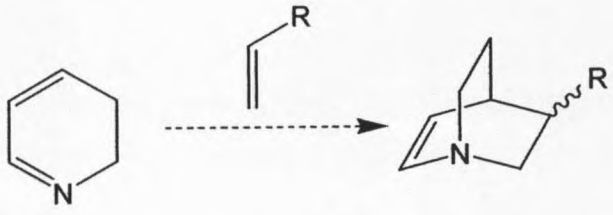
Figure 1



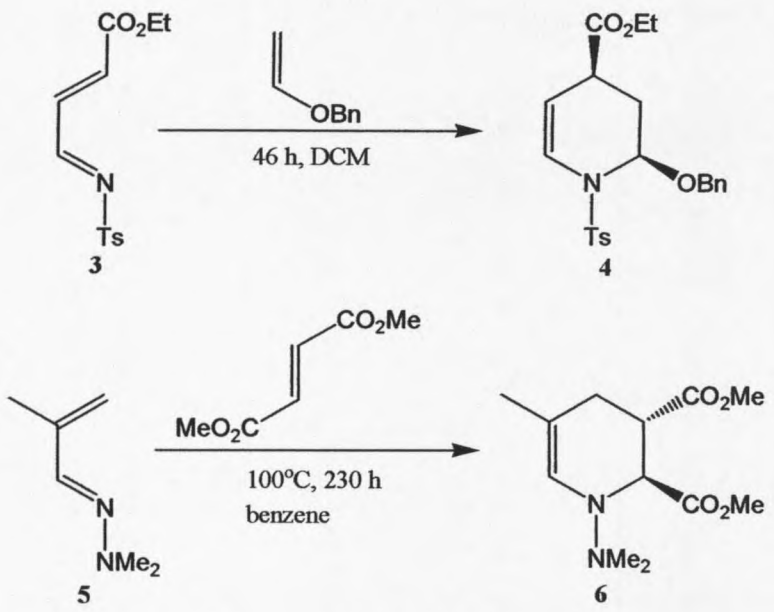
Scheme 1

2,3-Dihydropyridines

The aza-Diels-Alder reaction has the potential to be a very powerful method for the preparation of interesting nitrogen heterocyclic molecules. However, there is a large void in this area, as there are no examples of 2,3-dihydropyridines being utilized in the aza-Diels-Alder reaction (Scheme 2). This has made the synthetic preparation of quinuclidines significantly more complex than if an aza-Diels-Alder reaction could be used to assemble the quinuclidine core. The preparation of new 2,3-dihydropyridines and their attempted use in aza-Diels-Alder reactions is described in Chapter 2. Currently nearly all examples of 1-azadienes which undergo aza-Diels-Alder reactions are limited to acyclic unsaturated imines, two of which are shown in Scheme 3.[1,2] Two cases exist where the aza-dienes are cyclic, but are part of fused aromatic systems.[3,4] This will be discussed further in Chapter 2.



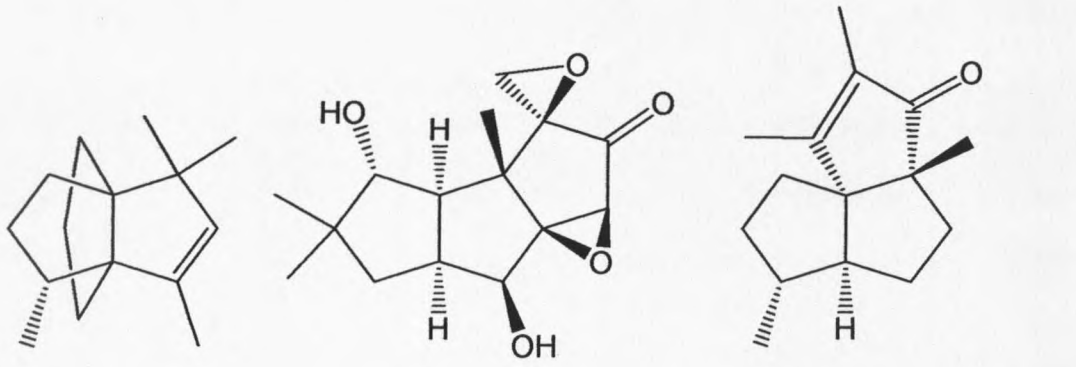
Scheme 2



Scheme 3

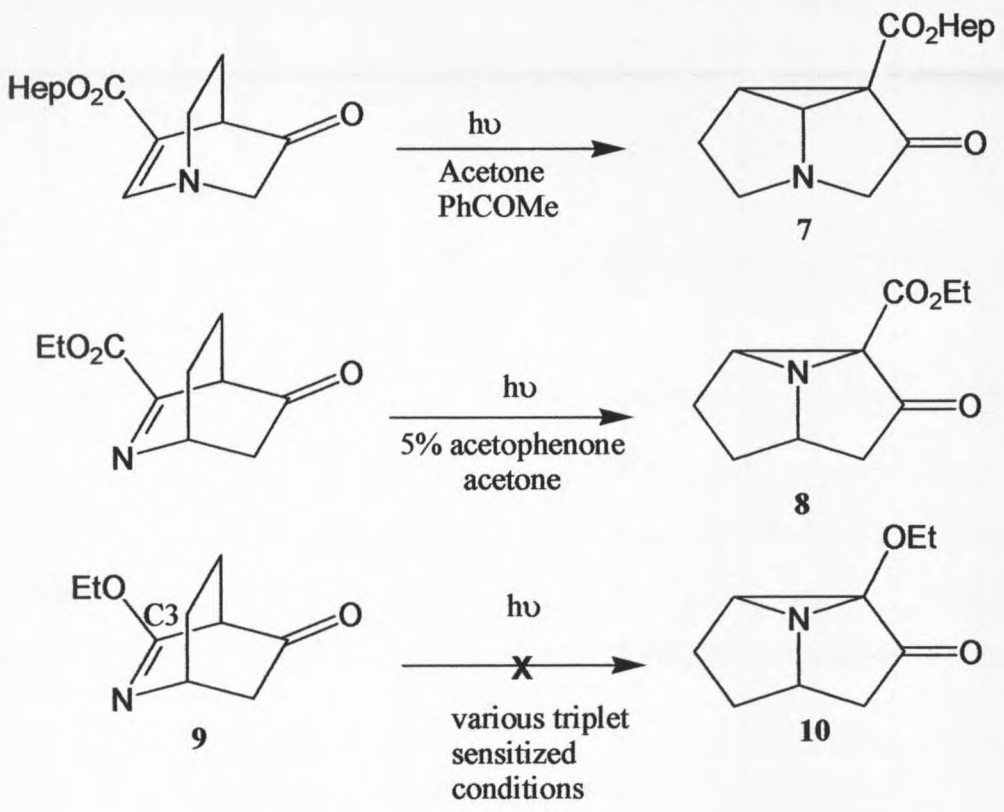
C3-Substituent Effects on the Oxa-Di-π-Methane Photoisomerization

The oxa-di-π-methane (ODPM) photoisomerization has proven to be a useful synthetic transformation.[5] Syntheses of several natural products have been realized using the ODPM photoisomerization.[6] Examples of these include Modhephene,[7] (-)-Coriolin,[8] and (-)-Silphiperfol-6-en-5-one[9] (Figure 2). Recently, the use of basic nitrogen containing substrates have been reported to react under ODPM conditions to produce the desired tricyclic compounds **7** and **8** (Scheme 4).[10,11,12] However, the reaction conditions did not prove to be general, and the conversion of imidate **9** to the desired photoproduct **10** was not observed (Scheme 4).[11] One other example of a failed ODPM photoisomerization where the C3-substituent was an electron donating alkoxy group has been found.[5d] The role of the C3-substituent on the ODPM photoisomerization is explored in Chapter 3.



Modhephene **(+/-)-Coriolin** **(-)-Silphiperfol-6-en-5-one**

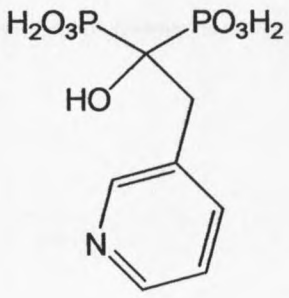
Figure 2



Scheme 4

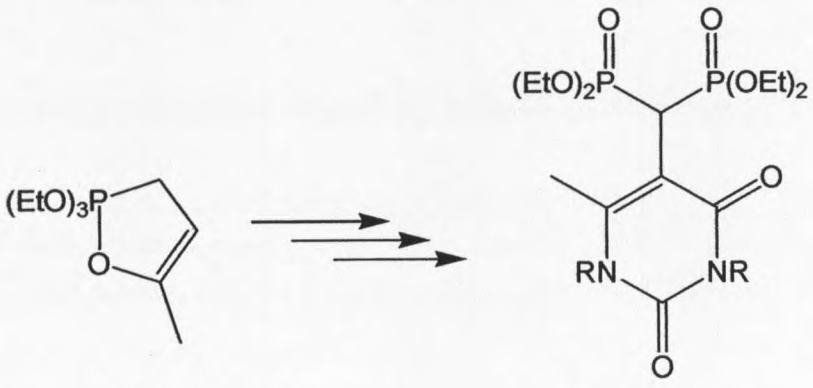
Bisphosphonomethyl-pyrimidinediones

Bisphosphonates such as risedronate[13] **11** (Figure 3) have been shown to be effective in the treatment of bone resorptive disorders such as osteoporosis and Paget's disease.[14] Several bisphosphonates have been studied by a number of pharmaceutical companies with the goal of enhancing activity against such bone resorptive disorders.[13,15] In pursuit of this goal, a new bisphosphonate **13** has been realized via synthetic methodologies developed in the McClure group (Scheme 5).[16] This work is described in Chapter 4.



11

Figure 3



12 **13**

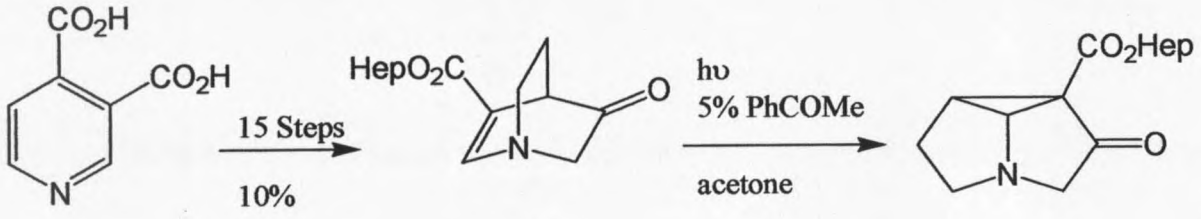
Scheme 5

CHAPTER 2

SYNTHESIS AND CHARACTERIZATION OF 2,3-DIHYDROPYRIDINES

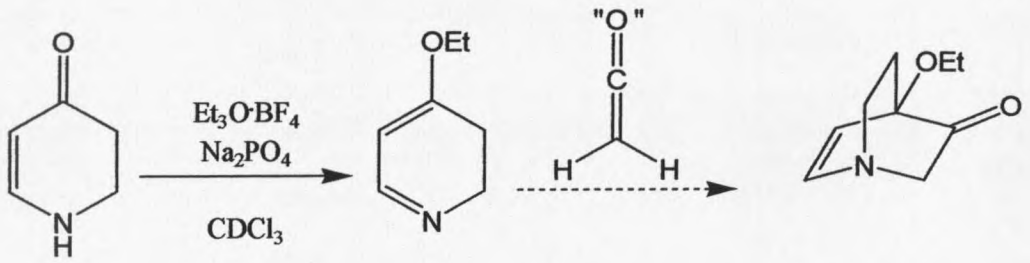
Introduction

In order to readily access variously substituted 1-azabicyclo[2.2.2]octenones for our photochemistry methodology, a program of study into the Diels-Alder reactivity of 2,3-dihydropyridines with ketene equivalents was begun. The interest in β,γ-enones stems from the development of a novel variant of the oxa-di-π-methane photoisomerization to include a basic nitrogen in the photoprecursors (Scheme 6)[10,11,12] The synthetic possibility of utilizing an aza-Diels-Alder reaction to efficiently construct these type of bicyclic systems was of great interest as the current synthetic route to photoprecursor **15** from cinchomeronic acid **14** consisted of many steps.[10,11,12] The desired aza-Diels-Alder reactions, such as shown in Scheme 7, could provide ODPM photoprecursors much more convienently than currently possible.



14 **15** **7**

Scheme 6

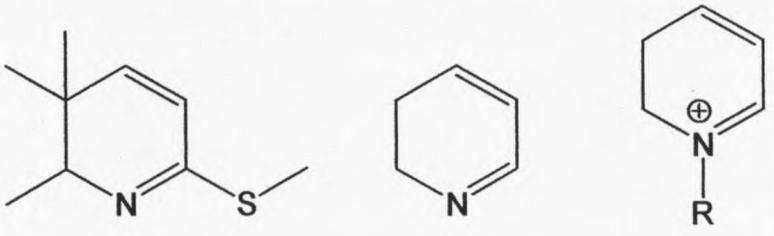


57 **1** **17**

Scheme 7

Review of 2,3-Dihydropyridines

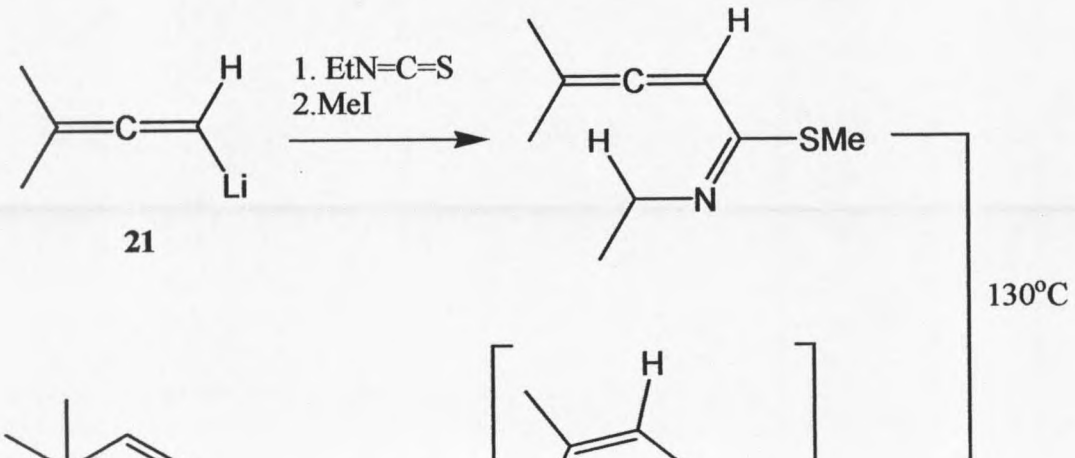
There are relatively few accounts of 2,3-dihydropyridines in the literature. The published 2,3-dihydropyridines fall in to two categories: those possessing geminal alkyl groups **18**,[17] and those prepared via extreme thermal conditions, such as **19**,[18] (Figure 4). 2,3-Dihydropyridines possessing geminal dimethyl groups are the most stable of the three types. Those formed by flash vacuum pyrolysis, have been noted to be less robust. These 2,3-dihydropyridines are discussed in turn below.



18 **19** **20**

Figure 4

Stable 2,3-dihydropyridines have been prepared which have geminal dimethyl groups. This has led to enhanced stability due to the molecules' inabiltity to aromatize to the corresponding pyridine. An example of the use of geminal dimethyls is the preparation of 2,3,3-trimethyl-2,3-dihydro-6-thiomethylpyridine **18** by Brandsma et al.[17] The dihydropyridine **18** was prepared from lithiated 1,1-dimethylallene[19] **21** over three steps (Scheme 8).

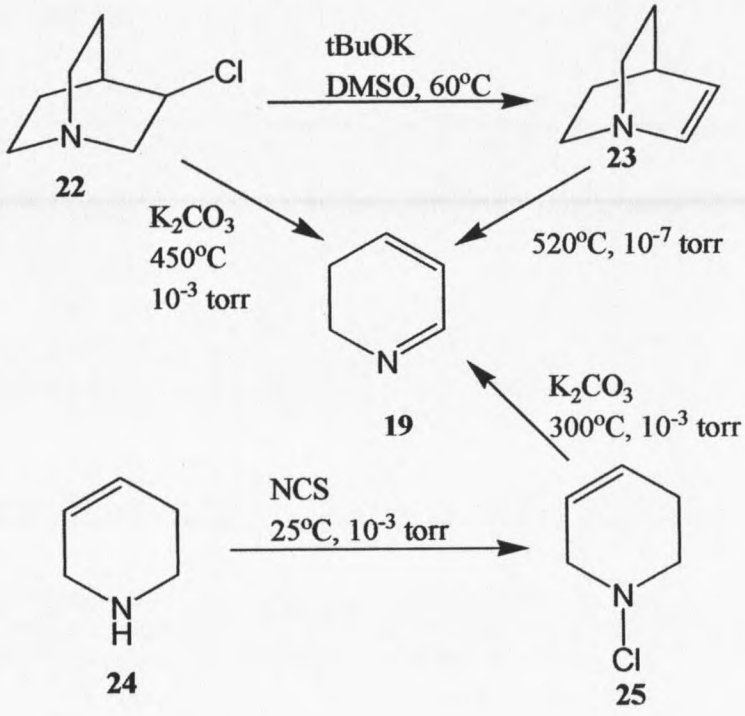


21 **18**

Scheme 8

Flash vacuum pyrolysis (FVP) has also given access to 2,3-dihydropyridines. Three related procedures for the preparation of the parent 2,3-dihydropyridine **19** were reported by Ripoll[18] (Scheme 9). Thus, 1-azabicyclo[2.2.2]oct-2-ene **23**, prepared via elimination of 1-azabicyclo[2.2.2]-3-chlorooctane **22**, was heated to 520°C at 10^{-7} torr, to produce the product **19**. The second procedure directly converted **22** to 2,3-

dihydropyridine by treatment with K_2CO_3 at 450°C at 10^{-3} torr. In the third route, N-chloro-1,2,3,6-tetrahydropyridine **25**, prepared via chlorination of 1,2,3,6-tetrahydropyridine **24**, was eliminated using K_2CO_3 at 300°C at 10^{-3} torr to produce dihydropyridine **19**. The 2,3-dihydropyridine **19** was characterized by low temperature ^{1}H-NMR as it was only stable in solution below -80°C. Allowing the temperature to rise above -80°C led to polymerization.



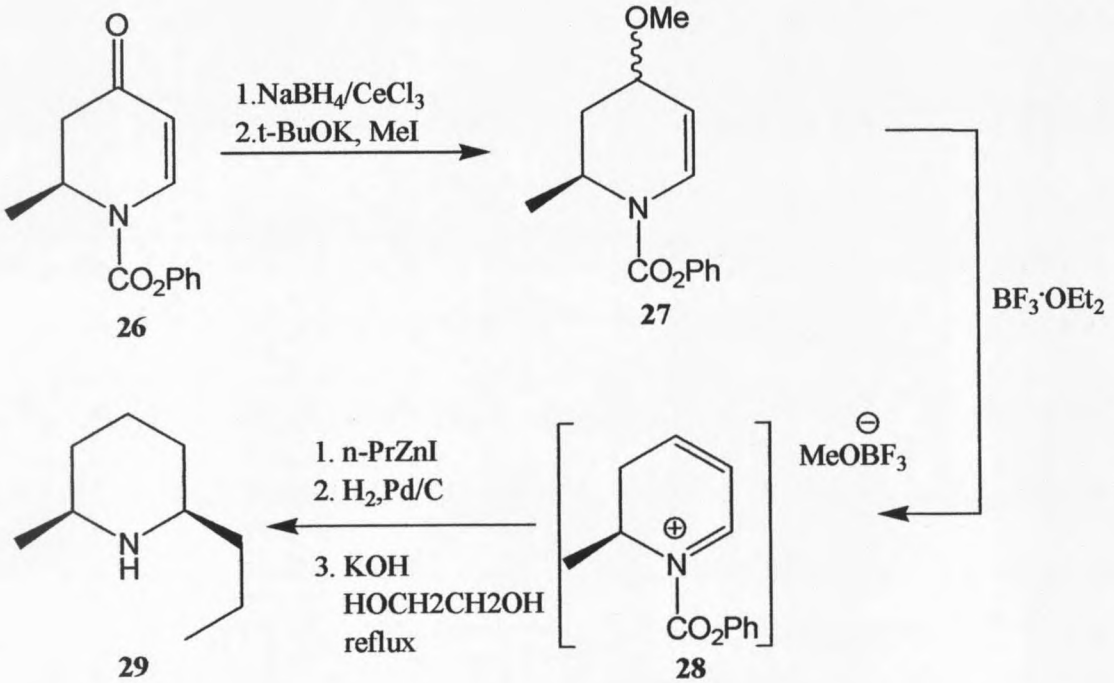
Scheme 9

Review of 2,3-Dihydropyridinium salts

The preparation and use of 2,3-dihydropyridinium salts has been around for several years. In many cases these 2,3-dihydropyridinium species have been prepared and subsequently reacted with various nucleophiles. Examples of 2,3-dihydropyridinium

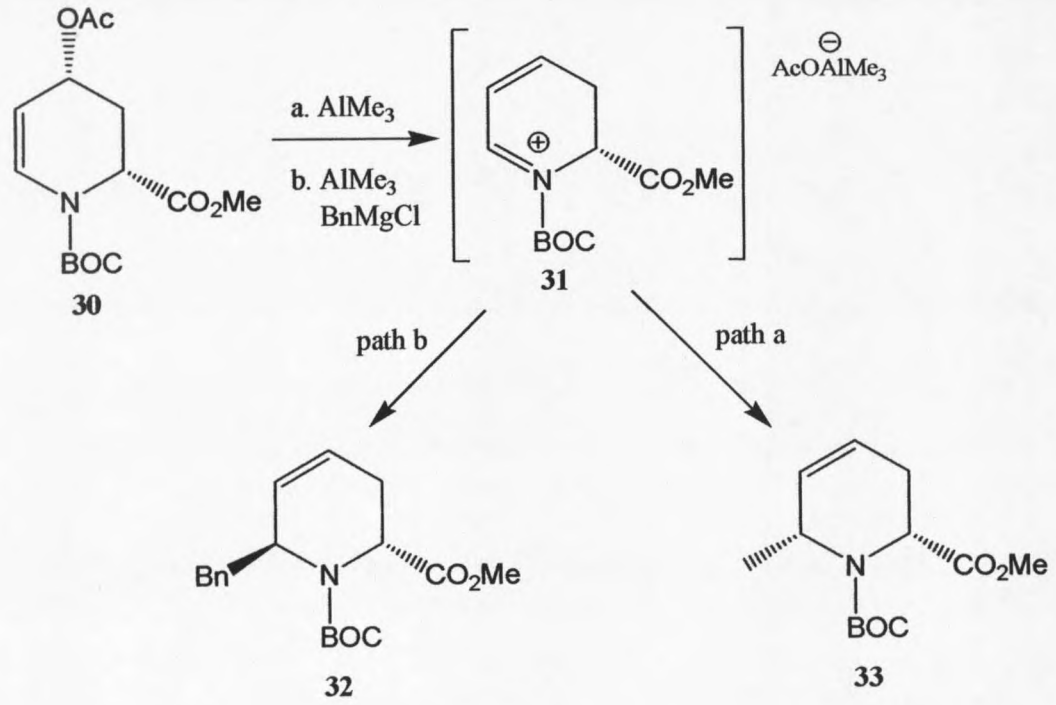
salts have been reported by Comins,[20] Hanson,[21] Meyers,[22] and Husson.[23] These examples will be discussed below in turn.

The use of *in situ* generated 2,3-dihydropyridinium salts has been used for the stereoselective synthesis of small natural products. Comins[20] reported the preparation of (+/-)-dihydropinidine **29** using a 2,3-dihydropyridinium salt **28** as the key intermediate for introduction of the relative stereochemistry between the C1 and C6 positions (Scheme 10). It was demonstrated that the use of n-propylzinc led to the cis alkylation product when added to 2-methyl-2,3-dihydropyridinium trifluoromethoxyborate **28**. Although the product was proposed to come from the intermediate 2,3-dihydropyridinium salt **28**, no spectral evidence was obtained to support it.[24]



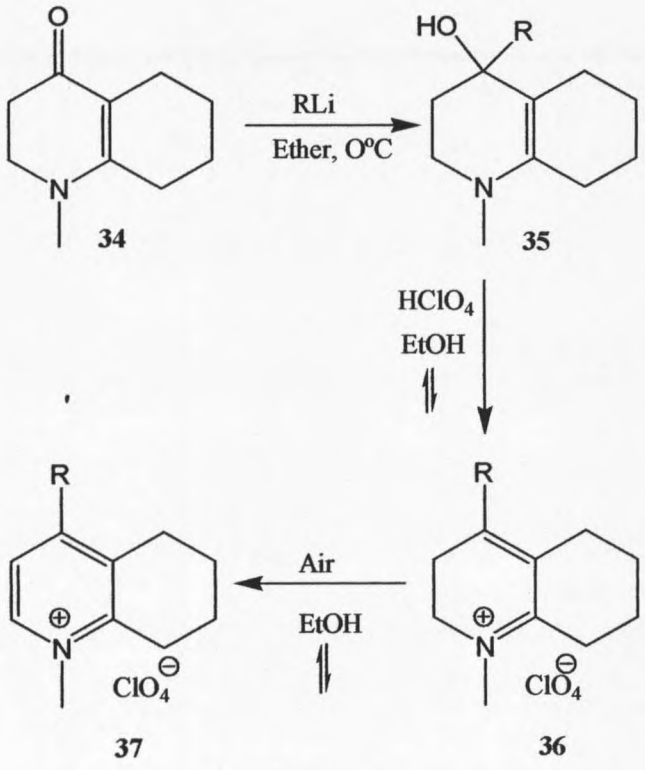
Scheme 10

Hanson[21] used an intermediate 2,3-dihydropyridinium salt **31** for the stereoselective preparation of pipecolic acid derivatives **32** and **33** (Scheme 11). When trimethyl aluminum was utilized, the cis alkylation product **33** was produced. It is of further interest that the trans alkylation product **32** was obtained through the use of benzylmagnesium chloride and aluminium chloride. This stereochemical change was thought to be due to complexation of the aluminum-magnesium species with the carbomethoxy group. No spectral evidence of the existence of the intermediate 2,3-dihydropyridinium species was offered. In both of the cases above, the structures of the dihydropyridinium salts were inferred from the reaction conditions and products.



Scheme 11

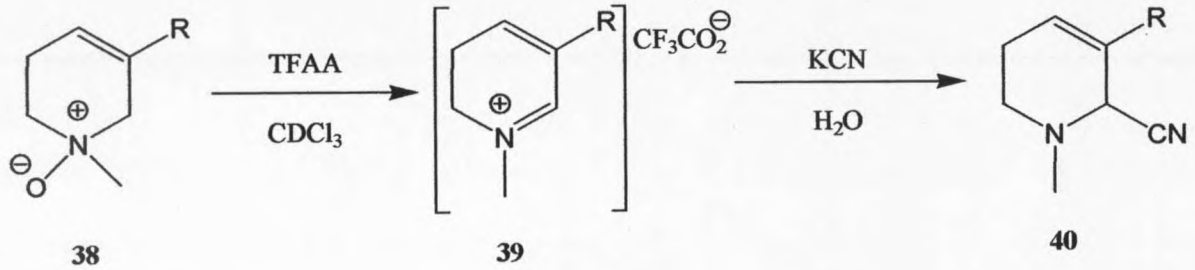
In 1969, Meyers[22] published examples of 2,3-dihydropyridinium salts derived from bi- and tricyclic dihydropyridones. An example of this work is shown in Scheme 12. Pyridone **34** was treated with methyl lithium to yield the corresponding enamine alcohol **35** which was smoothly converted to the dihydropyridinium salt **36** by treatment with cold perchloric acid. Here the dihydropyridinium perchorate salt **36** formed was found to be stable enough to obtain analytical data, including melting points. Further conversion of the dihydropyridinium perchlorate salt **36** to the corresponding pyridinium perchlorate salt **37** was easily accomplished via air oxidation in refluxing ethanol.



Scheme 12

In 1980, Husson[23] reported the preparation of N-methyl-2,3-dihydropyridinium salts via the Polonovski-Potier reaction.[25] An example of this work is the *in situ*

preparation of 1-methyl-2,3-dihydropyridinium tetrafluoroacetates **39** from 1-methyl-1,2,3,6-tetrahydropyridine N-oxides **38** by treatment with trifluoroacetic anhydride in $CDCl_3$ at 0°C followed by spontaneous elimination (Scheme 13). These 2,3-dihydropyridinium salts were prepared to investigate their reactivity with nucleophiles, and no indication was given that they pursued aza-Diels-Alder conditions with them. The use of $CDCl_3$ as solvent allowed Huson to obtain ^{1}H-NMR data for the 2,3-dihydropyridinium salts. This report is the only one, that we are aware of, which provides spectroscopic evidence of 2,3-dihydropyridinium salts.

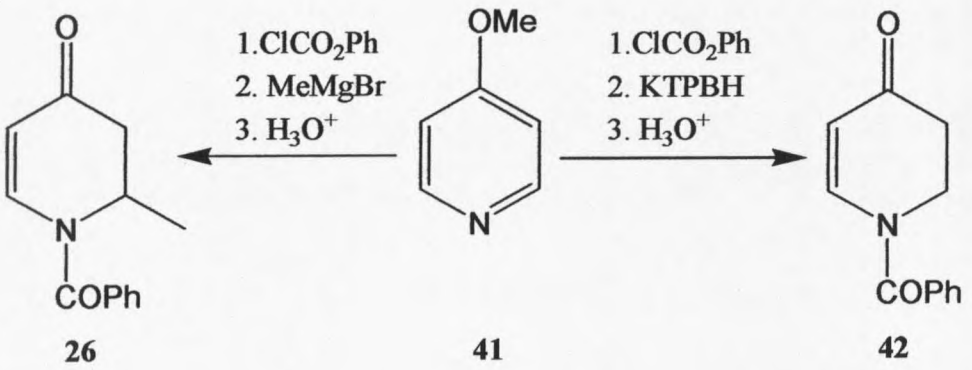


38 **39** **40**

Scheme 13

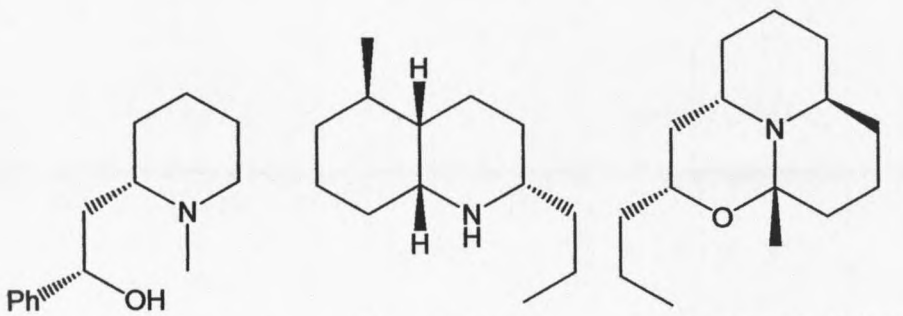
Review of 2,3-Dihydropyridones

Our approach to 2,3-dihydropyridines relied upon the availability of 2,3-dihydropyridones (Scheme 14). 2,3-Dihydropyridones have been employed as key synthetic intermediates for the preparation of several natural products, including the enantioselective syntheses of (-)-sedamine,[26] (-)-pumiliotoxin C,[27] and (-)-porantheridine[28] (Figure 5). All of these molecules were prepared via optically active 2,3-dihydropyridone derivatives derived from pyridinium salts.



26 **41** **42**

Scheme 14



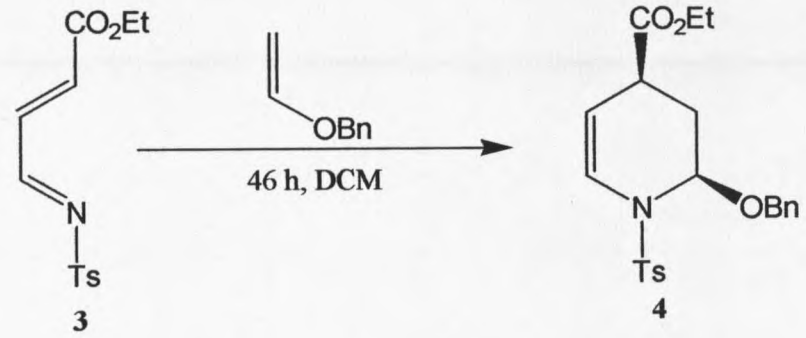
(-)-sedamine **(-)-pumiliotoxin** **(-)-porantheridine**

Figure 5

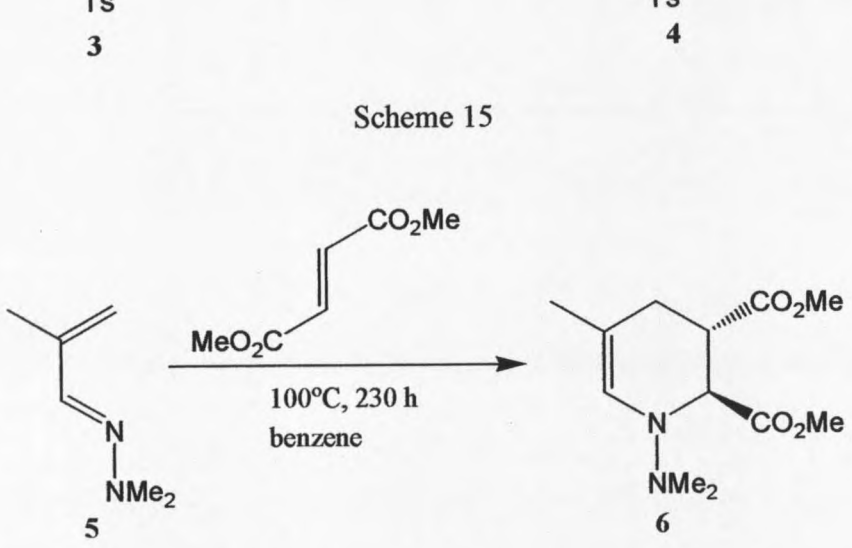
There are several published routes used to prepare 2,3-dihydropyridones.[29-34] Among them, the reduction of 4-alkoxypyridinium salts represents the most facile route. This method can be used to prepare both 2-alkylated and 2-H 2,3-dihydropyridones by selection of the reducing agent. When hydride sources such as sodium borohydride[29-31] and potassium tris-isopropoxyborohydride[29] (KTPBH) are employed, the 2-H 2,3-dihydropyridones, such as **42**, are produced. The use of a Grignard reagent such as methymagnesiun bromide produced the 2-alkylated product, such as **26**, in good yield (Scheme 14).[33, 34]

Aza-Diels-Alder Reactions

Hetero-Diels-Alder reactions have been an area of synthetic interest for many years, with the aza-Diels-Alder reaction being explored by several groups.[1-4] Most aza-Diels-Alder reactions of 1-aza-dienes involved dienes that were acyclic. Examples of these acyclic cases have been reported by Boger[1] and Ghosez[2]. Boger has effectively used dienes such as the unsaturated imine **3** in inverse electron-demand Diels-Alder reactions (Scheme 15).[1] Ghosez utilized the unsaturated imine **5** to react in the normal electron-demand mode with diethyl fumarate (Scheme 16).[2]

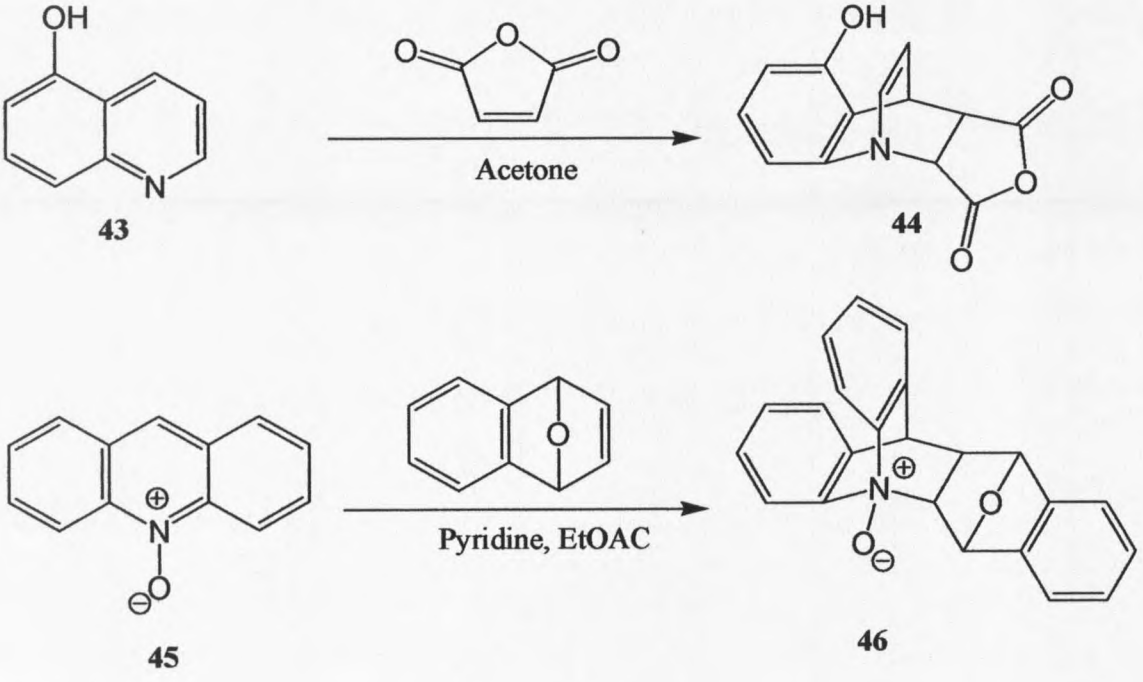


Scheme 15



Scheme 16

The use of cyclic 1-aza-dienes in aza-Diels-alder reactions is very limited, as searching the literature revealed only two such examples (Scheme 17). In both cases, the "aza-diene" moiety was imbedded in fused aromatic heterocycles. Rastogi[3] reacted 8-hydroxyquinoline **43** with maleic anhydride yielding the desired tricyclic adduct **44**. Wittig[4] utilized acridine N-oxide **45** as a 1-aza-diene by reacting it with 1,4-dihydro-1,4-epoxido-napthalene to give the Diels-Alder product **46**.

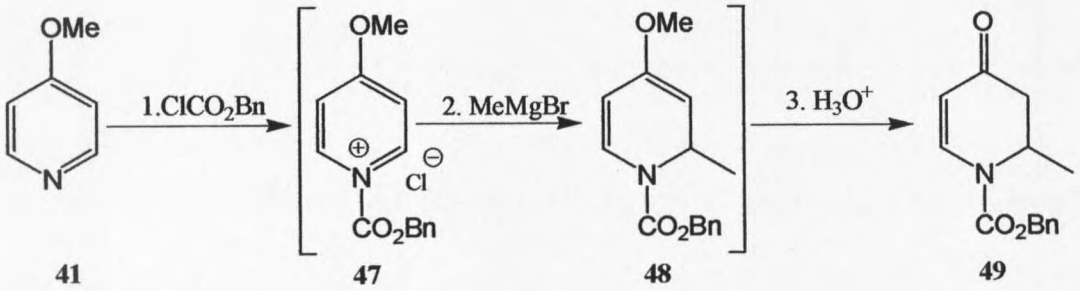


Scheme 17

Results and Discussion

Preparation of 2,3-Dihydropyridones

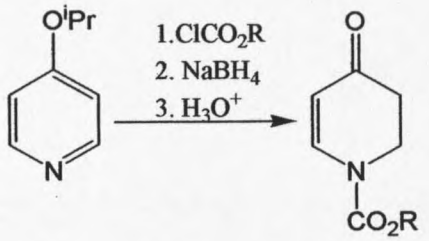
In order to explore the use of 2,3-dihydropyridines in aza-Diels-Alder reactions for the preparation of the desired photoprecursors (Scheme 7), the required 2,3-dihydropyridones were prepared. For this study, our 2,3-dihydropyridines were synthesized from the requisite 2,3-dihydropyridones. One-pot preparation of the N-carbobenzyloxy-2,3-dihydro-2-methylpyridone **49** was facilitated by the *in situ* generation of pyridinium salt **47** followed by addition of methyl magnesium bromide to yield the 1,2-dihydropyridine **48**. This was subsequently hydrolyzed to the desired dihydropyridone **49** in 89% overall yield (Scheme 18).



Scheme 18

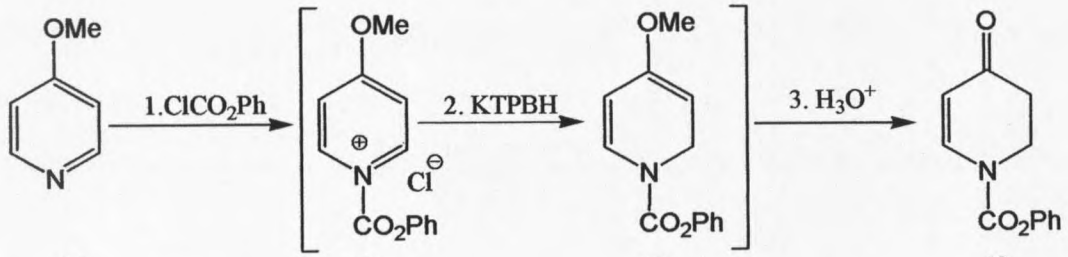
Preparation of the non-alkylated dihydropyridones from 4-methoxypyridine represented a combination of two common methods from the literature.[29-31] We chose to investigate the use of sodium borohydride in place of the potassium tris-isopropoxyborohydride (KTPBH) used by Comins'[29] after noticing the conditions demonstrated by Raucher[30] (**51**) and Yamada[31] (**52**) on 4-isopropoxypyridine **50** (Scheme 19). Comins stated that the reason for using the more exotic reducing agent was due to

the relatively poor yields (34%) when sodium borohydride was employed for the reduction of N-carbophenoxy-4-methoxypyridinium chloride **53** (Scheme 20), versus the use of KTPBH (53%).[29] However, we have found that sodium borohydride could be used to produce the related N-carbobenzyloxy-2,3-dihydropyridone **55** in similar yields (76%) to those found for Comins' KTPBH conditions (Scheme 21).



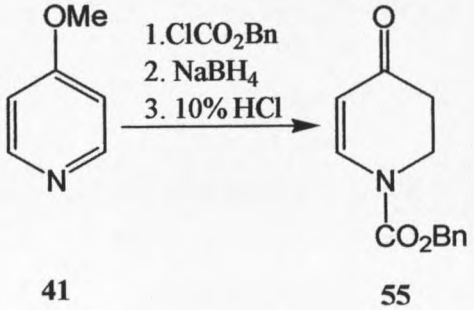
50 **51** R=Me
52 R=Bn

Scheme 19



41 **53** **54** **42**

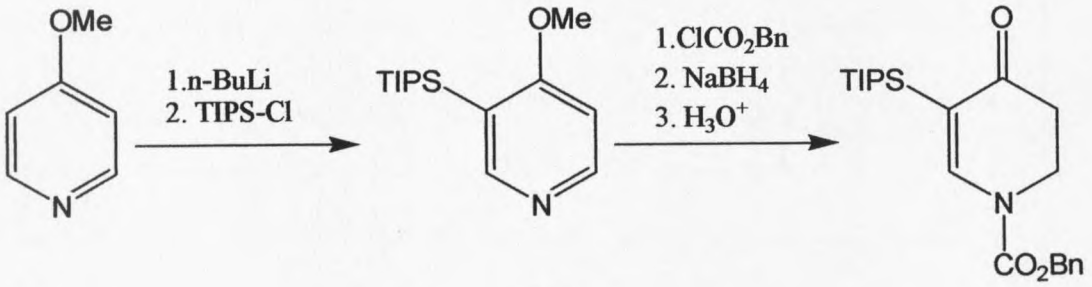
Scheme 20



41 **55**

Scheme 21

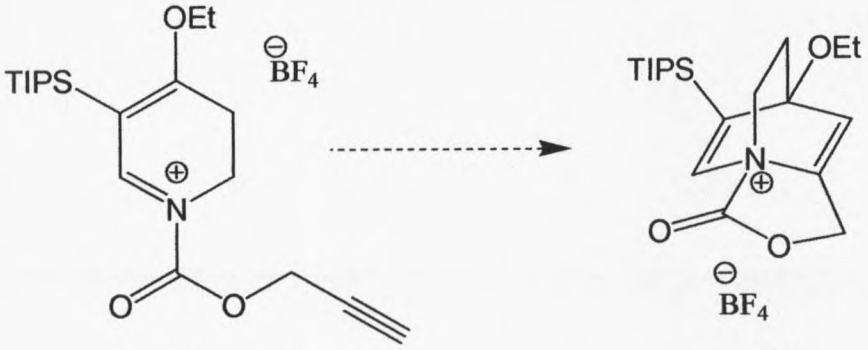
The preparation of 5-silyl-substituted 2,3-dihydropyridones was also accomplished using the conditions developed in this study. Using the Comins approach, the preparation of 4-methoxy-3-(triisopropylsilyl)pyridine **56** was accomplished by α-lithiation of 4-methoxypyridine **41**, followed by treatment with triisopropylsilyl chloride to produce the silylated pyridine **56** in yields comparable to those reported in the literature (Scheme 22).[35] With the silylated pyridine **56** in hand, it was easily transformed to the corresponding 2,3-dihydropyridone **57** in 75% yield using the conditions developed here, that is, by treatment with carbobenzyloxy chloride in the presence of sodium borohydride, followed by hydrolysis with 10% HCl (aq.) (Scheme 22).



41 **56** **57**

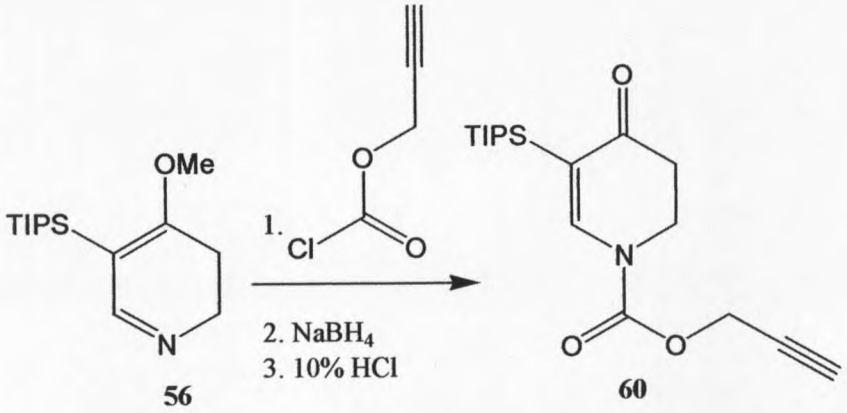
Scheme 22

N-Carbopropargyloxy-5-(triisopropylsilyl)-2,3-dihydropyridone **60** was prepared for the purpose of appending an intramolecular dienophile onto the dihydropyridinium salt **58** (Scheme 23). Dihydropyridone **60** was prepared in similar fashion to the previously described pyridones, from 3-(triisopropylsilyl)-4-methoxypyridine **56** in 75% yield (Scheme 24).



58 **59**

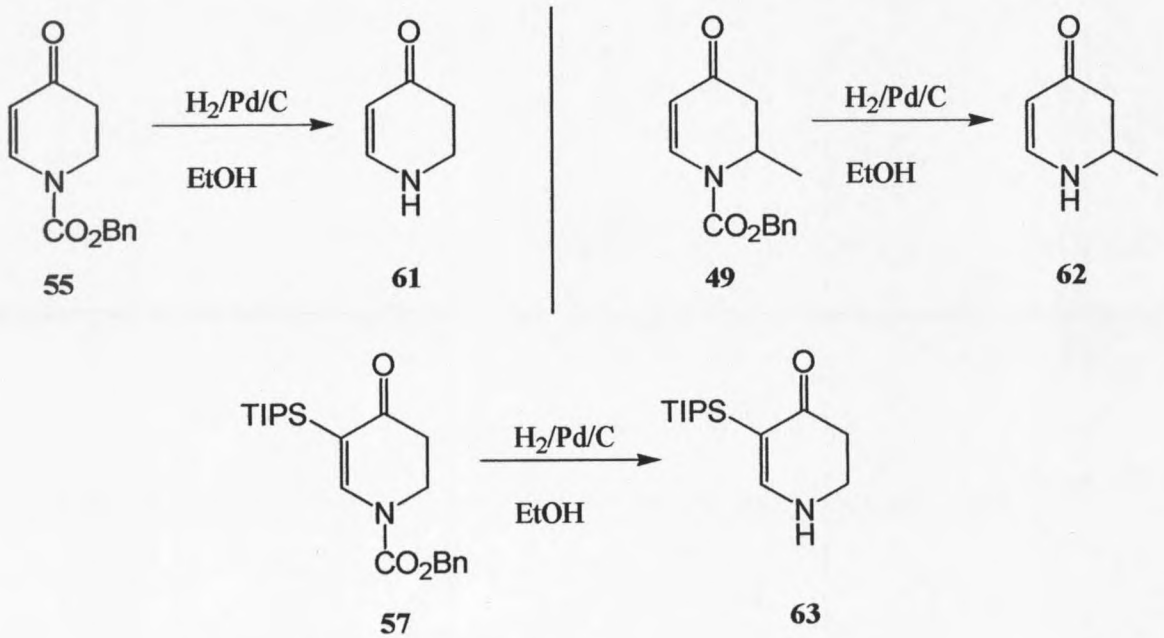
Scheme 23



56 **60**

Scheme 24

Removal of the carbobenzyloxy groups was carried out via standard hydrogenolysis[35] of the N-carbobenzyloxy-2,3-dihydropyridones **49**, **55** and **57** with palladium on carbon under a hydrogen atmosphere (Scheme 25). This procedure gave the parent 2,3-dihydropyridones **61**, **62** and **63** in high yield. With 2,3-dihydropyridones in hand, the transformation of them into the desired 2,3-dihydropyridines was possible.

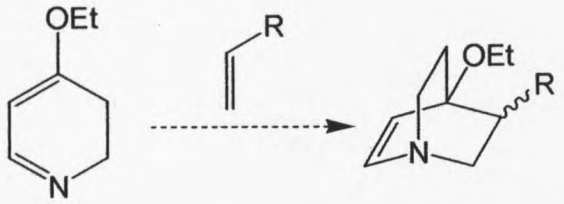


Scheme 25

Preparation of 2,3-Dihydropyridines

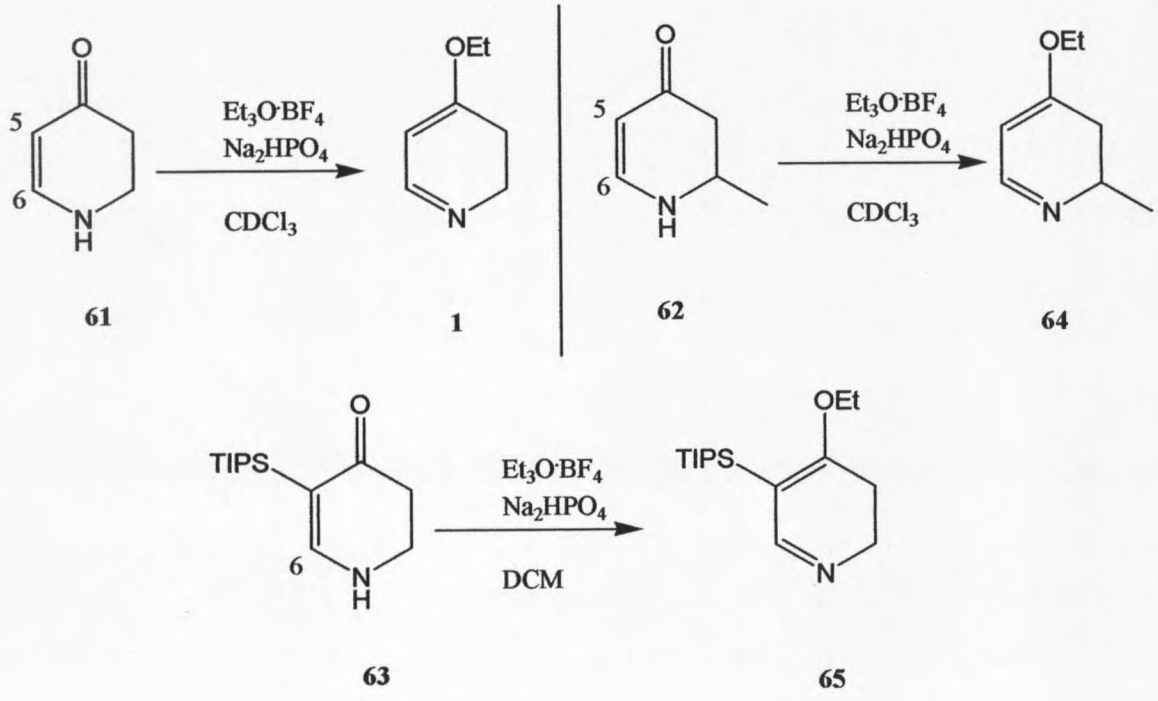
Preparation of the new 4-ethoxy-2,3-dihydropyridine derivatives, **1**, **64** and **65**, has been accomplished in good conversion by ^{1}H-NMR as outlined below. These dihydropyridines were prepared to investigate their reactivity under Diels-Alder conditions (Scheme 26). To access the 2,3-dihydropyridines, we have employed the known[29-31] and novel 2,3-dihydropyrid-4-ones **61**, **62** and **63** as starting materials. Transformation of pyridones **61** - **63** to the corresponding 2,3-dihydropyridines was

accomplished in high conversion by ^{1}H-NMR utilizing ethyl Meerwein's reagent[36] in the presence of dibasic sodium phosphate, a proton scavenger, to prevent formation of HF (Scheme 27). *In situ* identification of the dihydropyridines was accomplished via proton and carbon NMR spectroscopic techniques. See Appendix A for copies of the NMR spectra.



1

Scheme 26



61 **1** **62** **64**

63 **65**

Scheme 27

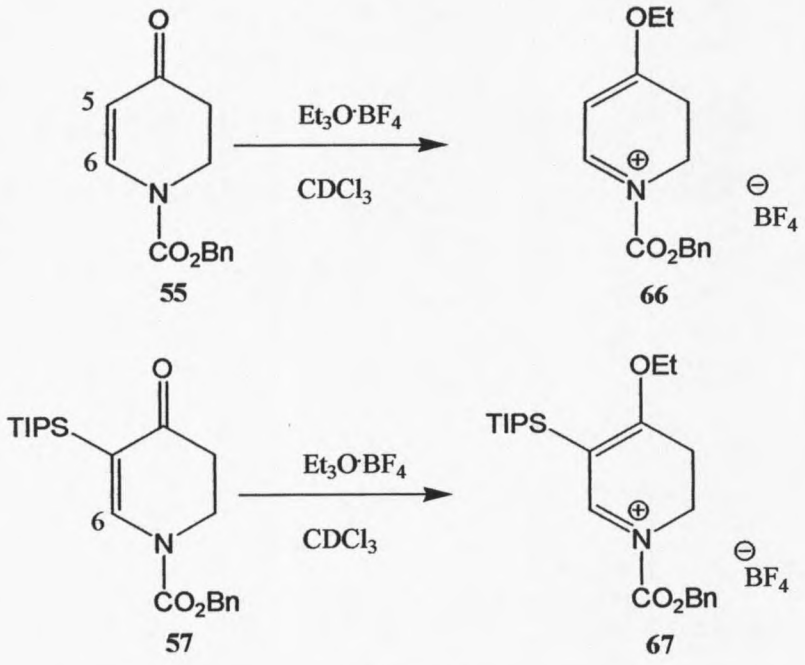
Central to the identification of the dihydropyridines were the ^{1}H-NMR signals representing the protons on C6 and C5, where applicable, and comparison to the chemical shifts of the dihydropyridone starting material (Table 1). The dihydropyridines exhibited a considerable downfield shift from their corresponding dihydropyridones. High resolution mass spectrometry data were obtained for the 2,3-dihydro-4-methoxypyridine **1**. The dihydropyridines were stable under anhydrous conditions for several days, but attempts to further purify them by vacuum distillation or chromatography on basic alumina led primarily to the parent pyridine and other unidentified decomposition products.

Dihydropyridone	C6	C5	Dihydropyridine	C6	C5
61	7.18	5.04	**1**	8.04	5.63
62	7.19	5.33	**64**	8.29	5.68
63	7.16	-	**65**	7.96	-

Table 1

Preparation of 2,3-Dihydropyridinium salts

The 2,3-dihydropyridinium salts **66** and **67** were prepared utilizing similar conditions to those described for the 2,3-dihydropyridines, but without the use of dibasic sodium phosphate (Scheme 28). The proton scavenger was not required as no HF would have been produced during the course of the reaction. The 2,3-dihydropyridinium salts were found to be much more sensitive to air oxidation and no further attempts to purify them was undertaken.



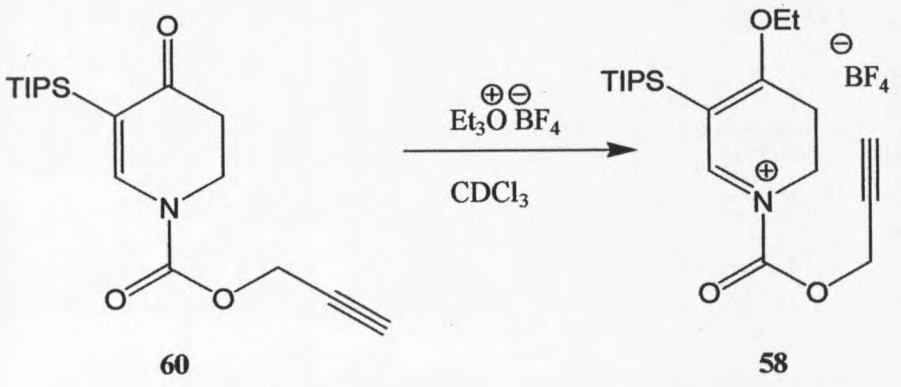
Scheme 28

The 2,3-dihydropyridinium tetrafluoroborate salts prepared here were identified by NMR spectroscopy and exhibited spectral features similar to those found for the 2,3-dihydropyridines. Again the chemical shifts of the protons on C6 and C5, where applicable, demonstrated a significant downfield shift from their corresponding dihydropyridones (Table 2). The instability to the atmosphere found for the dihydropyridinium salts prepared here, compared to the air stability of the dihydropyridinium salts prepared by Meyers,[23] may be due to the electronic differences between the nitrogen substituents; carbamates versus the methyl group used by Meyers. Additionally, the dihydropyridinium salts prepared by Meyers had an alkyl or aryl group at the C4 position versus the ethoxy group in our cases. The counterion may also play a role in the relative stabilities between these two different salts as well, as Meyers' examples had perchlorate counterions.

Compound #	C6	C5	Compound #	C6	C5
55	7.83	5.32	**66**	8.86	6.10
57	7.89	-	**67**	8.61	-
60	7.82	-	**58**	8.50	-

Table 2

Conversion of dihydropyridone **60** with the appended alkyne to dihydropyridinium salt **58** was accomplished under similar conditions that were employed for the N-carbobenzyloxy cases. Thus, addition of ethyl Meerwein's reagent to a solution of the dihydropyridone in $CDCl_3$ to give the desired dihydropyridinium salt **58** in good conversion by ^{1}H-NMR (ca ~ 72%). The NMR spectrum for dihydropyridinium salt **58** exhibited similar features as were noted for the other dihydropyridinium salts (Table 2).

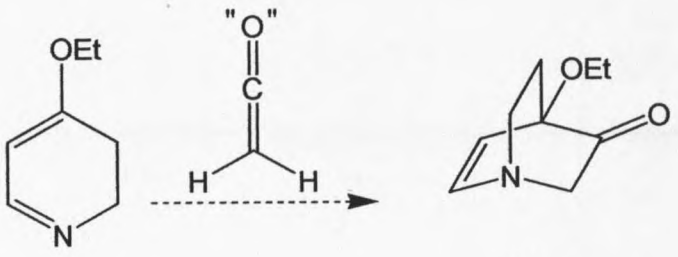


60 **58**

Scheme 29

Attempted Diels-Alder Cyclizations
Using 2,3-Dihydropyridines
and 2,3-Dihydropyrdinium salts .

As noted earlier, the described 2,3-dihydro-pyridines and -pyridinium salts were prepared to investigate their reactivity under Diels-Alder conditions. The aim was to react our aza-dienes with a ketene equivalent, thus generating the desired azabicyclo[2.2.2]octenones in a rapid and efficient manner (Scheme 30). To this end, various aza-Diels-Alder conditions were investigated.

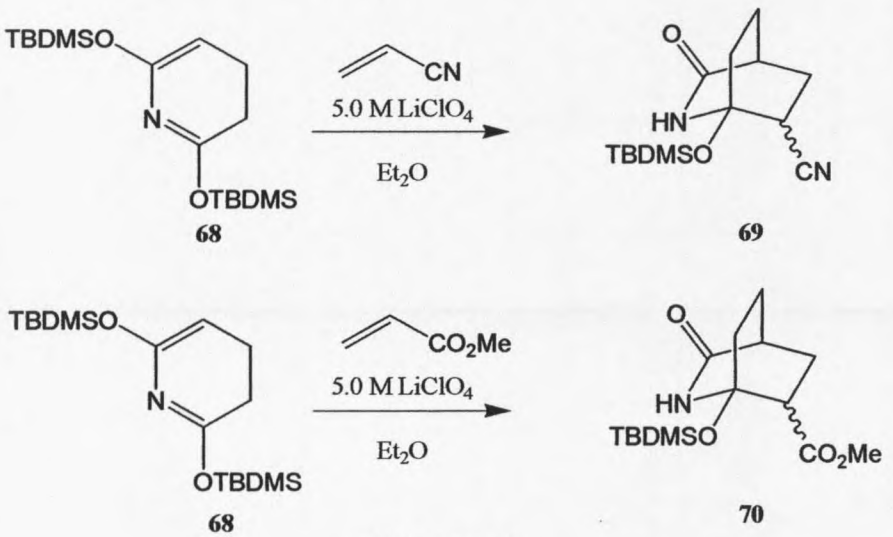


1 17

Scheme 30

Initially, the Diels-Alder reactions (Table 3) were run at room temperature in chloroform-d and followed by ^{1}H-NMR spectroscopy. The azadienes utilized are shown in Figure 7, and the dienophiles are shown in Figure 6. After several days, all of the reactions attempted yielded no products. The mixtures were then heated to reflux (61°C), but again no products were observed via NMR. This led to further attempts in refluxing toluene-d8 (110°C), again indicating no addition of product (NP) by ^{1}H-NMR spectroscopy. Following the lack of success utilizing traditional thermal conditions, the use of a non-traditional solvent media was investigated. The conditions developed by Grieco consisting of 5M lithium perchlorate in ether was selected.[37] This highly polar

media has been used, by Grieco, to effect aza-Diels-Alder reactions of the 2-aza-diene **68** with electron deficient dienophiles (Scheme 31).[37] Unfortunately, the highly polar media failed to produce the desired Diels-Alder adduct. These reactions were followed by TLC of the reaction looking for disappearance of the dienophile. Table 3 Summarizes the thermal and Grieco conditions attempted.



Scheme 31

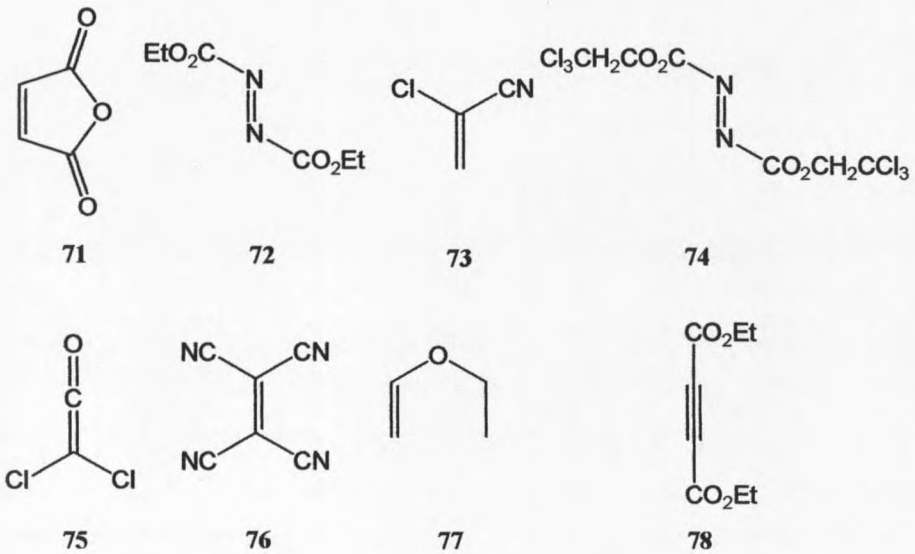


Figure 6

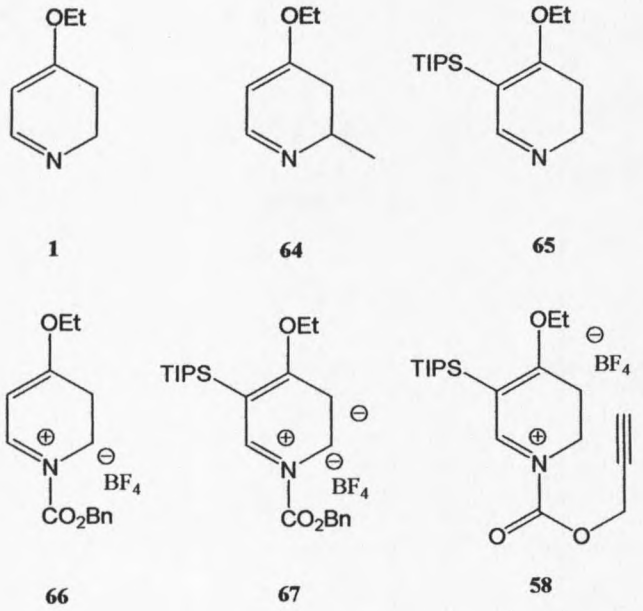


Figure 7

Entry	Aza-diene	Dienophile	Temperature	Solvent	Result
1	**64**	**71**	RT to 61°C	$CDCl_3$	NP
2	**64**	**72**	RT to 61°C	$CDCl_3$	NP
3	**64**	**73**	RT to 61°C	$CDCl_3$	NP
4	**64**	**74**	RT to 61°C	$CDCl_3$	NP
5	**64**	**71**	RT	5M $LiClO_4$-Et_2O	NP
6	**64**	**73**	RT	5M $LiClO_4$-Et_2O	NP
7	**1**	**73**	RT	5M $LiClO_4$-Et_2O	NP
8	**1**	**73**	RT	1M $LiClO_4$-Et_2O	NP
9	**1**	**75**	RT	Toluene-d8	NP
10	**1**	**73**	RT to 61°C	$CDCl_3$	NP
11	**1**	**73**	110°C	Toluene-d8	NP
12	**1**	**76**	RT to 61°C,	$CDCl_3$	NP
13	**1**	**76**	110°C	Toluene-d8	NP
14	**66**	**71**	RT	Acetone / DCM	NP
15	**66**	**77**	RT to 61°C	$CDCl_3$	NP
16	**66**	**73**	RT to 61°C	$CDCl_3$	NP
17	**66**	**73**	110°C	Toluene-d8	NP
18	**67**	**78**	RT	DCM	NP
19	**67**	**78**	100°C sealed vial	DCM	NP
20	**58**	-	RT to 61°C	$CDCl_3$	NP
21	**58**	-	RT	$Mg(ClO_4)_2$ (1 eq.) DCM	NP

Table 3

The final attempt to facilitate the aza-Diels-Alder reaction was via the use of microwave radiation. In order to follow the reactions by ^{1}H-NMR spectroscopy, they were performed in chloroform-d. Microwave radiation at 250 watts led to no observation of product (NP) at the temperatures used. As the temperature was increased, degradation of the aza-dienes was observed, but no aza-Diels-Alder adduct was obtained. Table 4 summarizes the microwave conditions attempted.

Entry	Aza-diene	Dienophile	Temp	Time	Result
22	**65**	**73**	150	10	NP
23	**65**	**73**	175	10	NP
24	**65**	**73**	180	10	Decomp
25	**68**	**73**	150	10	NP
26	**68**	**73**	175	10	NP
27	**68**	**73**	180	10	Decomp
28	**58**	-	150	10	NP
29	**58**	-	175	10	NP
30	**58**	-	180	10	Decomp

Table 4

In conclusion, the first room temperature stable 4-ethoxy-2,3-dihydropyridines derived from 2,3-dihydropyridones were prepared. They were generated under very mild conditions using ethyl Meerwein's reagent at room temperature. Although they proved to be non-isolable, they were stable for prolonged periods at and above room temperature in anhydrous solutions. They were also unreactive, to our dismay, to a variety of Diels-Alder conditions by failing to react with dienophiles. Exposure to air and extreme thermal conditions led to decomposition. Conditions for the preparation of 2,3-dihydropyridones was further optimized from those available in the literature, and the need for the use of the expensive reducing KTPBH was found to be unnecessary.

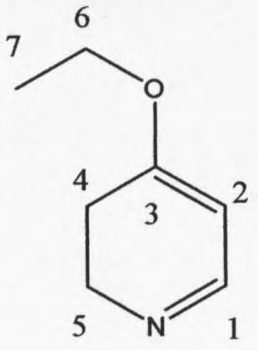
Experimental

General

All experiments were carried out under an atmosphere of dry argon in oven and/or flame dried glassware. ^{1}H, ^{13}C, ^{31}P NMR spectra were obatained on Bruker DRX-250, DPX-300, or DRX-500 spectrometers using $CDCl_3$ as solvent unless noted otherwise. Chemical shifts are reported in ppm downfield of the internal refernce tetramethysilane, or phosphoric acid (in the case of ^{31}P). Splitting patterns are designated as: s (singlet), d (doublet), t (triplet), q (quartet), pent (pentet), sext (sextet), sept (septet), and m (mulitplet); addition of b indicates broadened pattern, addition of app indicates and apparent signal, i.e. app pent = apparent pentet. Infrared spectra were taken on a Perkin-Elmer 1600 FTIR spectrophotometer as neat oils on NaCl plates or solid plates with KBr and are reported in cm^{-1}. Mass spectra were obtained on a VG70E_HF double focusing mass spectrometer. Gas chromatography was performed on a Hewlett-Packard model 5890A using a 30m DB-5 column (0.25 mm i.d., 0.25 mm film thickness), He flowrate 30 cm/sec calibrated at 200°C, start 50°C hold 5 min, ram 10°C/min to 300°C, hold until complete. Column chromatography was performed using Whatman 4790-250 silica gel. The solvent mixtures used from column chromatography are reported in volume/volume mixtures. R_f values refer to thin layer chromatography on Analtech 2.5 x 10 cm, 250M analytical plates coated with silica gel GF. Melting points were taken on Lab Device Mel-Temp and are uncorrected. CH_3CN, CH_2Cl_2 were distilled from CaH_2 under argon. THF, benzene, toluene, xylenes, and diethyl ether were distilled from sodium benzophenone ketyl before use.

Experimental

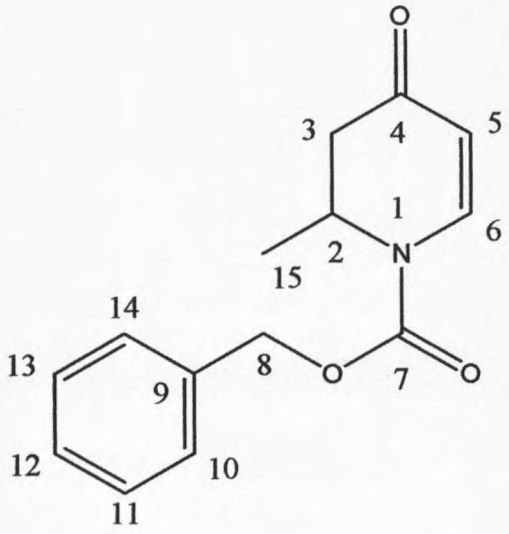
2,3-Dihydro-4-ethoxypyridine (1): An oven dried, Argon purged 50 mL round bottom flask was charged with 2,3-dihydropyrid-4-one **61** (884.6 mg, 9.1 mmol), and Na_2HPO_4 (1.55 g, 10.9 mmol). To this was added freshly distilled $CDCl_3$ (10 mL). A solution of ethyl Meerwein's reagent in $CDCl_3$ (9.1 mL, 9.1 mmol, 1M) was then added at room temperature in one portion. The reaction mixture was stirred at room temperature and followed by NMR until the reaction was completed at 2 days. The reaction mixture was then filtered to remove the phosphates and concentrated *invacuo*. Attempts to further purify the material led to decomposition.



^{1}H-NMR: 8.29 (1H, dd, *J*=5.6 Hz, *J*=1.0 Hz, H on C1), 5.68 (1H, *J*=5.7 Hz, H on C2), 4.20 (2H, q, *J*=7.1 Hz, H's on C6), 3.89 (2H, t, *J*=9.3 Hz, H's on C5), 2.76 (2H, t, *J*=9.3 Hz, H's on C4), 1.20, (3H, t, *J*=7.0 Hz, H's on C7). ^{13}C-NMR: 179.6 (C3), 166.2 (C1), 92.5 (C2), 66.2 (C6), 40.9 (C5), 27.3 (C4), 15.7 (C7). HRMS calculated for $C_7H_{11}NO$ 125.084064, Found 125.084206

N-Carbobenzyloxy-2,3-dihydro-2-methylpyrid-4-one (49): An oven dried, Argon purged 100 mL round bottom flask was charged with 4-methoxypyridine (1.08 g, 9.9

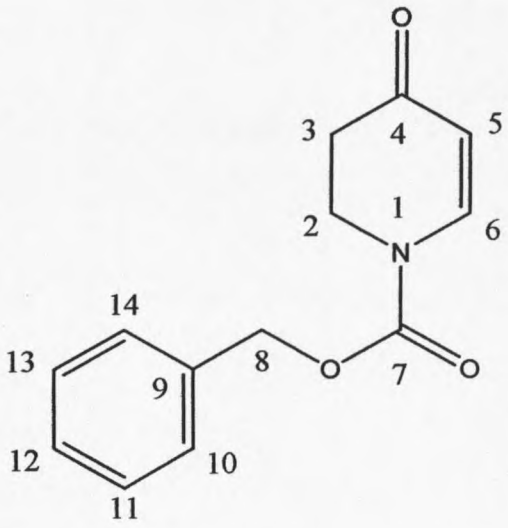
mmol) and dry THF (35 mL), and then cooled to -23°C. Carbobenzyloxy chloride (1.79 g, 10.5mmol) was added dropwise to the cooled solution, and the mixture stirred for an additional 30 minutes. To the cooled reaction flask, a solution of methyl magnesium bromide in butyl ether (1M, 12 mL, 12 mmol) was added dropwise. Following the addition, the reaction was stirred for an additional 30 minutes at -23°C. The reaction was then quenched by pouring the reaction mixture into a flask containing 10% HCl (aq) (50 mL) that had been cooled to 0°C. The reaction mixture was stirred to room temperature for 90 min. Ether (25 mL) was then added, and the mixture separated. The aqueous layer was extracted with ether (4x25 mL). The combined organic extracts were dried by filtration over K_2CO_3 and then concentrated *in vacuo*. Column chromatography on silica gel of the crude product eluting with 5% MeOH/DCM yielded the product as a yellow oil in 89% yield (2.16 g, 8.8 mmol).



^{1}H-NMR: 7.72 (1H, d, *J*=8.2Hz, H on C6), 7.32 (5H, bs, H's on C10, 11, 12, 13, 14), 5.31 (1H, d, *J*=8.9 Hz, H on C5), 5.25 (2H, d, *J*=2.1 Hz, H's on C8), 4.71 (1H, m, H on C2), 2.84 (1H, dd, *J*=16.5, 6.8 Hz, H on C3), 2.29 (1H, d, *J*=16.5 Hz, H on C3), 1.24 (3H,

d, J=6.8 Hz, H's on C15). ^{13}C-NMR: 192.8 (C4), 153.3 (C7), 141.6 (C6), 135.0 (C9), 128.7 (C's 11, 12, 13), 128.4 (C's 10, 14), 106.8 (C5), 69.0 (C8), 49.3 (C2), 41.8 (C3), 16.7 (C15). Spectral data are consistent with the values reported in the literature.[38]

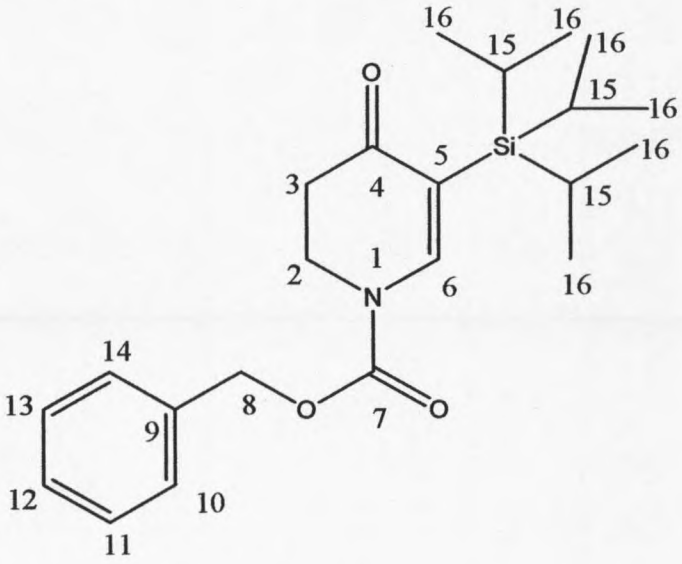
N-Carbobenzyloxy-2,3-dihydropyrid-4-one (55): An oven dried, Argon purged 250 mL round bottom flask was charged with sodium borohydride (2.43 g, 64.2 mmol) and dry methanol (50 mL). The flask was then cooled to -78°C. To this mixture, a solution of 4-methoxypyridine (4.3 g, 39.4 mmol) in dry methanol (50 mL) was added dropwise. Carbobenzyloxy chloride (7.07 g, 41.4 mmol) was then added dropwise to the cooled reaction mixture. Following the addition, the reaction was allowed to warm to room temperature overnight. The reaction was quenched by pouring the reaction mixture into a flask containing 10% HCl (aq) (120 mL) that had been cooled to 0°C. The reaction mixture was stirred to room temperature over 45 min. Ether (100 mL) was then added and the mixture separated. The aqueous layer was extracted with ether (4x100 mL) followed by extraction with DCM (5x200 mL). The combined organic extracts were concentrated *in vacuo*. Column chromatography on silica gel of the crude product with 5% MeOH/DCM yielded the product as a white solid, which was subsequently recrystalized from hexanes in 76 % yield (6.98 g, 30.2 mmol), mp 64.6 – 64.8 °C.



^{1}H-NMR: 7.83 (1H, bs, H on C6), 7.38 (5H, bs, H's on C10, 11, 12, 13, 14), 5.32 (1H, bs, H on C5), 5.25 (2H, s, H's on C8), 4.03 (2H, t, *J*=7.3 Hz, H's on C2), 2.55 (2H, t, *J*=7.3 Hz, H's on C3). ^{13}C-NMR: 193.3 (C4), 153.4 (C7), 149.1 (C6), 134.9 (C9), 128.8 (C's 11, 12, 13), 128.5 (C's 10, 14), 108.2 (C5), 69.1 (C8), 43.7 (C3), 36.6 (C2). IR: 3065, 3032, 2961, 1726, 1669, 1603, 1423, 1391, 1344, 1324, 1301, 1214, 1182, 1106, 998.

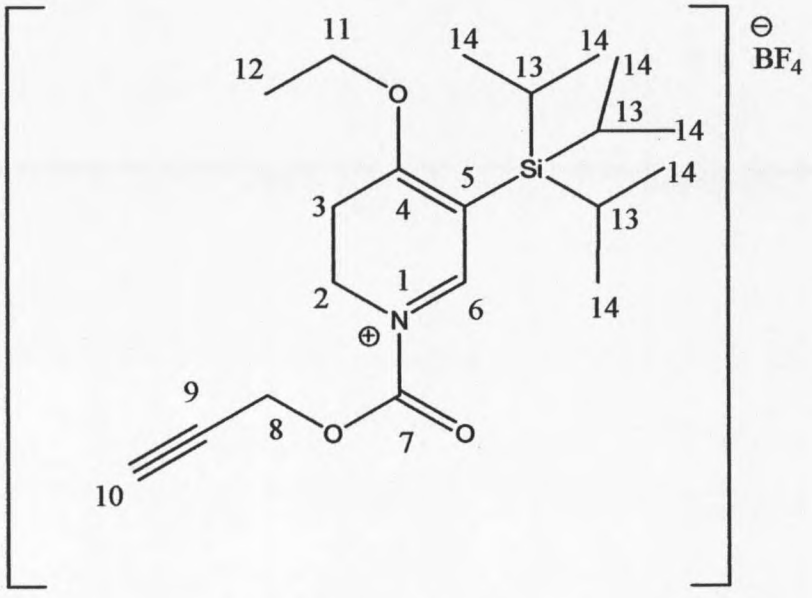
N-Carbobenzyloxy-5-triisopropylsilyl-2,3-dihydropyrid-4-one (57): An oven dried, Argon purged 50 mL round bottom flask was charged with sodium borohydride (153 mg, 4.1 mmol) and dry methanol (10 mL). The flask was then cooled to -78°C. To this mixture a solution of 4-methoxy-3-triisopropylsilylpyridine **56** (2.33 g, 8.8 mmol) in dry methanol (10 mL) was added. Carbobenzyloxy chloride (334.7 mg, 2.8 mmol) was added dropwise to the cooled reaction. Following the addition, the reaction was allowed to stir at -78°C for 2 hours, and then allowed to warm to room temperature overnight. The reaction was quenched by pouring the reaction mixture into a flask containing 10% HCl (aq) (5 mL) that had been cooled to 0°C. This mixture was stirred to room

temperature over 10 min. Ether (20 mL) was then added, and the mixture separated. The aqueous layer was extracted with ether (4x20 mL) followed by extraction with DCM (5x20 mL). The combined organic extracts were concentrated *in vacuo*. Column chromatography of the crude product with 20% Ether/Hexanes yielded the product as a colorless oil in 75% yield (453 mg, 1.2 mmol).



^{1}H-NMR: 7.89 (1H, bs, H on C6), 7.37 (5H, bs, H's on C10, 11, 12, 13, 14), 5.26 (2H, bs, H's on C8), 4.00 (2H, t, *J*=7.5 Hz, H's on C2), 2.53 (2H, t, *J*=7.4 Hz, H's on C3), 1.29 (3H, app. sept. *J*=7.4, H's on C's15), 1.16 (18H, d, *J*=7.3, H's on C's16). ^{13}C-NMR: 196.6 (C4), 152.8 (C7), 148.4 (C6), 135.2 (C9), 128.6 (C's 10, 11, 13, 14), 128.1 (C12), 111.7 (C5), 68.8 (C8), 42.4 (C2), 36.3 (C3), 18.7 (C's16), 11.1 (C's 15). IR: 2973, 2931, 2839, 1707, 1659, 1510, 1436, 1297, 1247, 1247, 1027. HRMS calculated for $C_{22}H_{33}NO_3Si$ (M+H) 388.229141, Found (M+H) 388.230798.

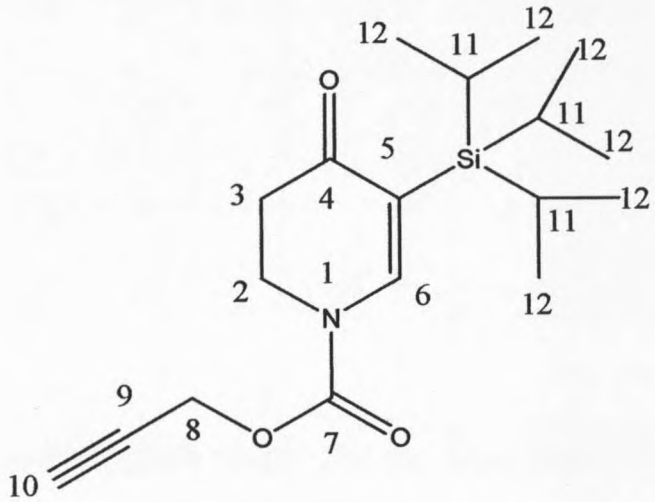
N-Carbopropargyloxy-2,3-dihydropyrid-4-ethoxy-5-triisopropylsilyl-pyridinium tetrafluoroborate (58): An oven dried, Argon purged 5 mL conical vial was charged with N-carbopropargyloxy-2,3-dihydro-5-(trisiopropylsilyl)pyrid-4-one **60** (500 mg, 1.5 mmol). To this was added freshly prepared solution of ethyl Meerwein's reagent in $CDCl_3$ (1.5 mL, 1.5 mmol, 1M) at room temperature. The reaction mixture was stirred at room temperature and followed by NMR until the reaction was completed at 2 d. Attempts to purify the material led to decomposition.



^{1}H-NMR: 8.50 (1H, s, H on C6), 4.75 (2H, m, H's on C11), 3.97 (2H, m, H's on C2), 3.40 (2H, m, H's on C3), 2.65 (1H, s, H on C10), 1.47 (3H, t, *J*=6.9 Hz, H's on C12), 1.25 (3H, m, H's on C's 14), 1.01 (18H, m, H's on C's13).

N-Carbopropargyloxy-5-triisopropylsilyl-2,3-dihydropyrid-4-one (60): An oven dried, Argon purged 250 mL round bottom flask was charged with sodium borohydride (532 mg, 13.8 mmol) and dry methanol (50 mL). The flask was then cooled to -78°C. To

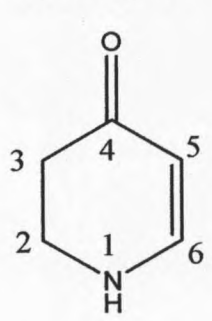
this mixture, a solution of 4-methoxy-3-triisopropylsilylpyridine **56** (2.33 g, 8.8 mmol) in methanol (50 mL) was added dropwise. Carbopropargyloxy chloride (1.22 g, 10.2 mmol) was added dropwise to the cooled reaction mixture. The reaction was then allowed to warm to room temperature overnight. The reaction was quenched by pouring the reaction mixture into a flask containing 10% HCl (aq) (30 mL) that had been cooled to 0°C. The mixture was stirred and allowed to warm to room temperature over 20 min. Ether (100 mL) was then added and the layers separated. The aqueous layer was extracted with ether (4x100 mL) followed by extraction with DCM (5x200 mL). The combined organic extracts were concentrated *in vacuo*. Column chromatography of the crude product with 20% Ether/Hexanes yielded the product as a colorless oil in 75% yield (2.21 g, 6.6 mmol).



^{1}H-NMR: 7.82 (1H, bs, H on C6), 4.83 (2H, d, *J*=2.4 Hz, H's on C8), 4.00 (2H, t, *J*=7.3 Hz, Hs on C2), 2.54 (3H, m, H's on C's 3 & 10), 1.29 (3H, app. pent, *J*=7.5 Hz, H's on C's 11), 1.02 (18H, d, *J*=7.35 Hz, H's on C's 12). ^{13}C-NMR: 196.7 (C4), 152.3 (C7), 148.3 (C6), 112.3 (C5), 76.9 (C9), 75.8 (C10), 54.5 (C8), 42.5 (C2), 36.2 (C3), 18.9

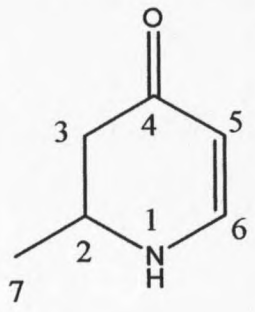
(C11), 11.0 (C12). IR: 3306, 3268, 2861, 2130, 1717, 1661, 1567. GC: Rt=25.8 min. MS: 292 (100). HRMS calculated for $C_{22}H_{33}NO_3Si$ (M-C_3H_7) 292.136848, Found (M-C_3H_7) 292.136897.

2,3-dihydropyrid-4-one (61): An oven dried, Argon purged 100 mL round bottom flask was charged with N-carbobenzyloxy-2,3-dihydropyrid-4-one (1.03 g, 4.4 mmol) and absolute ethanol (85 mL). To this solution 10% Pd/C (130 mg) was added. The flask was then purged with hydrogen gas, and a hydrogen atmosphere was maintained using balloons filled with hydrogen. The reaction was allowed to stir at room temperature for 15 h. After TLC indicated completion of the reaction, the mixture was filtered through Celite and $MgSO_4$. The resulting solution was concentrated *in vacuo*. The resulting oil was purified via column chromatography on silica gel eluting with 2% MeOH/DCM giving the product as a white solid, which was recrystalized from ether in 98 % yield (418 mg, 4.3 mmol), mp 38.9 - 39.4 °C (Lit. mp 38 – 40 °C[40]).



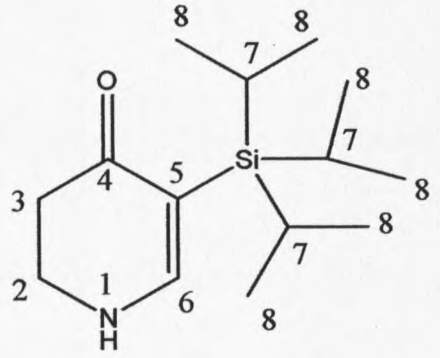
^{1}H-NMR: 7.18 (1H, t, *J*=6.7Hz, H on C6), 5.04 (1H, d, *J*=7.4 Hz, H on C5), 3.58 (2H, t, *J*=7.7 Hz, H's on C2), 2.50 (2H, t, *J*=7.7 Hz, H's on C3), 1.77 (1H, bs, H on N). ^{13}C-NMR: 193.0 (C4), 151.7 (C6), 100.3 (C5), 42.5 (C3), 36.6 (C2). Spectral data are consistent with values reported in the literature.[40]

2,3-dihydro-2-methylpyrid-4-one (62): An oven dried, Argon purged 100 mL round bottom flask was charged with N-carbobenzyloxy-2,3-dihydro-2-methylpyrid-4-one (3.18 g, 1.8 mmol) and absolute ethanol (80 mL). To this solution, 10% Pd/C (130mg) was added in one portion. The flask was then purged with hydrogen gas, and the hydrogen atmosphere was maintained using balloons filled with hydrogen. The reaction was allowed to stir at room temperature for 17 h. After TLC indicated completion of the reaction, the mixture was filtered through Celite and $MgSO_4$. The resulting solution was concentrated *in vacuo*. The resulting oil was purified via column chromatography on silica gel eluting with 2% MeOH/DCM yielding the product as a white solid, recrystallization from ether gave a white solid in 88% yield (1.26 g, 11.4 mmol), with a melting point of 28.5 – 28.9 °C (Lit. mp 28 – 30 °C[39]).



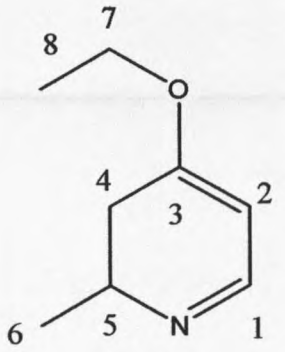
^{1}H-NMR: 7.19 (1H, t, *J*=6.3Hz, H on C6), 5.33 (1H, bs, H on N), 5.05 (1H, d, *J*=6.3 Hz, H on C5), 3.78 (2H, m, H on C2), 2.36 (2H, m, H's on C3), 1.30 (3H, d, *J*=6.5 Hz, H on C7). ^{13}C-NMR: 192.9 (C4), 150.8 (C6), 99.3 (C5), 49.3 (C3), 44.0 (C2), 20.2 (C7). Spectral data are consistent with values reported in the literature.[39]

5-triisopropylsilyl-2,3-dihydropyrid-4-one (63): An oven dried, Argon purged 50 mL round bottom flask was charged with N-carbobenzyloxy-5-triisopropylsilyl-2,3-dihydropyrid-4-one **57** (926 mg, 2.3 mmol) and absolute ethanol (40mL). To this solution, 10% Pd/C (283 mg) was added. The flask was purged with hydrogen gas, and a hydrogen atmosphere was maintained using balloons filled with hydrogen. The reaction stirred at room temperature overnight, at which time TLC indicated completion of the reaction. The mixture was filtered through Celite and $MgSO_4$. The resulting solution was concentrated *in vacuo*. The resulting oil was purified via column chromatography on silica gel eluting with 1% MeOH/DCM giving the product as a white solid, which was recrystallized from hexanes in 98% yield (571 mg, 2.25 mmol), mp 25.4 – 25.7 °C.



^{1}H-NMR: 7.16 (1H, d, *J*=6.1 Hz, H on C6), 5.09 (1H, bs, H on N1), 3.56 (2H, t, *J*=7.3 Hz, H's on C2), 2.48 (2H, t, *J*=7.5 Hz, H's on C3), 1.23 (3H, app. pent, *J*=7.6 Hz, H's on C's 7), 1.07 (18H, d, *J*=7.4 Hz, H's on C's 8). ^{13}C-NMR: 196.1 (C4) 156.4 (C6), 100.5 (C5) 41.8 (C3), 36.9 (C2), 18.9 (C8), 11.2 (C7). IR: 3220, 2942, 2862, 1744, 1606, 1566, 1461, 1312, 1157, 1016, 882. HRMS calculated for $C_{14}H_{28}NOSi$ (M+H) 254.194637, Found (M+H) 254.194018.

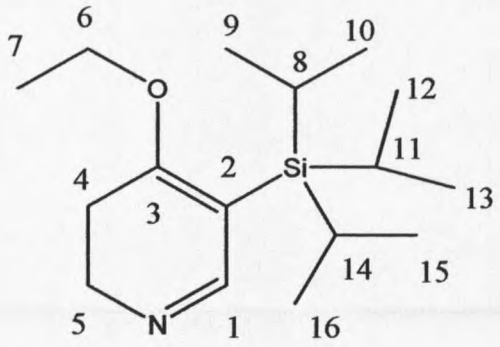
2,3-Dihydro-4-ethoxy-2-methylpyridine (64): An oven dried, Argon purged 25 mL round-bottom flask was charged with 2,3-dihydro-2-methylpyrid-4-one (655 mg, 5.6 mmol), and Na_2HPO_4 (973 mg, 13.9 mmol). To this was added freshly distilled $CDCl_3$ (5 mL). A solution of ethyl Meerwein's reagent in $CDCl_3$ (5.6 mL, 5.6 mmol, 1M) was added at room temperature. The reaction mixture was stirred at room temperature and followed by NMR until the reaction was completed at 2 days. The reaction mixture was then filtered to remove the phosphates and concentrated *in vacuo*. Attempts to further purify the material led to decomposition.



^{1}H-NMR: 8.04 (1H, d, *J*=5.4 Hz, N on C1), 5.63 (1H, d, *J*=5.6 Hz, H on C2), 4.11 (2H, q, *J*=7.1, H's on C7), 2.72 (2H, dd, *J*=18.1, 7.7 Hz, H's on C4), 2.52 (1H, dq, *J*=18.1, 6.3 Hz, H on C5), 1.32 (3H, d, *J*= 6.9 Hz, H's on C6), 1.18 (3H, t, *J*=7.1, H's on C8). ^{13}C-NMR: 179.3 (C3), 165.6 (C1), 92.1 (C2), 66.2 (C7), 48.9 (C5), 34.6 (C4), 15.7 (C6), 14.2 (C8)

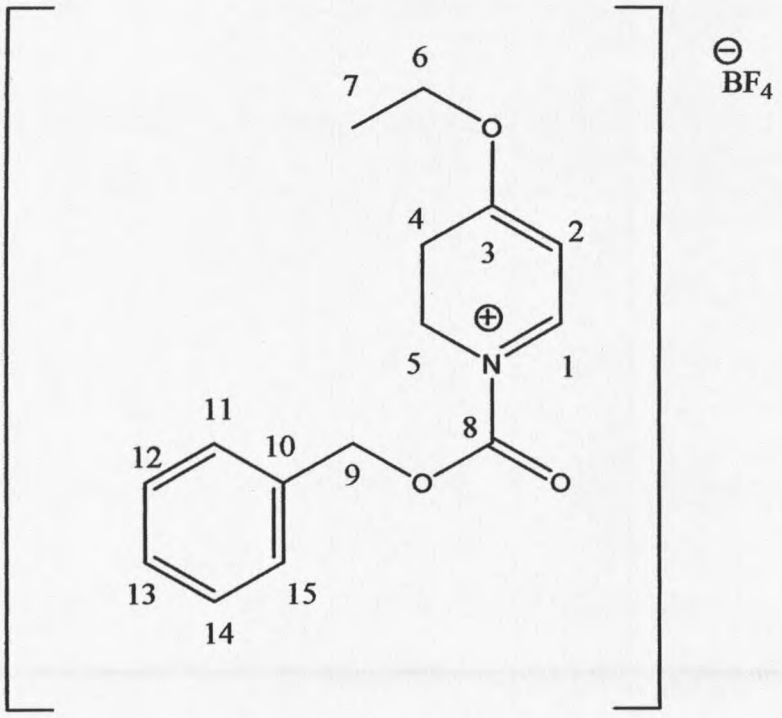
2,3-Dihydro-4-ethoxy-3-triisopropylsilylpyridine (65): An oven dried, Argon purged, 15 mL round-bottom flask was charged with 2,3-dihydropyrid-3-triisopropylsilyl-4-one **63** (303.3 mg, 1.2 mmol), and Na_2HPO_4 (204.4 mg, 1.4 mmol), and DCM (5 mL). A

solution of ethyl Meerwein's reagent in DCM (1.2 mL, 1.2 mmol, 1M) was added in one portion at room temperature. The reaction mixture was stirred at room temperature and followed by NMR until the reaction was completed at 2 days. The reaction mixture was then filtered to remove the phosphates and concentrated *in vacuo*. Attempts to further purify the material led to decomposition.



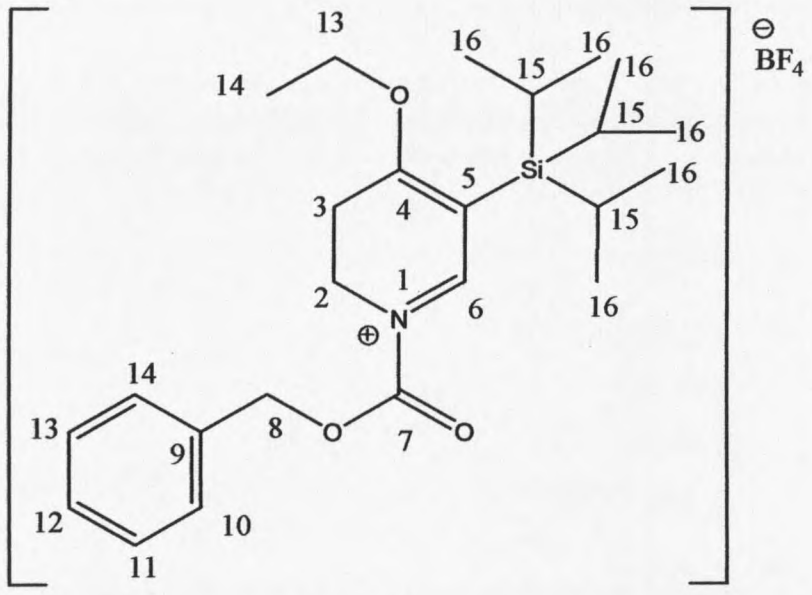
^{1}H-NMR: 7.96 (1H, d, *J*=7.65 Hz, H on C1), 4.32 (2H, q, *J*=7.0, H's on C6), 3.87 (2H, t, *J*=9.1 Hz, H's on C5), 2.95 (2H, t, *J*=9.3 Hz, H's on C4), 1.38 (3H, t, *J*=7.1 Hz, H's on C7), 1.25 (3H, app. septet, *J*=7.45 Hz, H's on C's 8,11,14), 0.99 (18H, d, *J*=7.14 Hz, H's on C's 9, 10, 12, 13, 15, 16). ^{13}C-NMR: 188.6 (C3), 169.1 (C1), 101.2 (C2), 66.1 (C6), 39.8 (C5), 24.2 (C4), 18.8 (C's 8, 11, 14), 15.6 (C7), 11.5 (C's 9, 10, 12, 13, 15, 16).

N-Carbobenzyloxy-2,3-dihydro-4-ethoxypyridinium Tetrafluoroborate (66): An oven dried, Argon purged 5 mL conical vial was charged with N-carbobenzyloxy-2,3-dihydropyrid-4-one **55** (462.9 mg, 2 mmol). To this was added freshly prepared solution of ethyl Meerwein's reagent in $CDCl_3$ (2 mL, 2 mmol, 1M) at room temperature. The reaction mixture was stirred at room temperature and followed by NMR until the reaction was completed at 2 d. Attempts to purify the material led to decomposition.



^{1}H-NMR: 8.86 (1H, d, *J*=6.9 Hz, H on C1), 7.23-7.36 (5H, m, H's on C's11-15), 6.10 (1H, d, *J*=7.0, H on C2), 5.52 (2H, s, H's on C9), 4.49 (2H, q, *J*=7.0 Hz, H's on C6), 4.21 (2H, t, *J*=8.7 Hz, H's on C5), 3.00 (2H, t, *J*=8.6 Hz, H's on C4), 1.42 (3H, t, *J*=7.0 Hz, H's on C7).

N-Carbobenzyloxy-2,3-dihydropyrid-4-ethoxy-5-triisopropylsilyl-pyridinium tetrafluoroborate (67): An oven dried, Argon purged 5 mL conical vial was charged with N-carbobenzyloxy-2,3-dihydro-5-(trisiopropylsilyl)pyrid-4-one **57** (132.1 mg, 0.3 mmol) and DCM (1 mL). To this was added freshly prepared solution of ethyl Meerwein's reagent in DCM (0.3 mL, 0.3 mmol, 1M) at room temperature. The reaction mixture was stirred at room temperature and followed by NMR until the reaction was completed at 2 d. Attempts to purify the material led to decomposition.



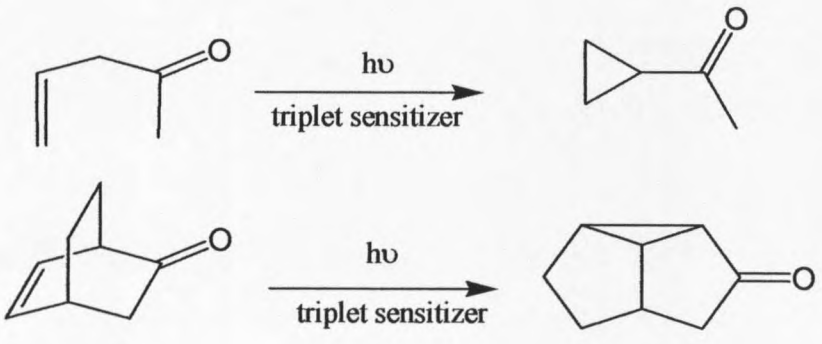
^{1}H-NMR: 8.61 (1H, s, H on C6), 7.35-7.41 (5H, m, H's on C10, 11, 12, 13, 14), 4.36 (2H, m, H's on C13), 4.09 (2H, m, H's on C2), 3.45 (2H, m, H's on C3), 1.53 (3H, t, *J*=7.1 Hz, H's on C14), 1.24 (3H, m, H's on C's 15), 1.06 (18H, d, *J*=7.3 Hz, H's on C's16).

CHAPTER 3

INVESTIGATION OF THE REACTIVITY EFFECTS OF C3 SUBSTITUENTS ON THE OXA-DI-π-METHANE PHOTOISOMERIZATION

Introduction

β,γ-enone photochemistry has been the subject of detailed investigations over the past several decades.[5, 6] The most commonly studied photochemical processes are the 1,3-acyl shift and the oxa-di-π-methane (ODPM) photoisomerizations. ODPM photoisomerization is the triplet sensitized rearrangement of β,γ-unsaturated carbonyl compounds resulting in the 1,2-acyl shift products (Scheme 32).



Scheme 32

The best chemical yields for the ODPM photoisomerization have been observed for systems that are conformationally rigid. Acyclic systems typically have low yields due to their high flexibility, where as [2.2.1]- and [2.2.2]-bridged molecules, which place the olefin and carbonyl groups in close proximity, exhibit higher yields.[5] The lower yields seen for bicyclo[3.2.2]nonenones reflect the "floppy" nature of those systems.[5]

The enhanced reactivity of the rigid bicyclo[2.2.2]octenones as ODPM substrates has been particularly useful to synthetic chemists.[5,6] Thus, the synthetic potential of the ODPM photoisomerization has been used to introduce significant molecular complexity from relatively simple starting materials. Several groups have illustrated this point in elegant syntheses of fused bi- and tricyclic molecules.[6] Modhephene,[7] (-)-Coriolin,[8] and (-)-Silphiperfol-6-en-5-one[9] are examples of synthetically interesting molecules which have been prepared via the ODPM photoisomerization (Figure 8).

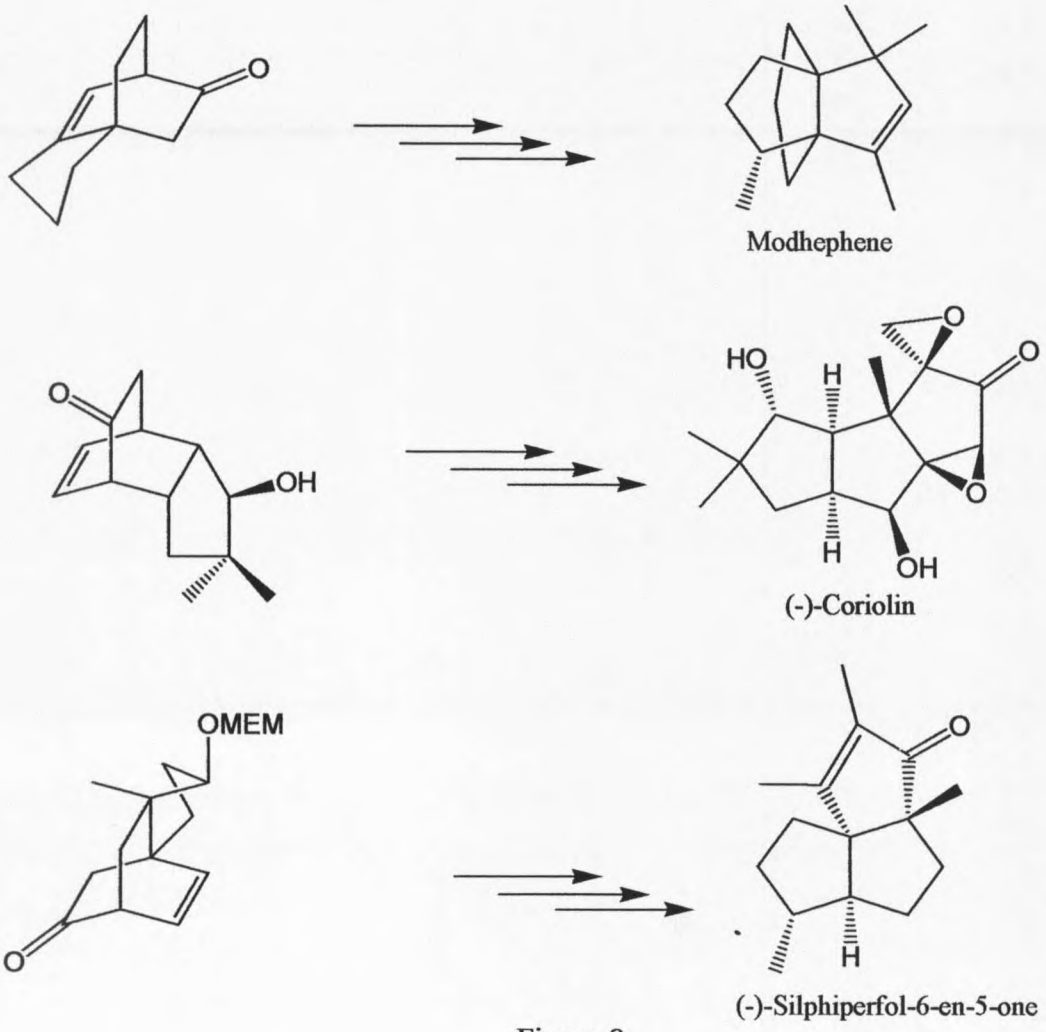
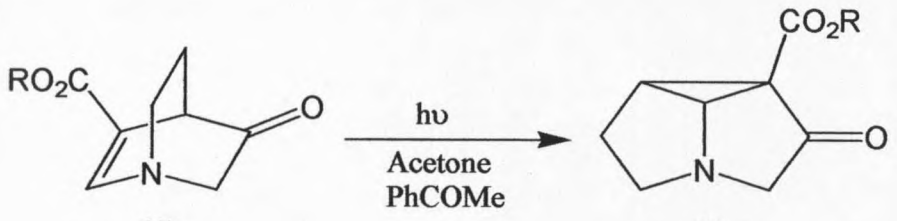


Figure 8

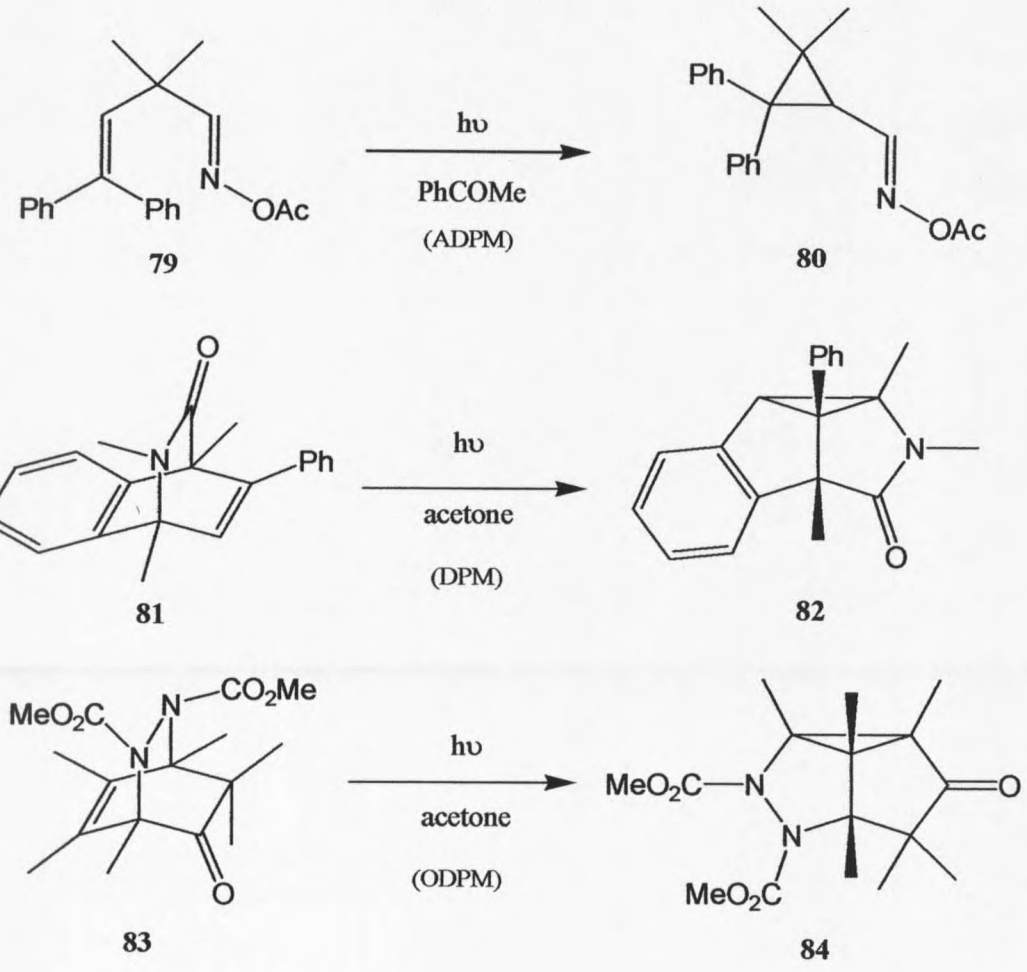
Recently, research by McClure, Kiessling and Link[10,11,12] led to the extension of this methodology to include basic nitrogen containing substrates in the ODPM photoisomerization. They reported the successful transformations of **15a,b** to **32a,b** under triplet sensitized photolytic conditions (Scheme 33). This represents the first occurrence of the ODPM photoisomerization proceeding with a basic nitrogen in the photoprecursor. Previous examples of substrates containing a nitrogen either underwent the related aza-di-π-methane (ADPM) photoisomerization, or the lone pair of electrons on the nitrogen were tied up as amides or carbamates, and the compounds reacted via ODPM or di-π-methane (DPM) rearrangements (Scheme 34).



15 **32**

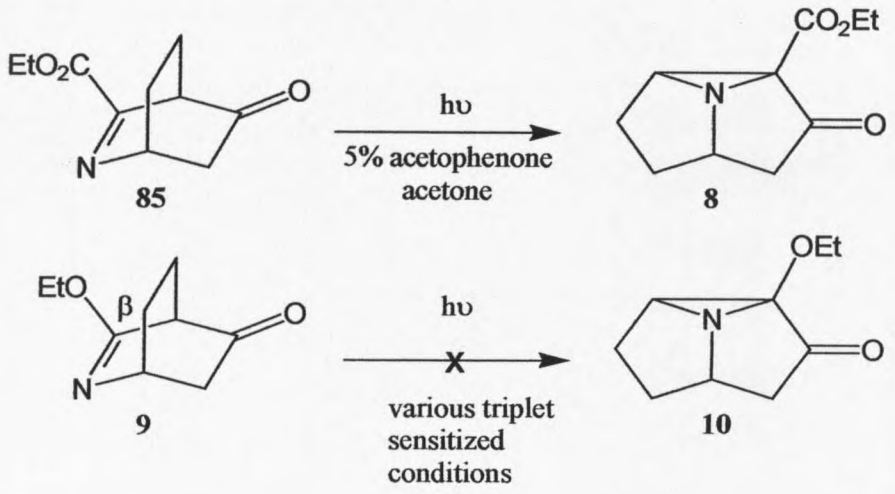
a: R = Me
b: R = Heptyl

Scheme 33



Scheme 34

Further studies by McClure and Link[11] have led to the investigation of the ODPM photoisomerization where the ring nitrogen was involved in the reactive portion of the molecule. Two examples of this work include the C-acyl imine **85** and imidate **9**. Imine **85** reacted as expected, under the standard photolysis conditions used by McClure et al., giving the desired tricyclic photoproduct **8** in 32% overall yield from the starting dienophile (Scheme 35). However, exhaustive photolysis under a variety of conditions failed to provide the photochemical rearrangement product from imidate **9**.



Scheme 35

Noting the unreactivity of imidate **9** led to a thorough search of the literature, yielding only one other example of an ODPM substrate containing an electron donating group at the β-position, 3-methoxybicyclo[2.2.2]oct-2-en-5-one **86**. It was reported that this compound also failed to produce the desired photoproduct upon exposure to photolytic conditions (Figure 9).[11] Aside from this singular example, we have not found any references, synthetic or theoretical, which describe this lack of reactivity, nor its origin. An attempt has been made to construct an empirical model for the prediction of ODPM reactivity, but the model does not hold for several important cases.[5]

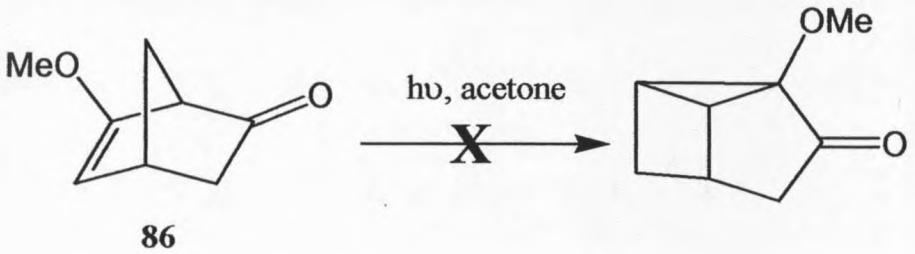
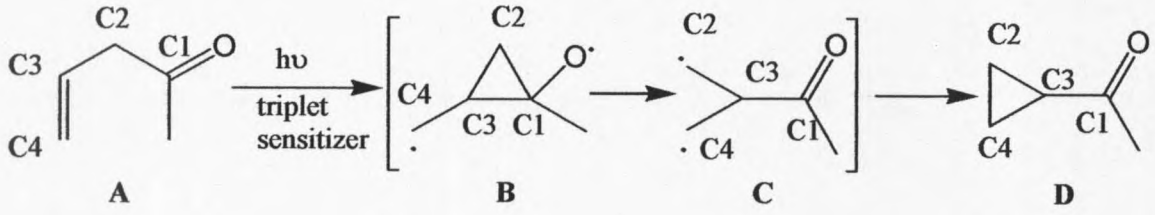


Figure 9

The earliest molecular mechanism for the ODPM photoisomerization[41] indicated that upon triplet sensitization, the substrate undergoes vinyl-carbonyl bridging to give diradical **B**, which subsequently rearranges to diradical **C**. Spin-flip then leads to bond formation to produce ODPM product **D** (Scheme 36). This mechanism has provided the basis for theoretical investigations by Shuster,[42] Houk,[43] Robb,[44] and now here. These previous investigations have been aimed at confirming and refining the proposed mechanism. Our goal was not to confirm the mechanism of the ODPM photoisomerization, but to study the mechanism in enough detail to eventually lead to a predictive model which could be employed by synthetic chemists to assist them in designing ODPM photoprecursors.



Scheme 36

Computational Investigations of
the Oxa-Di-π-Methane Mechanism

The mechanism of the ODPM photoisomerization has been previously studied by various theoretical methods.[42-44] The earliest example is a semi-emperical INDO-MO investigation by Schuster.[42] For this study, the lowest triplet state of 3-butene leading to ODPM photoisomerization was implicitly assumed to be n $\rightarrow$ π^* of the carbonyl (hereafter refered to as n $\rightarrow$ π_{co}^*). The reactivity of the n $\rightarrow$ π_{co}^* triplet state of 3-butenal

was proposed to be due to spin polarization of the olefinic region by the excited state carbonyl via the bridging methylene group. This spin polarization was proposed to lead to electron pairing between the π_{co}* electron and a spin of opposite sign on the olefin at the β-carbon. Closely following this report in a paper by Houk,[43] an alternative explanation was proposed based on the mixing of non-bonded electrons on the oxygen (n), the π orbital on the olefin (π_{cc}), the π* orbital on the olefin (π^*_{cc}) and the π* orbital on the carbonyl (π^*_{co}) orbitals using a more accurate semi-empirical method, CNDO/S, on trans-4-hexen-2-one (Figure 10). From these calculations, the ODPM photoisomerization reactivity was described by the computational observation that the π_{cc}* orbital indicated a C1-C3 bonding interaction. Houk, on the basis of the molecular orbitals, supported the vinyl-carbonyl bridging interaction of the proposed mechanism of the ODPM (Scheme 36). However, neither of these studies went beyond the starting material's vertical excitation (VE) to the triplet state.

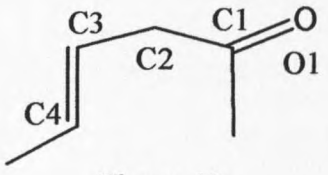


Figure 10

The most recent and more complete theoretical investigation of the ODPM mechanism was reported by Robb[44] and co-workers in 1996. This was the first study which explored the reaction beyond the initial excitation, and gave a global picture of the potential energy surface. This study used Complete Active Space – Self Consistent Field (CAS-SCF) method to locate key intermediates and transition states (Figure 13). These

intermediates and transition states were connected by qualitatively drawn triplet and singlet surfaces. The simplest "model" ODPM substrate, 3-butenal **87**, was used in their calculations. The initial step of the mechanism discussed in Robb's study was consistent with those previously suggested,[43] with the addition of the geometrically relaxed intermediate 1 (I1) from the initial vertical excitation (VE). Two triplet surfaces, the T_1 ($\pi_{cc} \rightarrow \pi_{cc}^*$ of the olefin, red line in Figure 13) and T_2 ($n \rightarrow \pi_{co}^*$) of the carbonyl, green line in Figure 11) excitations, were explored by calculating the structures of intermediates and transition states corresponding to I1, transition state 1 (TS1), intermediate 2 (I2), transition state 2 (TS2), and intermediate 3 (I3). The first excited singlet (S_1) surface ($n \rightarrow \pi_{co}^*$ blue line Figure 11) was generated in the same fashion. Since Robb did not calculate an intermediate specie preceeding TS2 on the S_1 surface, this point on the surfaces appears not to be a true transition state; however, Robb indicated it as a transition state and qualitatively drew a minimum nearby.[44]

The potential energy surfaces drawn based on the relative energies of these structures showed that the two triplets at I2 indicated that the ODPM process could be accessed from both triplet surfaces. Robb[44] suggested, based on the conical intersection at I2, that the reaction continued on the singlet surface S_1 at I2 toward I3 where the S_1 surface crossed the ground state closed shell singlet (S_0) surface leading to product (P) (Figure 11). Robb concluded that the surface and conical intersections were "well represented at the MC-SCF/6-31G* level", but that "computed barrier heights will be sensitive to the treatment of dynamic electron correlation".[44] Most importantly, he speculated that substituent effects would be observed in computed barrier heights.

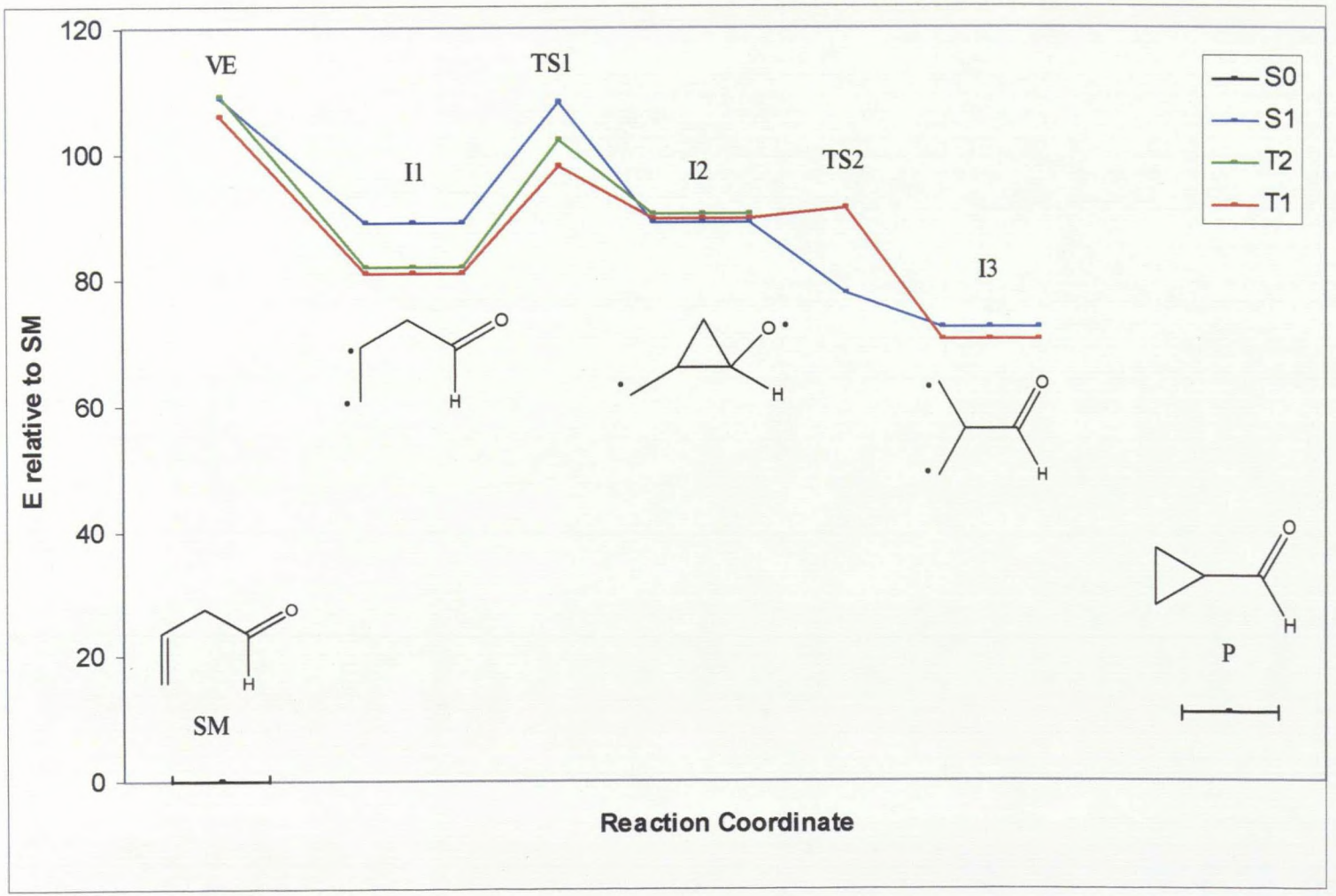

120
100
80
60
40
20
0
E relative to SM
VE
TS1
I1
I2
TS2
I3
S0
S1
T2
T1
SM
P
Reaction Coordinate

Figure 11

Project Aim

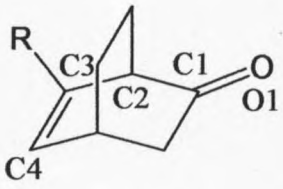
The aim of this project was to deduce the origin of the reactivity differences that have been noted, and to attempt to provide a quantitative description of the β-substituent (C3) effects. In order to achieve this goal, key molecular descriptors, such as atomic charges, bond orders, geometric parameters, etc., that account for the observed experimental reactivities needed to be identified. These descriptors could then be employed in a simple model to be used by experimental organic chemists without a deep knowledge of sophisticated theoretical methods, such as multireference CAS-SCF calculations, to predict the ODPM reactivity of photoprecursors possessing various substituents at the C3 position.

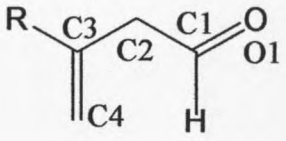
Computational Methods

The Density Functional Theory (DFT)[45] is one of the most popular computational methods, and was employed to perform the calculations described herein. DFT is a superior method to another well known *ab initio* method, Hartree-Fock (HF),[46] by its more complete treatment of electron-electron correlation interactions. The method is based on the Kohn-Sham equation, which operates on electron density, and divides the total energy operator into four terms: kinetic, potential, coulombic and exchange/correlation functionals.[47] This method is particularly attractive since it involves a significant amount of electron correlation in addition to the exchange interactions in the form of an appropriate exchange correlation functional, whereas the HF methods require additional post-SCF methods to take into account electron correlation.[48] Another benefit of DFT method is that it typically scales better, roughly as

the cube of the number of electrons (~N^3), than comparable correlated post-HF methods (N^4-N^7).[49] For the calculations presented here, the B3LYP set of functionals were used.[50] This functional (Becke 3-parameter exchange and Lee-Yang-Parr correlation) was chosen because it was empirically corrected for use in calculations on small organic molecules.

The calculations described herein involved acyclic and bicyclic molecules, that is, appropriately substituted bicyclo[2.2.2]octenones **88** - **91** and the 3-butenals **87**, **92** - **94** (Figure 14). These were selected based on their similarity to known ODPM substrates,[5] as well as their simplicity for the purpose of allowing for detailed potential energy surface studies at a reasonable computational cost. The two molecule sets were labeled as shown in Figure 12.





88 R=H
89 R=Me
90 R=OMe
91 R=COOMe

87 R=H
92 R=Me
93 R=OMe
94 R=COOMe

Figure 12

Ground and excited state calculations were performed by single point SCF energy calculations with and without altering the occupation of molecular orbitals. The vertical excitation (VE) energies were calculated by energy differences (ΔSCF)[51] of ground and excited states. In addition, time-dependant DFT (TD-DFT)[52] calculations were also carried out which are based on the SCF solution of a time-dependant perturbation of the

ground state electron density. This approach can provide reasonable excitation energies for the lower lying excited states.[52]

Geometry optimizations and relaxed potential energy surface scans were performed to locate the intermediates, transition states and the connecting pathways. Stationary points were confirmed by frequency calculations to be true equilibrium geometries as they must not have any imaginary components of the normal mode vibrational frequencies.

The two methods employed to compute atomic charges and atomic spin densities were Mulliken[53] and natural population analysis (NPA)[54]. The major difference between these computational methods is the way the electron density is divided up among the nuclear centers. Mulliken population analysis equally distributes the electron density, while Weinhold's NPA method uses a set of core, valence and Rydberg natural orbitals to fit the electron density. NPA was selected for this study because it tends to be more sensitive to subtle electronic effects and provide chemically more reasonable charge distributions. Mulliken atomic spin densitites were used to uniquely assign the electronic states based on the localization of spin densities.

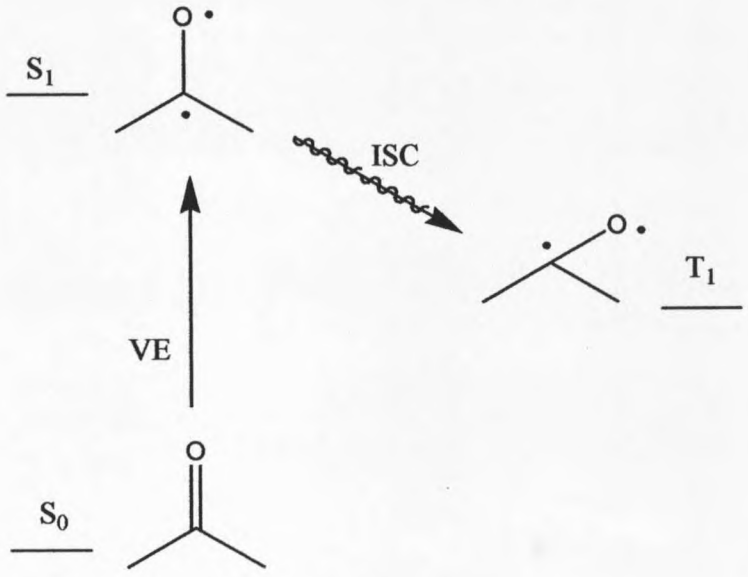
Calculations were performed using the Gaussian 98[55] and Spartan'02[56] computational packages. Three basis sets were employed in this study: 6-31G* (called hereafter BS1), 6-311G* (called hereafter BS2), and 6-311++G** (called hereafter BS3).[57] The hardware used for this study consisted of single processor 2.4 GHz Dell desktops used alone or parallelized in clusters of 3, 6, and 10 processors. Unless

otherwise noted all units are reported as follows: energy in kcal/mol, distances in Angstroms, and angles in degrees.

Results and Discussion

Calibration of B3LYP/BS3 Level of Theory Using Acetone

The ODPM photoisomerization is a triplet sensitized rearrangement which involves a sensitizer molecule that absorbs the direct irradiation, followed by intersystem crossing to its triplet state without any further reaction until it transfers the triplet energy to the acceptor molecule of interest (Scheme 37). The most common triplet sensitizer used in the ODPM photoisomerization is acetone, which is often used as the solvent as well.[58] The frequent application of acetone is due to its short singlet lifetime (10^{-9} sec), long lived triplet state (10^{-5} sec), and its quantum yield of intersystem crossing (ISC) of 1.0.[58]



Scheme 37

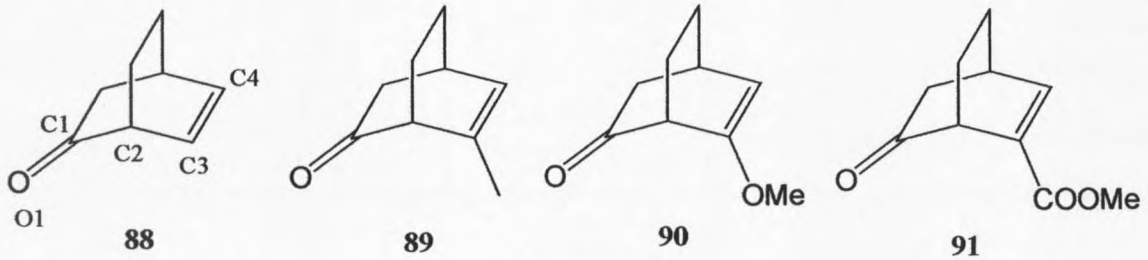
As a means of calibrating the computational method for our study the ground state, VE and geometrically relaxed first triplet state were calculated for acetone using B3LYP/BS3 and compared to available experimental spectroscopic data. These DFT calculations gave a relaxed triplet state energy of 76 kcal/mol, which is close to the reported experimental value of 78 kcal/mol.[58] To further refine the triplet energy of acetone, solution phase calculations were also performed and gave a triplet energy of 77 kcal/mol, which further supports the good agreement. These results indicated that this combination of method and basis set should be sufficient for the calculations to be used in this ODPM photoisomerization study. In addition, the anticipated solvent effects are small, and therefore gas-phase calculations should already provide reasonable energies.

Examination of VE Energies

In a general physical organic picture, the VE of ODPM photoisomerization substrates may be affected by the electronic character of the C3-substituent. Cases with strong electron donating groups at the C3 position would not be sensitized to the reactive triplet state since the strong electron donation should lower the HOMO energy of the ground state and therefore increase the VE energy. Therefore, these groups should not give product upon exposure to photolytic conditions. To investigate this hypothesis, four molecules were selected to probe the C3-substitent effect: **88** – **91** (Figure 13). The four different C3-substituents convey different electronic interactions with the olefin. The methyl ester acts as a resonance withdrawing group, the hydrogen is essentially a very mild inductively active electron donor, the methyl substituent acts as a mild electron

donating group via hyperconjugation, and the methyl ether acts as a strong electron donor via resonance.

Geometries for the four molecules were optimized as singlet ground states (Figure 13). The singlet ground state geometries had olefin and carbonyl bond lengths typical for these systems (Table 5). Single point energy (SPE) calculations were performed on the singlet geometries in the triplet state to calculate the VE values via ΔSCF.



88 **89** **90** **91**

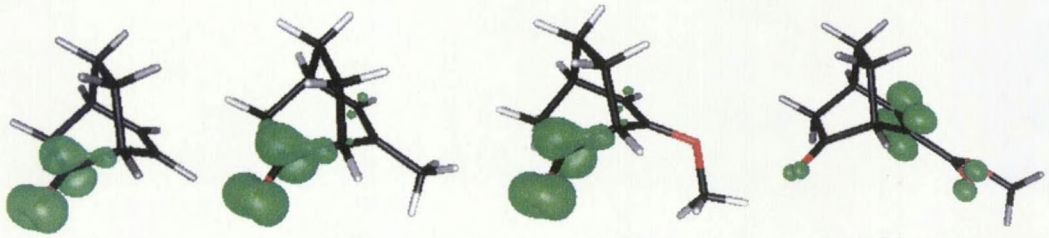
Figure 13

C3 R-group	O1-C1 (Å)	C1-C2 (Å)	C1-C3 (Å)	C2-C3 (Å)	C2-C4 (Å)	C3-C4 (Å)	C3-R (Å)
H	1.21	1.53	2.44	1.51	2.40	1.34	1.08
Me	1.21	1.53	2.45	1.52	2.39	1.34	1.50
OMe	1.21	1.53	2.44	1.52	2.41	1.34	1.37
CO_2Me	1.21	1.53	2.45	1.51	2.41	1.34	1.48

Table 5

Spin density plots for the triplet state indicated, surprisingly, an $n \rightarrow \pi_{co}^*$ excitation for three of the four cases. The ester substituent was the only case where the VE was $\pi_{cc} \rightarrow \pi_{cc}^*$. Plots of the atomic spin densities, clearly indicating the nature of the excited state, are shown in Figure 14. TD-DFT calculations also supported the $n \rightarrow \pi_{co}^*$ excitation for all cases except the ester. VE energies were also calculated taking

solvation interactions into account, and its effect on these VE energies was negligible, as was observed in the acetone case. These calculations indicated that no correlation existed between VE and the electronic character of the C3-substituent for compounds **88 - 91** (Table 6). The lack of any correlation was not too unexpected for the three cases where the excitation was $n \rightarrow \pi_{co}^*$ on the C=O bond, as the C3-substituents were two σ bonds away from the location of the excitation. However, the VE for **91** with the ester C3 substituent varied some from the other three cases due to its $\pi \rightarrow \pi^*$ VE.



88 **89** **90** **91**

Figure 14

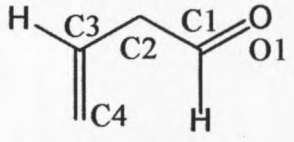
Molecule	C3 R-Group	VE(Δ-SCF) (kcal/mol)	VE(Δ-SCF) w/solvation (kcal.mol)	TD-DFT (kcal/mol)
88	**H**	84.7	85.3	82.7
89	**Me**	84.6	85.0	82.5
90	**OMe**	85.1	85.6	82.9
91	**CO_2Me**	81.9	81.4	75.3

Table 6

From the atomic spin densities (Figure 14) it was apparent that the calculated triplet states for three cases (**88 – 91**) was that of an $n \rightarrow \pi^*$ excitation. These results seem to contradict what has been found in the literature[43,44] as the previous studies were based on $\pi \rightarrow \pi^*$ excitation of the olefin leading to ODPM products. To assure that the $n \rightarrow \pi^*$ excitation was not an artifact of the DFT method used here, other theoretical methods were also considered. To evaluate other theoretical methods for this study, a calibration scheme was constructed based on 3-butenal, as was used in Robb's calculations. This scheme focused on the nature of the VE based on spin densities. A theoretically converging series of theoretical methods, such as Hartree-Fock (HF),[46] Moller-Plessett[59] second order correlation (MP2), MP3, MP4, and quadratic configuration interaction of singles and doubles (QCISD)[60] were selected and compared to B3LYP[50] using BS1. Ground state geometries were optimized, starting from the bond lengths and angles from Robb's paper, for HF and MP2 methods. MP3, MP4, and QCISD calculations used the geometry obtained from the MP2 optimization. VE energies were calculated similarly to the bicyclic cases via the ΔSCF procedure (Table 7). Moller-Plesset (MP) methods showed that the nature of the excitation could not be assigned unambiguously. The spins were located on the oxygen and carbons 1, 3 and 4. It was not until the QCISD method, which was the highest in the above series, was applied that the atomic spin densities clearly indicated the nature of the lowest lying triplet state as $n \rightarrow \pi_{co}^*$ (Table 7, column 1).

The spin densities obtained from QCISD calculations, as the highest level of theory explored, agreed with the B3LYP $n \rightarrow \pi_{co}^*$ assignment for the first triplet excited

state. Therefore, the n $\rightarrow$ π_{co}* may well be the lowest triplet state for certain β,γ-unsaturated carbonyl compounds. For additional confirmation, the initial orbital occupations, shown in Table 7 (column 2), were altered to choose the π_{cc} $\rightarrow$ π_{cc}* excitation of 3-butenal **87** (Figure 15). The results (Table 7, column 2) indicated that at all levels of theories, the π_{cc} $\rightarrow$ π_{cc}* excitation of the olefin was significantly higher in energy than that of the optimized wavefunctions starting from n $\rightarrow$ π_{co}* excitations. It should be noted here that even starting from the initial π_{cc}* $\rightarrow$$\pi_{cc}$ excited wavefunction in B3LYP led to the n $\rightarrow$ π_{co}* triplet state. These calculations were repeated with a larger basis set BS2 to determine if the results showed any basis set dependence (Table 7, columns 3 & 4). Columns 3 and 4 compared to columns 1 and 2 (Table 7), respectively, show that the larger basis set had little or no effect on the observed spin densities. With this calibration in hand it could be concluded that 6-311++G** (BS3) already represents a theoretically converged basis and the use of a larger basis would not improve the computational results.



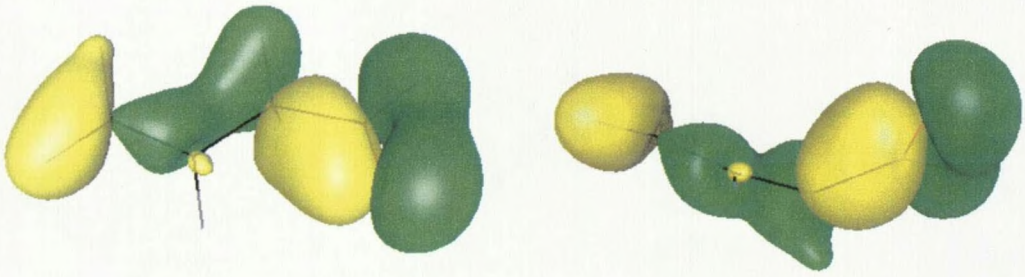
84

Figure 15

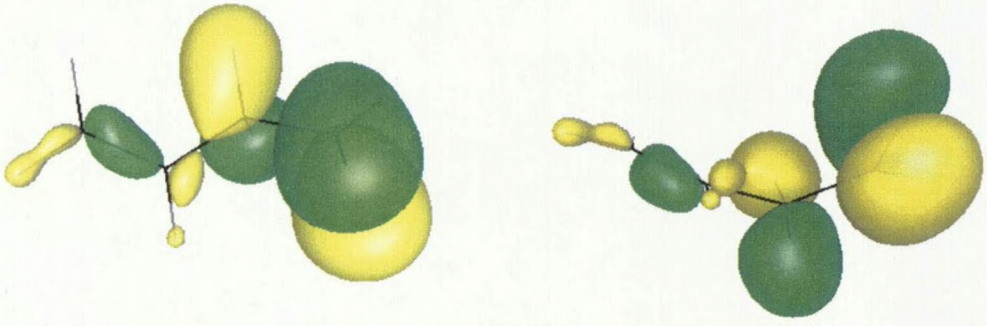
		Initial Wavefunctions			
		$n \rightarrow \pi^*$	$\pi \rightarrow \pi^*$	$n \rightarrow \pi^*$	$\pi \rightarrow \pi^*$
		1	2	3	4
Method		Δ-SCF/BS1	Δ-SCF/BS1	Δ-SCF/BS2	Δ-SCF/BS2
HF	**E_{rel} (kcal/mol)**	**73**	**83**	**72**	**83**
Spin Densities	O1	1.1	0.0	1.1	-0.2
	C1	0.9	0.1	0.8	0.1
	C3	-0.2	1.2	-0.1	1.2
	C4	0.2	1.2	0.2	1.2
MP2	**E_{rel} (kcal/mol)**	**102**	**106**	**100**	**106**
Spin Densities	O1	1.0	0.2	1.1	0.2
	C1	0.8	-0.1	0.8	-0.1
	C3	1.5	1.1	1.7	1.1
	C4	-1.5	1.2	-1.7	1.2
MP3	**E_{rel} (kcal/mol)**	**92**	**102**	**89**	**102**
Spin Densities	O1	1.1	0.1	1.1	0.1
	C1	0.8	-0.1	0.8	-0.1
	C3	1.2	1.1	1.3	1.1
	C4	-1.2	1.2	-1.3	1.2
MP4	**E_{rel} (kcal/mol)**	**93**	**102**	**89**	**102**
Spin Densities	O1	1.0	0.1	1.1	0.1
	C1	0.8	-0.1	0.8	-0.1
	C3	1.0	1.1	1.0	1.1
	C4	-0.9	1.1	-1.0	1.2
QCISD	**E_{rel} (kcal/mol)**	**89**	**101**	**87**	**101**
Spin Densities	O1	1.0	0.0	1.0	0.0
	C1	0.8	0.0	0.8	0.0
	C3	0.0	1.1	0.0	1.1
	C4	0.0	1.1	0.0	1.2
B3LYP	**E_{rel} (kcal/mol)**	**85**	**85**	**85**	**85**
Spin Densities	O1	0.9	0.9	0.9	0.9
	C1	0.7	0.7	0.7	0.7
	C3	0.0	0.0	0.0	0.0
	C4	0.1	0.1	0.1	0.1

Table 7

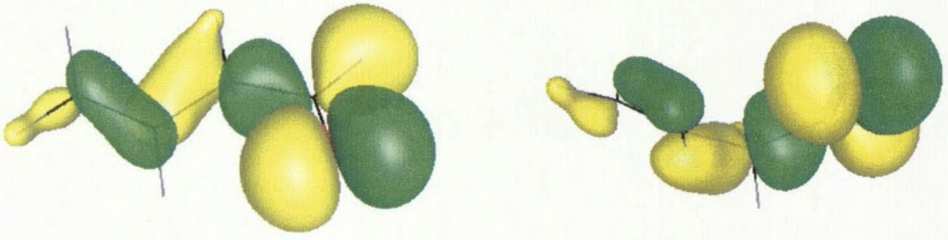
Naturally, reproduction of the results published by Robb[44] were attempted. The aim of these calculations was to directly compare the published results on the unsubstituted case with those bearing a C3-substituent. To accomplish this, the initial geometry for 3-butenal **87** was generated from the bond lengths and angles reported by Robb. The structure was fully optimized at HF/6-31G*, and frequency calculation showed no imaginary frequencies. The seven active space orbitals selected by Robb were the n orbital on the oxygen, the π and π^* orbitals on the carbonyl and olefin, and σ and σ^* orbitals on the α-carbon. The active space orbitals used here were selected to be as close as possible to those described in Robb's calculations (occupied MOs Figure 16, unoccupied MOs Figure 17). The CAS-SCF calculations were carried out using the HF optimized singlet ground state geometry. The ground state singlet (Root=1) was calculated and the energy (-229.89138 a.u.) was 7.4 kcal/mol lower than the the CAS optimized geometry reported by Robb (-229.8802a.u.). The first excited singlet state (Root=2) was calculated (-229.70121 a.u.) to be 3.5 kcal/mol higher in energy than that reported by Robb (-229.7067 a.u.). The lowest triplet state (Root=1) was calculated (-229.72307 a.u.) and found to be 7.3 kcal/mol lower in energy than that reported by Robb (-229.7114 a.u.). The excited state triplet (Root=2) could not be obtained due to convergence issues in both state-specific and state-averaged calculations. These issues with reproducing published results discouraged us from continuing with multireference methods, which could easily overgrow the original aim of this investigation.



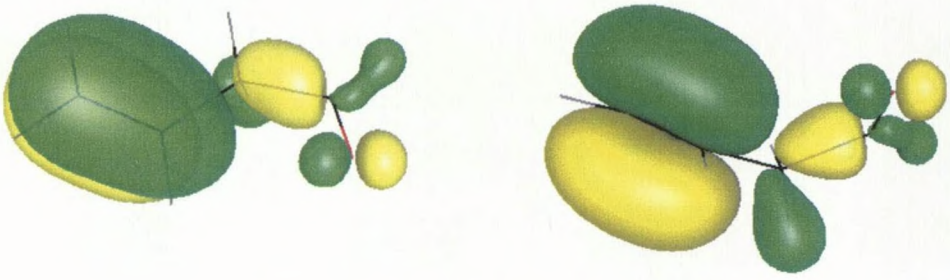
MO 11 C_{α}-C_{CO}



MO 16 π_{CO}

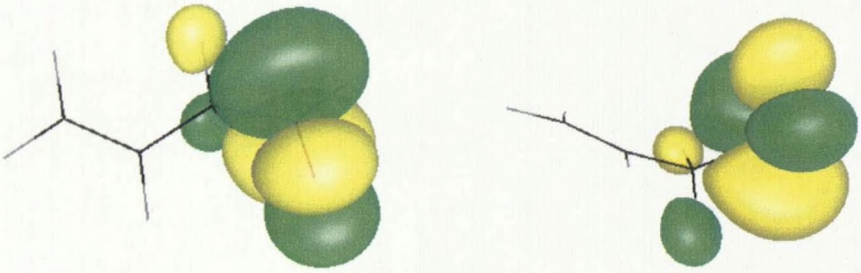


MO 18 n_O

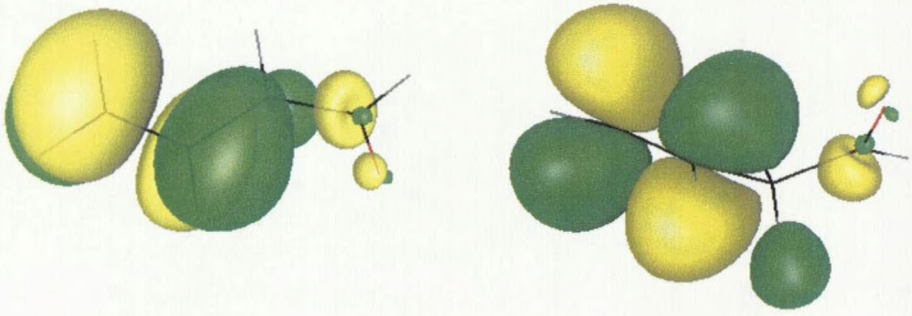


MO 19 π_{CC}

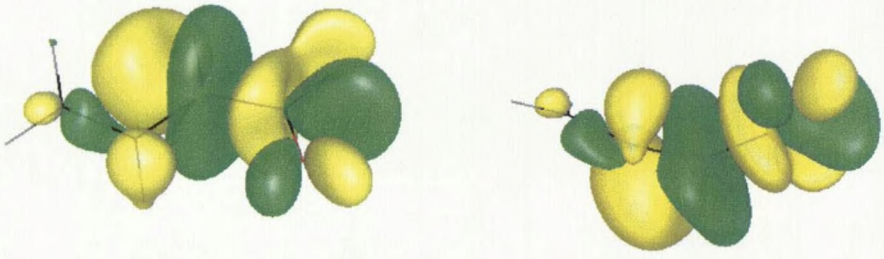
Figure 16



MO 20 π_{CO}*



MO 21 π_{CC}*

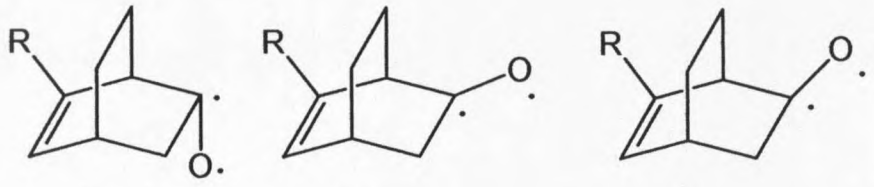


MO 29 $\sigma_{C\alpha\text{-}Cco}$*

Figure 17

To further investigate the n $\rightarrow\pi_{co}$* excitation, we calculated optimized geometries for the triplet excited state for all 4 bicyclic systems **88 - 91** (Figure 18). Intermediate 1 (I1) equilibrium triplet geometries were found and the energies were compared with respect to the C3-substituent in Table 10. These optimizations gave structures where the carbonyl group was bent indicating that the hybridization of the carbonyl carbon had changed due to excitation localized on the carbonyl. Two isomers for this intermediate

were found, exo and endo, with respect to the orientation of the carbonyl oxygen to the ring system. Based on the geometric requirements of the reaction, the exo isomer should be the reactive isomer and lead to product formation, where as the endo isomer would eventually recombine back to the ground state. It was assumed that the methoxy C3-substituent might affect the relative energies favoring the endo isomer and therefore act as a sink to hinder its reactivity. To investigate this, both exo (Table 8) and endo (Table 9) structures for all four bicyclic systems **88 - 91** were optimized, as well as the transition state (TS0) that connected the two isomers. The exo and endo isomers were found to be nearly degenerate with a small barrier (TS0) between them (Table 10), therefore it was concluded that the C3 substituent does not have any influence on the relative energies of the I1 intermediates.



I1endo TS0 I1exo

Figure 18

C3 R-group	O1-C1 (Å)	C1-C2 (Å)	C1-C3 (Å)	C2-C3 (Å)	C2-C4 (Å)	C3-C4 (Å)	C3-R (Å)
H	1.29	1.59	2.46	1.50	2.39	1.34	1.08
Me	1.29	1.59	2.46	1.50	2.38	1.34	1.50
OMe	1.29	1.60	2.45	1.49	2.39	1.35	1.36
CO_2Me	1.29	1.58	2.46	1.50	2.39	1.34	1.48

Table 8

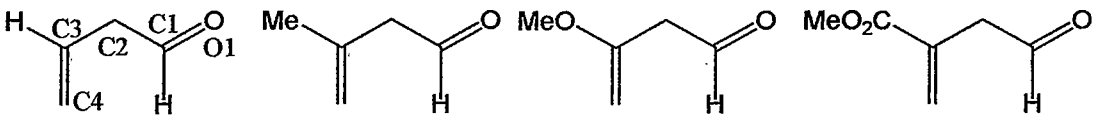
C3 R-group	O1-C1 (Å)	C1-C2 (Å)	C1-C3 (Å)	C2-C3 (Å)	C2-C4 (Å)	C3-C4 (Å)	C3-R (Å)
H	1.29	1.60	2.50	1.50	2.39	1.34	1.08
Me	1.29	1.60	2.50	1.50	2.38	1.35	1.50
OMe	1.28	1.61	2.49	1.49	2.40	1.36	1.36
CO_2Me	1.29	1.59	2.49	1.50	2.40	1.35	1.48

Table 9

Molecule	C3 R-group	$I1_{co}$ (endo) (kcal/mol)	TS0 (kcal/mol)	$I1_{co}$ (exo) (kcal/mol)
88	**H**	74.0	78.6	74.7
89	**Me**	73.8	78.4	74.4
90	**OMe**	73.0	77.3	73.7
91	**CO_2Me**	73.7	78.3	74.5

Table 10

In order to be able to map the potential energy surface of the reaction, and stay within reasonable computational cost, it was decided to switch from the bicyclo[2.2.2]octenones to the simpler acyclic 3-butenal series with substituents placed at the 3-position (Figure 19 & Table 11). For the purpose of completeness, the VE energies were calculated by both ΔSCF and TD-DFT methods for the four acyclic cases, and again no correlation was observed with respect to the C3 substituent (Table 12). Both VE methods indicated n $\rightarrow$ π_{co}* assignments for all but the ester case, similarly to the bicyclic cases. $I1_{co}$ geometries were also calculated for each of the four molecules (Figure 20 & Table 13). These acyclic $I1_{co}$ structures, like the bicyclic structures previously mentioned, have similar energies and no correlation to reactivity could be drawn.



87 **92** **93** **94**

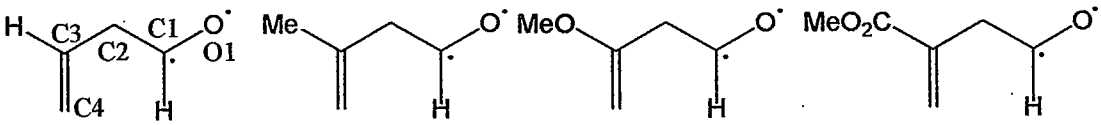
Figure 19: Starting Material Ground State (S_o) Structures

R-group	O1-C1 (Å)	C1-C2 (Å)	C1-C3 (Å)	C2-C3 (Å)	C2-C4 (Å)	C3-C4 (Å)	C3-R (Å)
H	1.20	1.52	2.51	1.51	2.51	1.33	1.09
Me	1.21	1.52	2.52	1.52	2.48	1.33	1.51
OMe	1.21	1.52	2.52	1.51	2.51	1.33	1.38
CO_2Me	1.21	1.52	2.52	1.51	2.50	1.34	1.49

Table 11

R-group	VE(D-SCF) (kcal/mol)	VE(TD-DFT) (kcal/mol)	$I1_{co}$ (kcal/mol)
H	83.2	82.0	72.8
Me	82.7	81.4	71.9
OMe	82.6	80.3	71.1
CO_2Me	82.4	76.6	74.7

Table 12



87 **92** **93** **94**

Figure 20: Intermediate 1_{co} ($I1_{co}$) Structures

R-group	O1-C1 (Å)	C1-C2 (Å)	C1-C3 (Å)	C2-C3 (Å)	C2-C4 (Å)	C3-C4 (Å)	C3-R (Å)
H	1.30	1.55	2.51	1.50	2.50	1.33	1.09
Me	1.30	1.55	2.51	1.50	2.47	1.34	1.50
OMe	1.30	1.56	2.57	1.50	2.49	1.34	1.36
CO_2Me	1.30	1.54	2.51	1.50	2.50	1.34	1.50

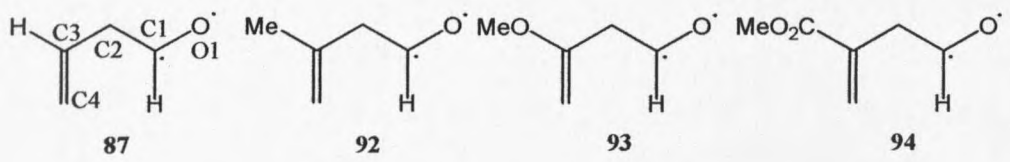
Table 13

In summary, on the basis of the B3LYP calculations the C3-substituent does not appear to affect the VE energies or corresponding I1 energies. The first triplet state appeared to be n $\rightarrow$ π_{co}* for all cases except the ester, which was $\pi_{cc} \rightarrow \pi_{cc}$*. The observed difference in the nature of the VE in the ester case may be due to the electronic effect of the ester to effectively lower the π^*_{cc} orbital making the $\pi_{cc} \rightarrow \pi_{cc}$* transition lower in energy with respect to the n $\rightarrow$ π^*_{co} excitation. Calculations indicated that the excitation will occur for all substrates regardless of the electronic nature of the C3-substituent. This can be easily rationalized, since the excitation is localized away from the olefin in all cases except the ester.

Examination of I1 to I2 Barrier Heights

Robb[44] speculated that the experimentally observed selectivity must be due to the barrier height variation. We therefore studied whether the barrier between $I1_{co}$ and I2 (TS1) would be affected by the C3 substituent since this part of the mechanism involves the formation of a bond between C3 and C1. The anticipated result from these calculations was that the relative height of TS1 would be greatest for the methoxy substituent and lower for the other substituents. To probe this, several attempts were made to calculate geometries for the first transition state (TS1) starting from various initial structures having the correct imaginary frequency for the C1-C3 bond formation without any success. These attempts gave stationary points corresponding to either I1 or I2 geometries. This difficulty can be attributed to the observed flat potential energy surfaces and the small activation barrier. An alternate solution was devised whereby the surface was mapped by performing relaxed potential energy surface (PES) scans at set

intervals along the reaction coordinate. The reaction coordinate was driven to give an approximate potential energy function connecting $I1_{co}$ and I2 by constraining the C1-C3 distance from 2.5 Å to 1.4 Å. Results of this scanning are shown in Figure 23. Starting from $I1_{co}$, the surface energy gradually increased as expected until the C1-C3 distance reached 2.3 Å to 2.1 Å, depending on the substituent. The $I1_{co}$ surface (Figure 23, T2: dotted lines) then collapsed to the $I1_{cc}$ triplet surface (Figure 23, T1: solid lines). This collapse was due to the localization of spin density distributions of $I1_{co}$ (Table 14) on O1 and C4 as the surfaces approached I2, and importantly varied with the C3-substituent (Figure 21). At shorter C1-C3 distances, proper electronic structures corresponding to the $I1_{co}$ were located, however all optimizations led to the $I1_{cc}$ surface. At similar C1-C3 distances the $I1_{cc}$ (Table 15) surface has the spin densities mostly localized on the olefin.

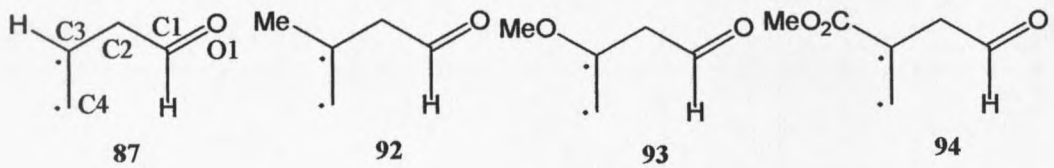


87 **92** **93** **94**

Figure 21: Intermediate 1_{co} ($I1_{co}$) structures

R-Group	O1	C1	C3	C4
H	0.8	0.5	0.0	0.6
Me	0.8	0.6	-0.1	0.7
OMe	0.8	0.7	0.0	0.4
CO_2Me	0.9	0.6	0.0	0.4

Table 14



87 **92** **93** **94**

Figure 22: Intermediate 1_{cc} ($I1_{cc}$) structures

R-Group	O1	C1	C3	C4
H	0.2	0.0	0.7	1.1
Me	0.2	0.5	0.8	0.9
OMe	0.2	0.5	0.7	0.8
CO_2Me	0.2	0.4	0.7	0.9

Table 15

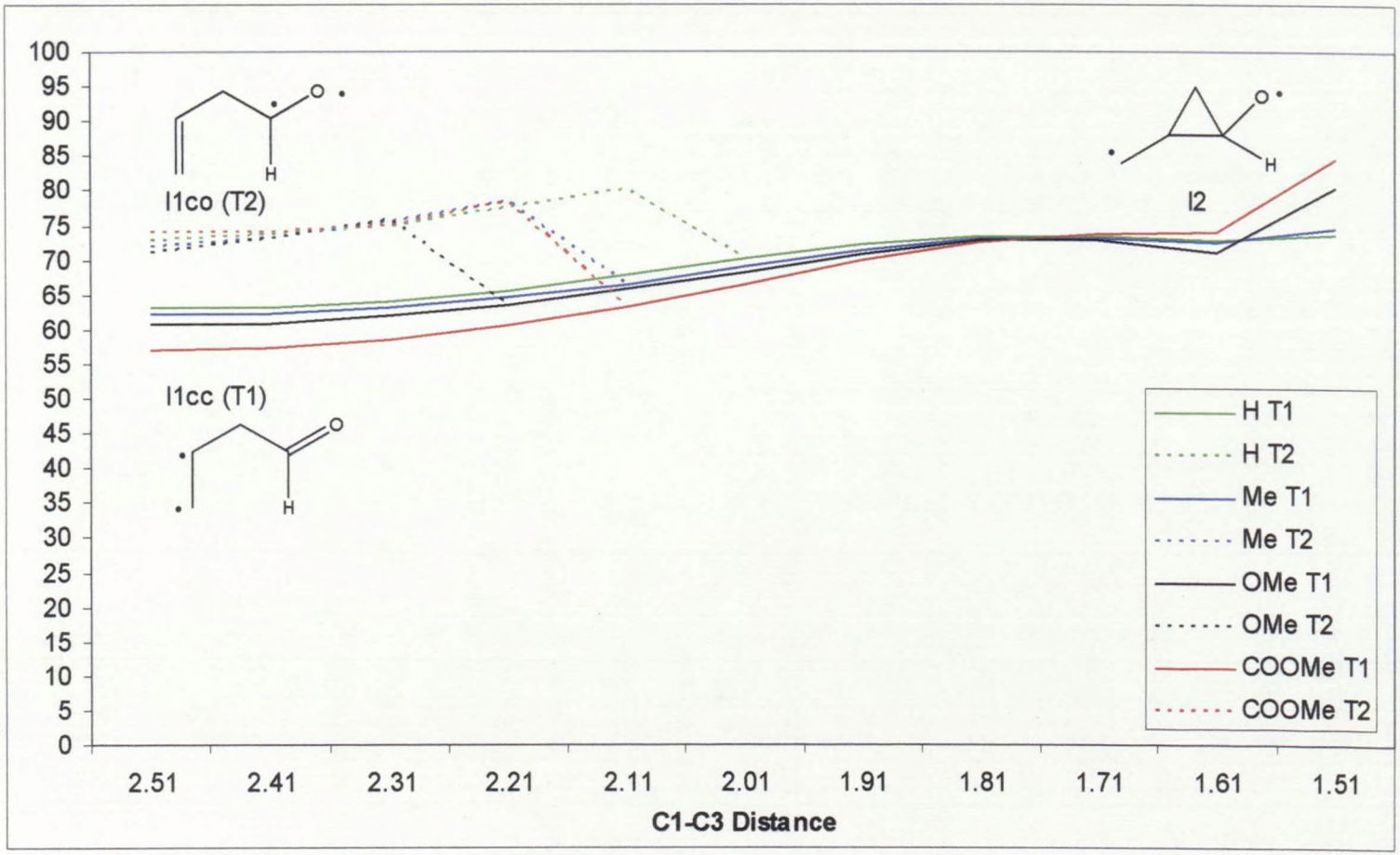
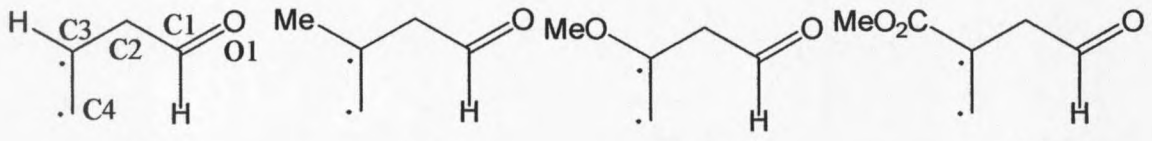

100
95
90
85
80
75
70
65
60
55
50
45
40
35
30
25
20
15
10
5
0
2.51
2.41
2.31
2.21
2.11
2.01
1.91
1.81
1.71
1.61
1.51
C1-C3 Distance
I1co (T2)
I1cc (T1)
I2
H T1
H T2
Me T1
Me T2
OMe T1
OMe T2
COOMe T1
COOMe T2

Figure 23

The $I1_{cc}$ triplet surface was probed in the same manner as the $I1_{co}$ surface, that is, stepping toward I2 by constraining the C1-C3 distance (Figure 23) of optimized $I1_{cc}$ geometries (Figure 24). Important bond lengths are shown in Table 14. The $I1_{cc}$ (T1) surfaces showed barriers that were nearly identical for all cases (Figure 23). However, and most importantly, the largest barrier was calculated for the ester case. Since the ester case produce the ODPM product, this barrier height between $I1_{cc}$ and I2 cannot explain the observed reactivity.



87 **92** **93** **94**

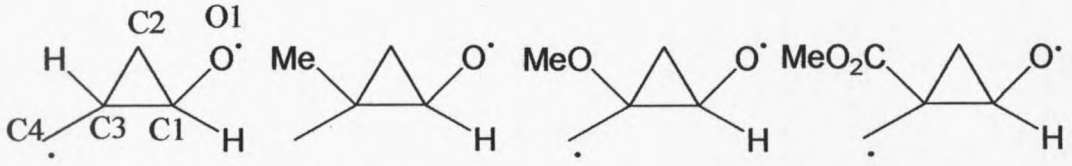
Figure 24: Intermediate 1_{cc} ($I1_{cc}$) Structures

Molecule	O1-C1 (Å)	C1-C2 (Å)	C1-C3 (Å)	C2-C3 (Å)	C2-C4 (Å)	C3-C4 (Å)	C3-R (Å)
87	1.20	1.51	2.51	1.49	2.51	1.46	1.09
92	1.19	1.52	2.51	1.49	2.52	1.46	1.51
93	1.21	1.52	2.50	1.52	2.52	1.46	1.37
94	1.18	1.52	2.52	1.51	2.50	1.47	1.49

Table 16

Analysis of the I1 to I2 surfaces indicated that molecules possessing a hydrogen, methyl or methoxy C3-substituent, will be excited to their first triplet state ($n \rightarrow \pi_{co}^*$), then relax to the intermediate $I1_{co}$, and travel along the reaction coordinate (Figure 24, dashed lines) until the T2 surface collapses to the $I1_{cc}$ (T1) surface (Figure 23, solid lines) continuing to the $I1_{cc}$ minimum. The methyl ester case will be excited to its $\pi_{cc} \rightarrow \pi_{cc}^*$

triplet state and relax to $I1_{cc}$. The conclusion of these results is that it may not matter which triplet excited state is accessed, VE_{co} or VE_{cc}, since molecules excited to the $I1_{co}$ intermediate have a path to the $I1_{cc}$ minimum. Furthermore, the similar barriers in going from $I1_{cc}$ to I2, and no observed correlation with respect to C3-substituent, indicated that all molecules excited can reach I2 (Figure 25 & Table 17).



87 **92** **93** **94**

Figure 25: Intermediate 2 (I2) Structures

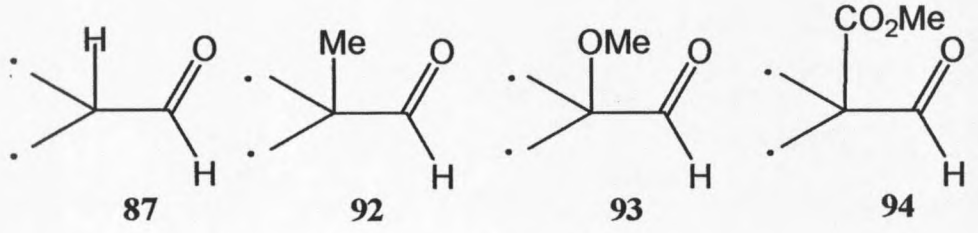
R-group	O1-C1 (Å)	C1-C2 (Å)	C1-C3 (Å)	C2-C3 (Å)	C2-C4 (Å)	C3-C4 (Å)	C3-R (Å)
H	1.29	1.61	1.58	1.48	2.57	1.46	1.08
Me	1.27	1.60	1.57	1.48	2.53	1.47	1.51
OMe	1.28	1.60	1.58	1.47	2.56	1.47	1.38
CO_2Me	1.28	1.59	1.57	1.50	2.55	1.47	1.51

Table 17

Examination of I2 to I3 Barrier Heights

Following the investigation of the $I1_{co}$ and $I1_{cc}$ to I2 triplet surfaces, it was concluded that no correlation existed between reactivity and the intermediates and barrier heights from I1 to I2. Based on the mechanism by Robb,[44] the transition state between I2 (Figure 25) and I3 (Figure 26) (TS2) could hold the key to the C3 substitiuent effect on reactivity. The expectation was that this barrier would be the largest for the methoxy and smaller for all other cases. In order to address this hypothesis the potential energy

surface was mapped in a stepwise fashion similar to the process used to scan the I1 to I2 surfaces. To accomplish this, optimized structures for I3 (Figure 26 & Table 18) were generated and the surface was driven by constraining the C1-C2 distance from 2.5 Å to 1.5 Å (Figure 26). From these results it was determined that no correlation existed between the substituent and the barrier height. Furthermore, this mapping, along with the I1 to I2 mapping, showed the surface around I2 to be quite flat indicating that molecules reaching I2 on the PE surface would eventually reach I3. From this we concluded that the triplet surfaces offered no quantitative answer to the origin of the non-reactivity of ODPM photoisomerization substrates bearing an electron donating group at the C3 position.



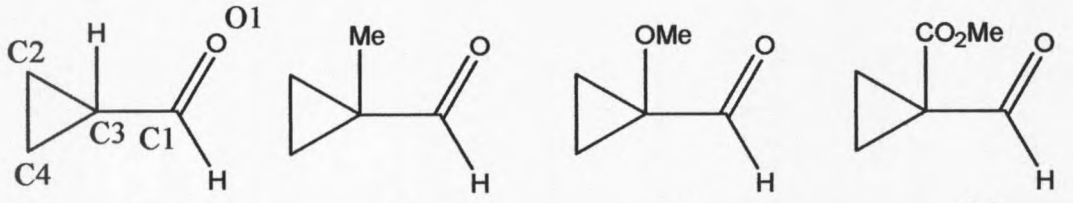
87 **92** **93** **94**

Figure 26: Intermediate 3 (I3) Structures

Molecule	O1-C1 (Å)	C1-C2 (Å)	C1-C3 (Å)	C2-C3 (Å)	C2-C4 (Å)	C3-C4 (Å)	C3-R (Å)
87	1.20	2.46	1.54	1.50	2.51	1.49	1.11
92	1.20	2.50	1.55	1.49	2.49	1.51	1.55
93	1.20	2.53	1.58	1.49	2.50	1.49	1.43
94	1.20	2.52	1.56	1.49	2.50	1.50	1.55

Table 18

The next step in this study was to investigate the closed shell singlet state potential energy surface (PES) connecting I3 with the product to determine the property of a pathway for I3 to reach product (P) (Figure 27 and Table 19). Intersection of the I3 triplet (Figure 28, solid line) and P closed shell singlet (Figure 28, dashed line) surfaces were probed by mapping the two surfaces with respect to the C2-C4 distance by constraining it between 2.5 and 1.8 Å. The resulting intersections are shown in Figure 29. From the figure it can be seen that all four cases behave similarly and the intersection occurs at about 2.45 Å. These results indicated that any molecule reaching I3 on the triplet surface (T_1) would eventually be converted to the desired product via intersystem crossing to the closed shell singlet surface of the product.



87 **92** **93** **94**

Figure 27

Molecule	O1-C1 (Å)	C1-C2 (Å)	C1-C3 (Å)	C2-C3 (Å)	C2-C4 (Å)	C3-C4 (Å)	C3-R (Å)
87	1.21	2.57	1.48	1.53	1.50	1.53	1.08
92	1.21	2.54	1.48	1.53	1.50	1.53	1.52
93	1.21	2.53	1.48	1.53	1.50	1.53	1.41
94	1.20	2.54	1.49	1.53	1.50	1.53	1.51

Table 19

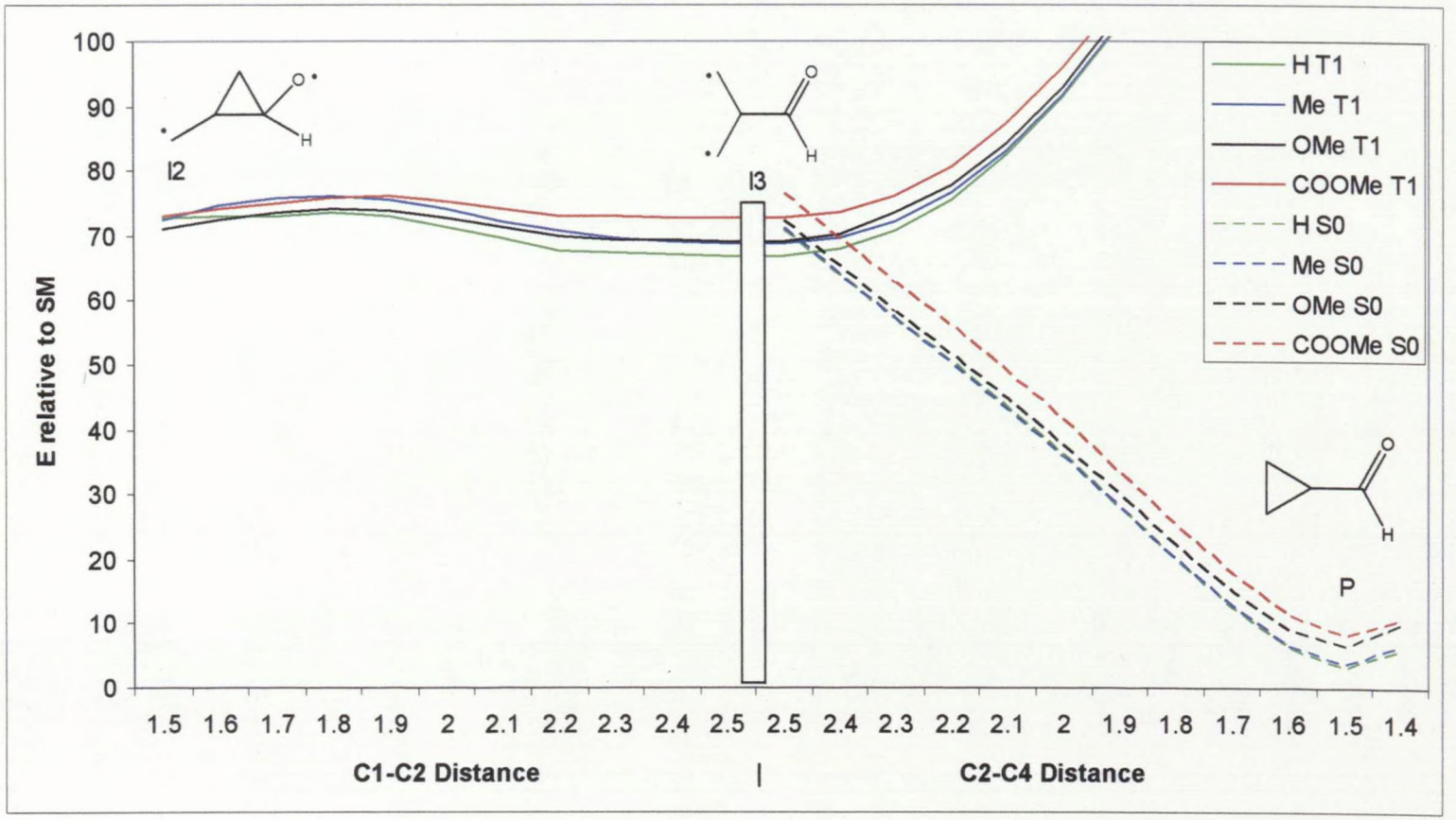

E relative to SM
100
90
80
70
60
50
40
30
20
10
0
I2
I3
P
H T1
Me T1
OMe T1
COOMe T1
H S0
Me S0
OMe S0
COOMe S0
1.5 1.6 1.7 1.8 1.9 2 2.1 2.2 2.3 2.4 2.5 2.5 2.4 2.3 2.2 2.1 2 1.9 1.8 1.7 1.6 1.5 1.4
C1-C2 Distance
C2-C4 Distance

Figure 28

Mapping of the Starting Material (SM)
Singlet Potential Energy Surface (S_0 PES)

In the mechanistic paper by Robb et al.,[44] multiple surfaces were discussed. Central to his discussion was the conical intersection of the triplet and singlet surfaces found around I2. On the basis of lacking any significant difference in the barriers on the triplet surfaces investigated with respect to the selectivity, intersystem crossing at I2 should describe the observed reactivity differences. This can occur as crossing of the triplet and two singlet states. In DFT, the open-shell singlet calculations collapsed to the closed shell singlet wavefunction. The corresponding open shell singlet surface could not be studied due to the limitations of the method, therefore only the closed shell singlet surface is discussed here. If the SM S_0 surface crossed the triplet surface before I2 in the methoxy case, it would provide a pathway for spin recombination leading back to the ground state yielding no product. The SM surface would then have to cross the triplet surface after I2 in the hydrogen, methyl, and methyl ester cases allowing them to proceed to I3 and eventually give the product. To define the S_0 surface starting from SM, the already optimized SM geometries were employed and the surfaces were mapped by constraining the C1-C3 distance, as was done in the I1 to I2 surface mapping (Figure 29). The SM S_0 surface (Figure 29, dashed lines) mapping showed similar behaviors for all four cases, and no correlation to the C3-substituent on the SM S_0 surface could be drawn. The finding that the triplet and closed shell singlet surfaces did not show any correlation with reactivity indirectly implies that the reactivity should originate from surface crossing of the triplet and open shell singlet surfaces at I2. From Robb's calculations, the surface crossing for the hydrogen case **87** is known, and it was found to be located beyond I2.

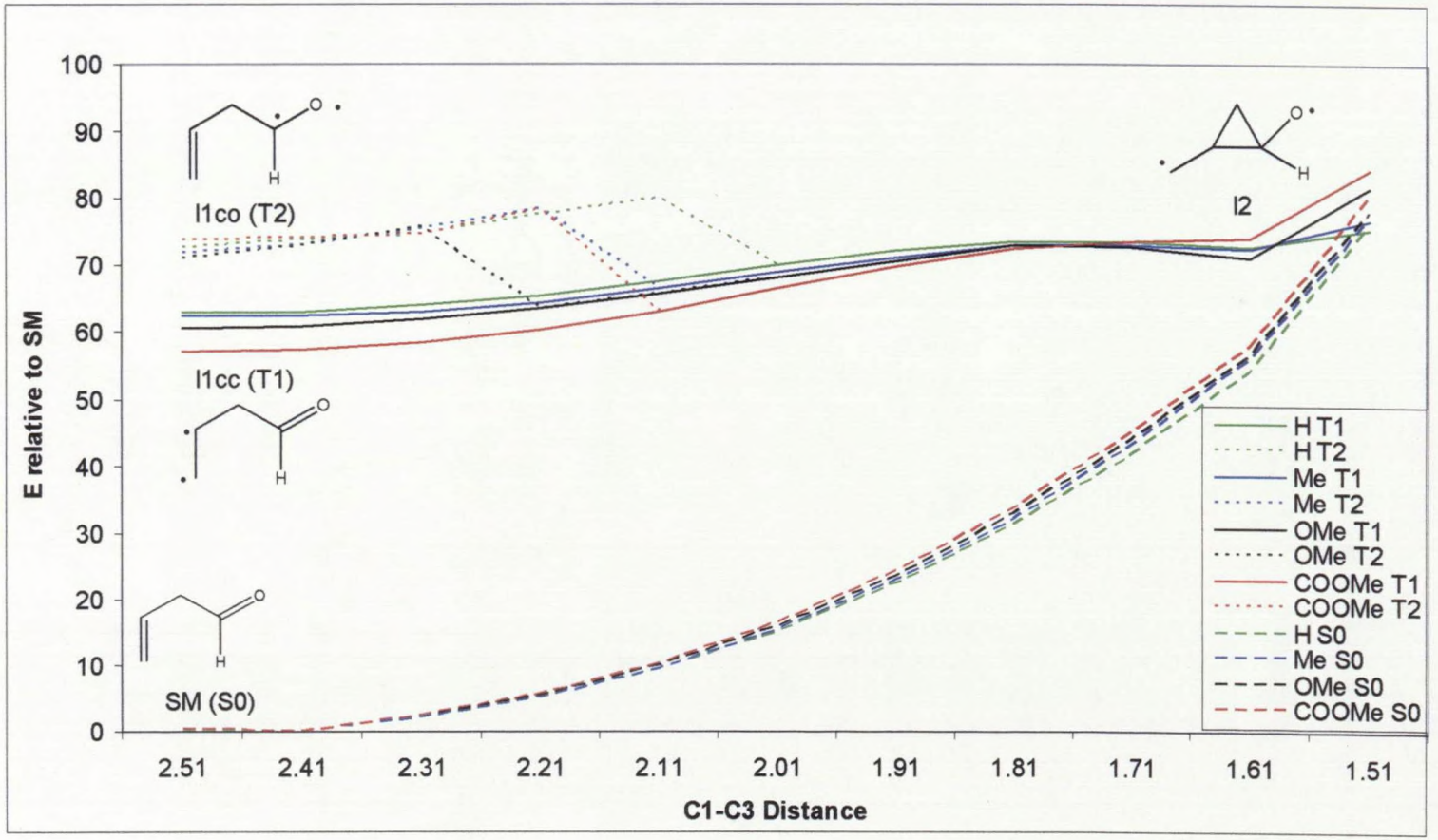
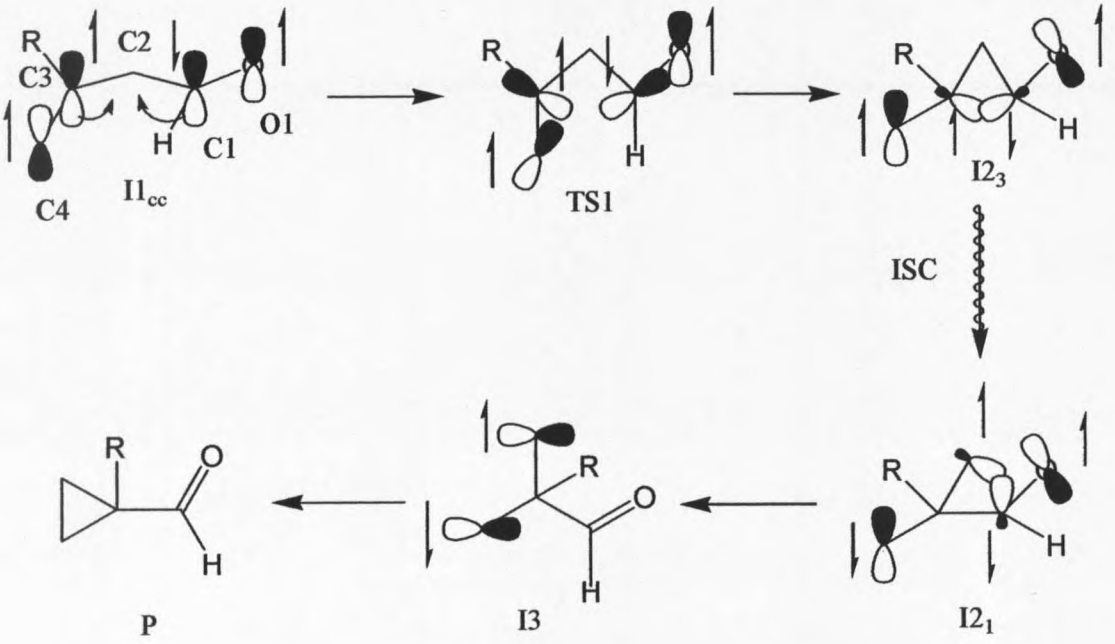

E relative to SM
C1-C3 Distance
100
90
80
70
60
50
40
30
20
10
0
2.51
2.41
2.31
2.21
2.11
2.01
1.91
1.81
1.71
1.61
1.51
I1co (T2)
I1cc (T1)
SM (S0)
I2
H T1
H T2
Me T1
Me T2
OMe T1
OMe T2
COOMe T1
COOMe T2
H S0
Me S0
OMe S0
COOMe S0

Figure 29

Inductive Effect Model

Based on the surface calculations performed using density functional calculations, it was deduced that the origin of the reactivity with respect to the C3-substituent is likely to come from crossing of the S_1 and T_1 surfaces at I2. In Robb's calculations, this crossing occurred after I2 on the rising slope of the I2-I3 triplet surface.[44] An indirect indication of the selective surface crossing can be found in the behaviour of the $I1_{co}$ to I2 surfaces. In order to fulfill the original goal of this project, to construct a simple computational model which correlates the reactivity differences with C3 substituents, a model based on the electronic features of I2 structures was designed. NPA atomic charges were computed to investigate this electronic effect for the four C3-substituent cases. These C3-substituent charges should indicate the effective electron-withdrawing strength by induction of the C3-substituent, and their overall effect on the C1-C3 bond. This effect, combined with the inherent bond angle strain in cyclopropanes, can describe the observed reactivities. This model shows a reactivity correlation with respect the C3 substituent's inductive electronic effect. Scheme 38 shows the orbitals involved in the mechanism of the ODPM photoisomerization. The results of the PES scanning indicated that all substrates have a path to $I1_{cc}$, either from sensitized excitation to $I1_{cc}$ (ester case) or via sensitized excitation to $I1_{co}$ followed by travel along the PES to $I1_{cc}$, as was demonstrated by both Robb[44] and us. Starting from triplet $I1_{cc}$, as the molecule progresses toward I2 the singly occupied MO (SOMO) at C3 rotates to form a bonding interaction with C1. The formation of the new C1-C3 bond should be most influenced by inductive effects in the course of the reaction. At $I1_{cc}$, the unpaired electrons are

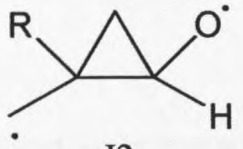
localized on the olefin carbons (C3 & C4). As found by Robb (Figure 13) and us (Figure 30) after the intersystem crossing (conical intersection at I2) the unpaired electrons remain localized on C1 and C4, however they are now antiparallel (I2-open shell singlet state). Cleavage of the C1-C2 bond will give I3 and consequently P. TS1 is a late transition state that connects $I1_{cc}$ and I2. At $I2_3$ (I2-triplet state) the unpaired electrons are separated by a distance of three σ bonds and localized on the olefin carbon (C4) and carbonyl oxygen (O1).



Scheme 38

In the case of the methoxy substituted molecule, the newly forming C1-C3 bond, will be weakest due to its strong electron withdrawing nature by induction. After ISC, instead of cleaving the C1-C2 bond, the weaker C1-C3 bond will be cleaved and it will eventually relax to the stating material ground state through an open shell singlet surfaces

and later a closed shell singlet surface. In order to quantitate this, atomic point charges were calculated using the Natural Population Analysis method for optimized I2 geometries. The result of these computations ranked the C3-substituents, in order of electron withdrawing to electron donating by induction, from methoxy to the methyl ester then methyl and finally hydrogen (OMe, CO_2Me, Me, H) (Figure 30 & Table 20). This provides a quantitative correlation with observed reactivity.



I2

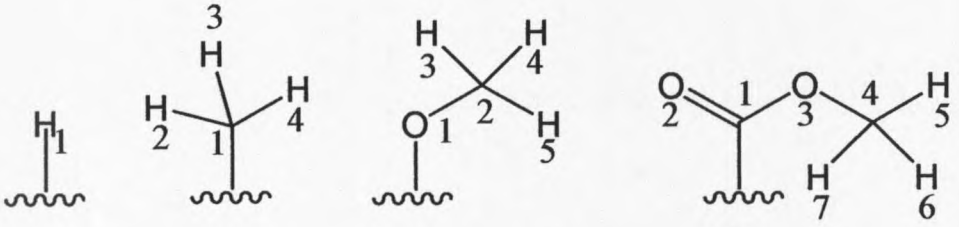


Figure 30

R	R-Group NPA Charge	1	2	3	4	5	6	7
H	0.24	0.24						
Me	0.07	-0.56	0.20	0.21	0.22			
OMe	-0.27	-0.59	-0.20	0.19	0.17	0.16		
COOMe	0.04	0.83	-0.61	-0.54	-0.21	0.19	0.19	0.19

Table 20

This model can satisfactorily describe the observed reactivity in a fashion that could be readily utilized by synthetic chemists. The main difference to the original proposal is that the selectivity originates from I2 instead of the SM, and is related to inductive instead of resonance effects. This inductive effect model could be applied to potential ODPM photoisomerization precursors to determine their likely reactivity. Further experimental and theoretical studies need to be conducted to verify its reproducibility for C3-substituents other than those studied here.

Conclusions

Potential energy surfaces of the ODPM photoisomerization for four acyclic photoprecursors were studied using DFT. The surface mapping calculations of gave similar triplet surfaces to those described by Robb[44] for the hydrogen C3-substituent case. In addition, this study determined that the hypothesis of the relative barrier heights being responsible for observed reactivities did not apply to substituent effects at C3. Investigation of the triplet and closed shell singlet surfaces indicated that all substrates may undergo the ODPM photoisomerization and yield the desired photoproducts. However, as noted in the introduction, synthetic examples contradict this behavior; therefore, there must be some feature of the reaction's potential energy surface that is selective with respect to the C3-substituent. Examination of the PE surfaces published earlier and obtained in this work indicated that a possible location for the origin of selectivity is the intersystem crossing at I2. At I2 intersystem crossing occurs between triplet and singlet surfaces in the form of a conical intersection, and can lead back to the

starting material for substrates known not to form ODPM products under photolytic conditions. In order to quantitatively address this possibility it would be necessary to employ mulitreference methods, such as CAS-SCF, due to the limitations of calculations of open shell singlet surface crossing inherent to DFT. However, these calculations require a significantly more elaborate approach and would not be practical for synthetic organic chemists.

The $n \rightarrow \pi_{co}^*$ triplet state was found to be the most likely state to interact with the triplet sensitizers in β,γ-enones, excepting those possessing an ester group at C3. This result seems to contradict previous computational reports, but does not influence the chemical outcome of the reaction, as the T_1 surfaces lead to the T_2 surfaces, thereby allowing for conversion of $I1_{co}$ to $I1_{cc}$, then to I2 through small barriers.

Based on the behavior of the triplet surfaces, a general model has been proposed here that allows for prediction of ODPM reactivities based on the inductive electronic effect of the C3-substituent. This model will be relatively simple to implement by experimental chemists with common computational packages such as Spartan™. The model appears to be consistent with observed ODPM reactivities. Future work, both experimental and theoretical, shall further determine its broader relevance to the C3-substituent effect.

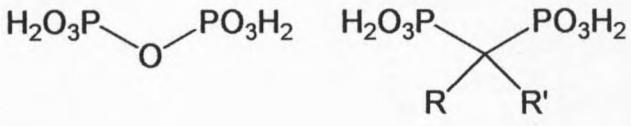
CHAPTER 4

SYNTHESIS OF BISPHOSPHONOMETHYL-PYRIMIDINDIONES

Introduction

Historical Background

Bisphosphonic acids, pyrophosphoric acid analogs where a methylene group has replaced the central oxygen (Figure 31), have been known and utilized since the 19th century.[14] These compounds are often referred to by the general name of bisphosphonates; due to acidity of the acidic protons *in vivo* they are commonly bisphosphonate salts. Their common industrial uses have included antiscaling, anticorrosive, and complexing agents.[14] In the 1960's, bisphosphonomethyl compounds were found to be effective in the treatment of bone mineral diseases.[61] Of particular interest is their activity against disorders such as Paget's disease and osteoporosis.[14]



pyrophosphoric acid bisphosphonic acid

Figure 31

The bioactivity of bisphosphonate compounds are thought to be due to two interactive regions. These regions are referred to as the "bone hook" and "bioactive" regions (Figure 32).[13] The "bone hook" or bisphosphonate region chelates calcium to

locate the molecules on bone surfaces. Chelation has been found to be enhanced when a hydroxyl group has been added to the carbon bearing the phosphonate groups. The "bioactive" region is the portion of the molecule responsible for repelling or deactivating the osteoclast cells which mine the bone for calcium.[14] This mining process is responsible for half of the dynamic process of remodeling bones. When this process is balanced it leads to healthy bones, however, when the balance is lost, disorders such as osteoporosis and Paget's disease set in and lead to bone degradation.

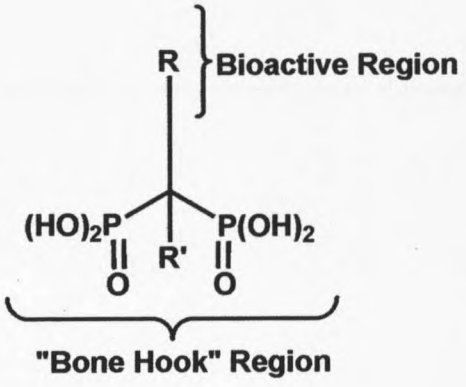
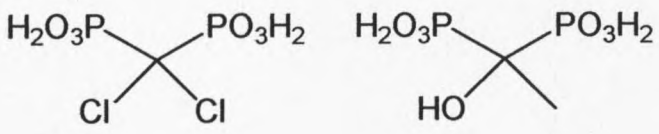


Figure 32

Although many studies have been aimed at identifying the exact mode of action, none have clearly demonstrated how the bisphosphonates interact with the osteoclasts.[15] This is unfortunate, since binding site information and knowledge of the parameters leading to inhibition of osteoclasts could direct the systematic design of potential inhibitors. Without this information, investigators have had to infer information about the bisphosphonate-osteoclast interactions from the screening results of many synthetically prepared bisphosphonates.[15]

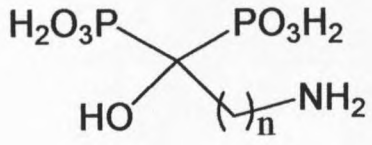
The first-generation of bisphosphonates were relatively simple molecules that demonstrated modest bioactivity. Etidronic acid and chloridronic acid are important examples of first-generation bisphosphontes (Figure 33).[15] Etidronic acid was prepared over 100 years ago and was the first to treat human disorders.[15]



Chlodronic acid Etidronic acid

Figure 33

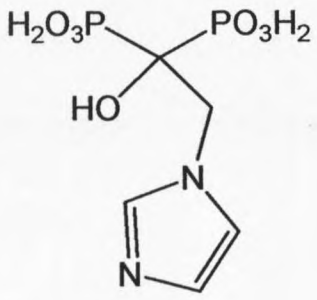
Pamidronate, a second-generation bisphosphonate, demonstrated enhanced anti-bone resorptive activity compared to first-generation bisphosphonates.[15] This led researchers to investigate nitrogen tether length to determine if bioactivity varied with nitrogen-bisphosphonate distance. An optimized nitrogen-bisphosphonate distance of 5 atoms, alendronate, was observed from the ED_{50} values of a series of bisphosphonates (Figure 34).[15]



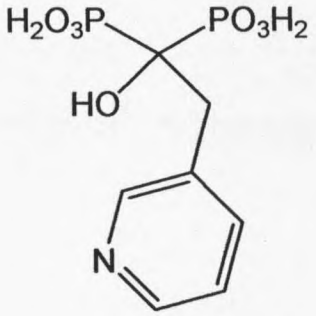
n	Name	ED_{50} (μg/Kg)
1	-	150
2	Pamidronate	61
3	Alendronate	8
4	-	20
5	Neridronate	60

Figure 34

Risedronate[13] and Zometa[15] represent the third-generation bisphosphonates (Figure 35). Third-generation bisphosphonates incorporate a heterocyclic moiety containing one or more nitrogens in the bioactive region of the molecule. These bisphosphonates typically exhibit enhanced bioactivity compared to first- and second-generation bisphosphonates. For example Zometa has an ED_{50} value of 0.07 μg/Kg, where as alendronate, a highly active second-generation bisphosphonate, has an ED_{50} value of 6 μg/Kg.[15]



Zometa
(Novartis)



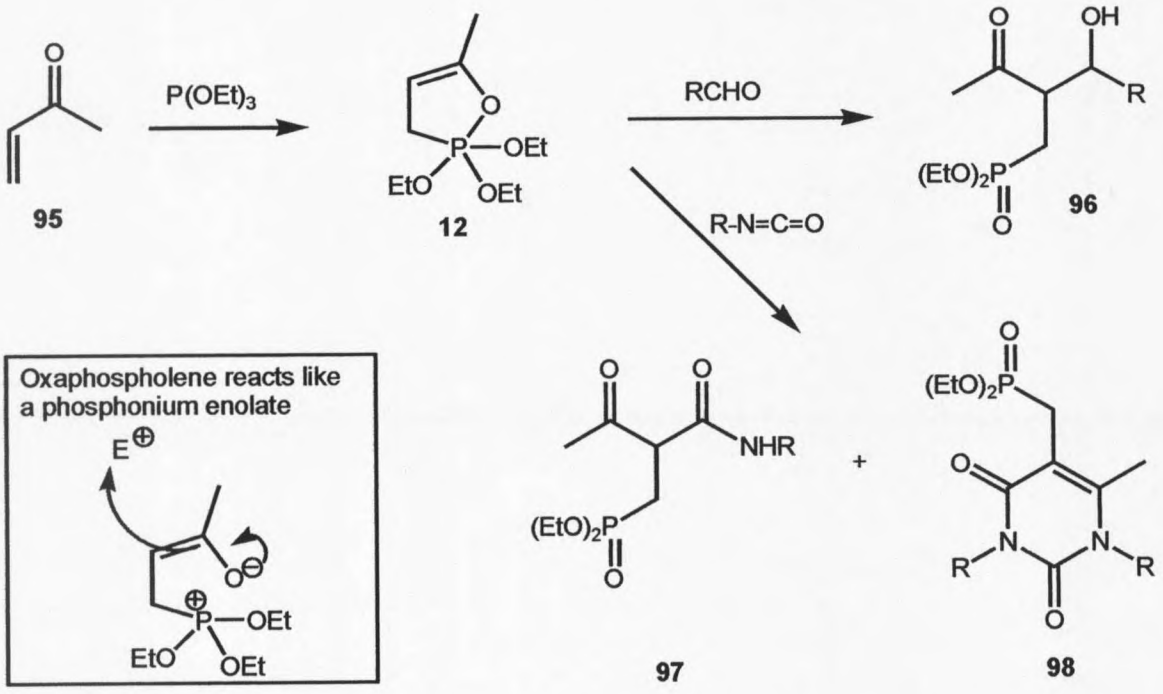
Risedronic acid
(Proctor and Gamble)

Figure 35

Oxaphospholene Methodology

Oxaphospholenes **12** have been extensively used by the McClure research group for the production β-hydroxyketones with appendant phosphonomethylene groups (Scheme 39).[16] This work featured an aldol-type reaction where the nucleophilic oxaphospholene was reacted with aldehydes. The reaction of oxaphospholene **12** with isocyanates followed as an extension of this work.[62] The anticipated product was the β-

ketoamide **97**. However, the reaction yielded a mixture of the expected β-ketoamide **97** as well as the heterocycle **98** arising from reaction of two equivalents of isocyanate with the oxaphospholene **12** (Scheme 39).

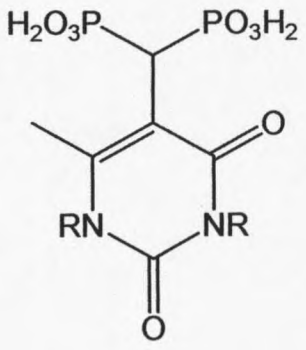


Scheme 39

Project Scope

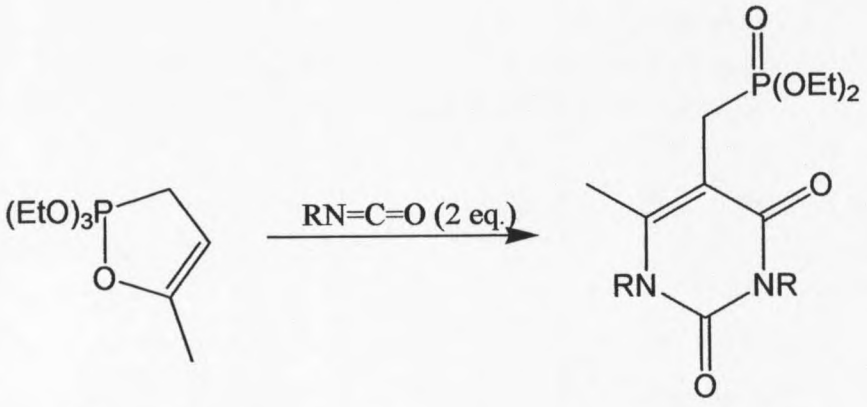
Based on the above information, a program of study was begun to produce new bisphosphonomethyl pyrimidinediones **2** (Figure 36) to be investigated as possible bone antiresorptives. This preparation utilizes the reaction previously discovered in this group between oxaphospholenes and isocyanates to yield phosphonomethyl pyrimidindiones **98** (Scheme 40). This reaction has proved to be a facile route to interesting monophosphono-heterocycles. The goal of this project was to extend the heterocycle

forming reaction into a process that could produce a variety of potentially useful bisphosphonomethyl-pyrimidindiones **2**.



2

Figure 36



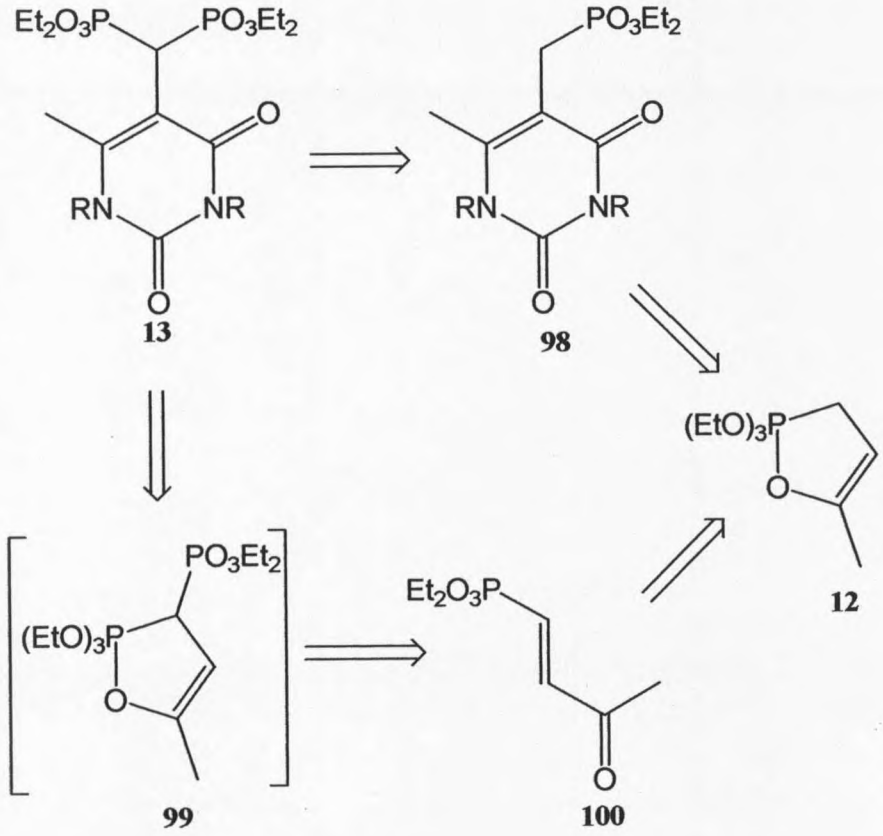
12 **98**

Scheme 40

Results and Discussion

Retrosynthetic Analysis

Our goal for this project was the production of variously N,N-disubstituted bisphosphono-pyrimidinediones **13** (R=Ar, Bn, H). To access these targets, we developed the following synthetic strategy (Scheme 41). The desired bisphosphonates could be produced from two penultimate intermediates, the mono-phosphonate **98** or phosphono-oxaphospholene **99** as shown in Scheme 41.



Scheme 41

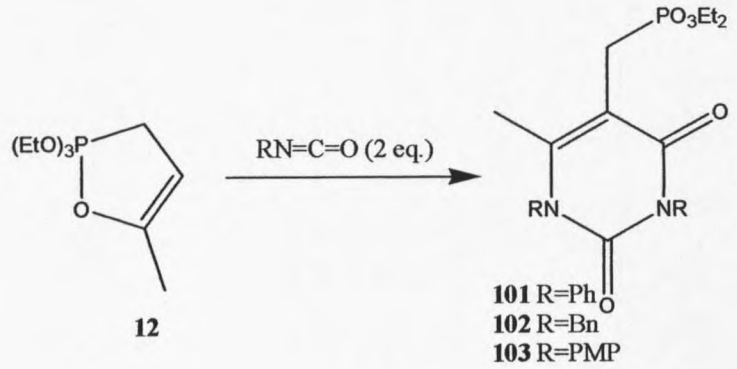
The first synthetic path to be considered involved phosphorylation of monophosphono heterocycles. This approach drew on the swift availability monophosphono heterocycles **98** from oxaphospholene **12**. The utility of this route would depend on the efficiency and selectivity of phosphorylation of the dianion of phosphonate **98** (Scheme 41).

The alternate synthetic plan involved the preparation of a new phosphono-oxaphospholene **98** (Scheme 41). It was envisioned that this new nucleophile could be prepared from the ketovinyl phosphonate (KVP) **100** and triethylphosphite. The preparation of KVP from oxaphospholene **12** and bromine followed by elimination has been previously described by this group.[63]

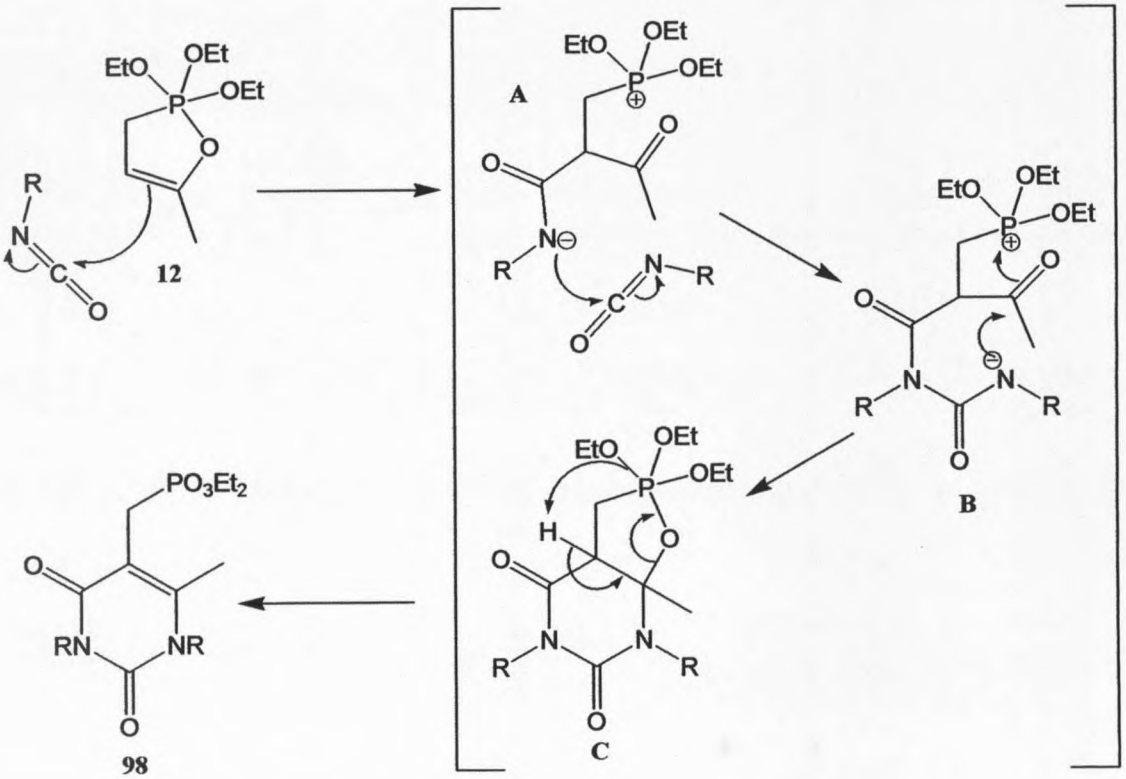
Preparation of Monophosphonates

Monophosphonomethyl pyrimidindiones **98** were prepared by the addition of oxaphospholene **12** to two equivalents of benzyl or aryl isocyanates in DCM (Scheme 42).[62,63] This procedure afforded the desired heterocycles in good yields (ca. 73-84%). This procedure was used to prepare three N,N-disubstituted pyrimidinediones **101** (R = Ph, 79%), **102** (R = $PhCH_2$ = Bn, 84%), and **103** (R = $pMeOC_6H_4$ = PMP, 73%). Attempts to prepare N,N-disubstituted pyrimidindiones from para-nitrophenylisocyanate and tert-butylisocyanate failed to produce the desired products. The molecules were presumed to be formed via the mechanism shown in Scheme 42. This mechanism shows the nucleophilic attack on the first equivalent of the isocyanate leading to formation of the amide anion intermediate **A**, which further reacts with the second equivalent of the isocyanate, to give the second amide anion intermediate **B** (Scheme 43). This anion

undergoes intramolecular ring closing onto the ketone giving the heterocyclic intermediate **C**, and the reaction is finished by elimination to give the product **98** (Scheme 43).



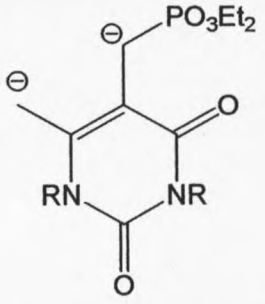
Scheme 42



Scheme 43

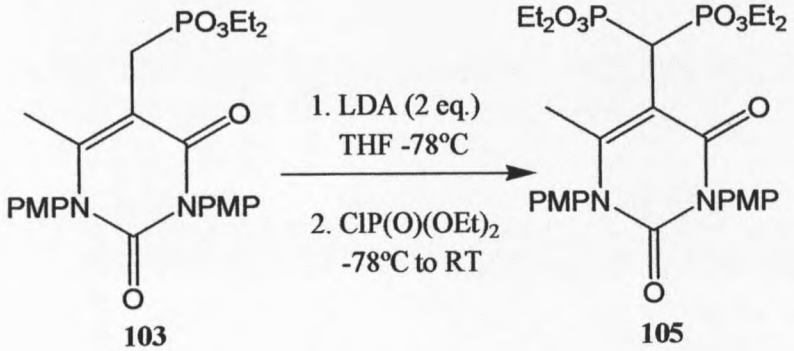
Phosphorylation of Monophosphonates

With the desired monophosphonates in hand, the next step was to convert them to their corresponding bisphosphonates. This was attempted via the generation of dianion intermediate **104** (Figure 37) of the monophosphonate followed by quenching with chlorodiethyl phosphate (Scheme 44). In the case where the R groups were PMP groups (**103**), the phosphorylation proceeded smoothly yielding the desired bisphosphonate in 42% yield. This process failed to produce the desired bisphosphonate where R was benzyl (**102**). The conditions instead yielded a variety of products, none of which were the desired geminal bisphosphonate.



104

Figure 37

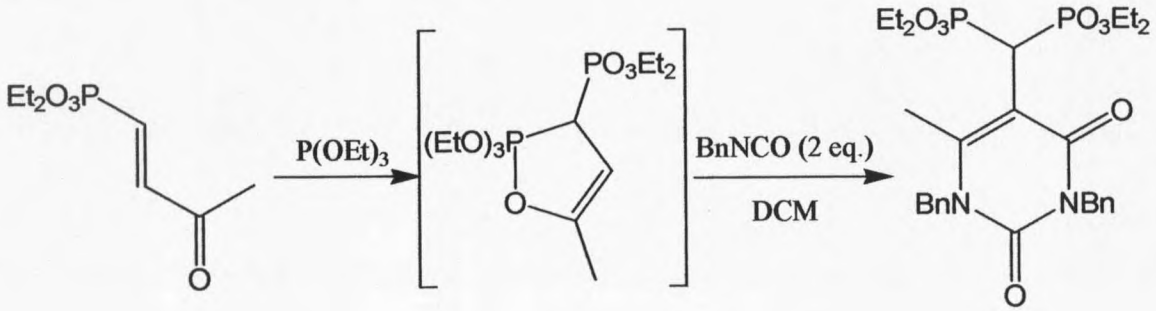


103 **105**

Scheme 44

Preparation and Use of a
Phosphono-Oxaphospholene

Due to the failure of the phosphorylation method to produce all of the desired bisphosphonates cleanly, it was decided that the alternate synthetic path would be undertaken. This route avoided the late introduction of the second phosphonate group by installing it regioselectively on the oxaphospholene. The phosphono-oxaphospholene **99** was easily prepared from KVP **100** and triethylphosphite. The phosphono-oxaphospholene was prepared neat *in situ*, then dissolved in dry DCM and benzyl isocyanate was added (Scheme 45). This reaction yielded product bisphosphonate **106** in only 3% yield.



100 **99** **106**

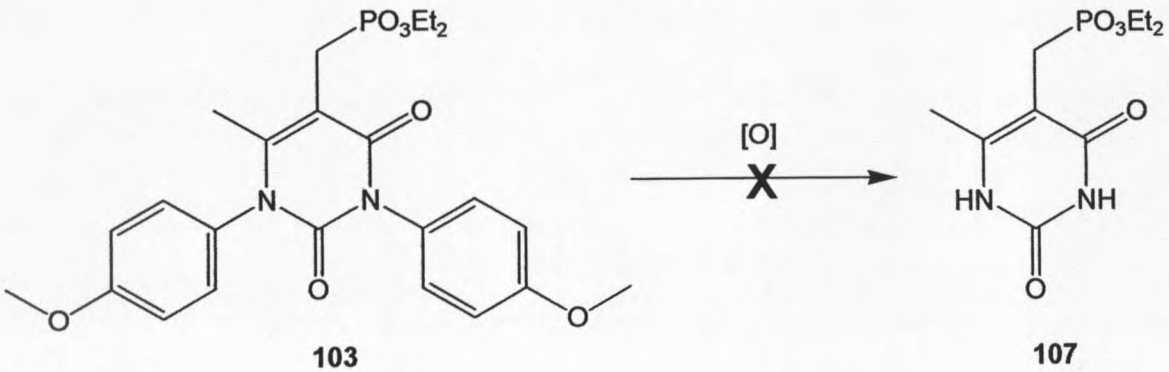
Scheme 45

In an attempt to boost the yield of this reaction, additives were employed but showed no effect in increasing the yield. The additives that were used included: magnesium bromide-diethyl etherate, magnesium sulfate, tetrabutylammonium bromide, potassium trimethylsilyloxide, and 4Å sieves. These additives were selected for screening in this reaction as they were fairly mild and would not promote the reversibility

of the formation of the phosphono-oxaphospholene. Clearly this method, although regioselective, was not an ideal route to the desired bisphosphonates.

Deprotection of the PMP-Phosphonates

The paramethoxyphenyl protecting group was selected based on its use in the synthesis of β-lactams. There it was demonstrated that PMP groups could be oxidatively cleaved from the nitrogen of the β-lactams via the use of ceric ammonium nitrate (CAN)[71] and other mild oxidants. The deprotection conditions were attempted on the mono-phosphonate **103** to determine which one would be most likely to succeed on the bisphosphonates (Scheme 46). The conditions attempted are summarized in Table 19. The data showed that under none of the conditions were the PMP groups successfully removed. These conditions ranged from the mild CAN to the stronger oxidative conditions of silver oxide. The use of sonication was employed in an attempt to enhance the rate of electron transfer. Ozonolysis was also attempted to facilitate cleavage of the PMP group. The harsh conditions of ozonolysis led to complete decomposition of the starting material yielding no product.



103 **107**

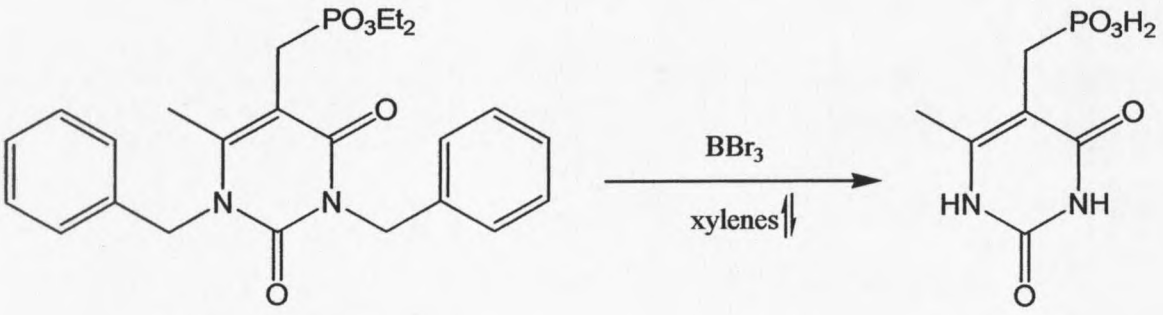
Scheme 46

Oxidant System	Solvent(s)	Temperature	Result
CAN	MeCN/H_2O	RT	NR
CAN	MeCN/H_2O	150°C sealed tube	NR
CAN	MeCN/H_2O Sonication	60°C	NR
DDQ	DCM, H_2O	RT	NR
$AgNO_3$	MeCN/H_2O	RT	NR
$AgNO_3$	MeCN/H_2O Sonication	60°C	NR
$AgNO_3$ Ammonium Persulfate	MeCN/H_2O	RT	NR
$AgNO_3$ Ammonium Persulfate	MeCN/H_2O Sonication	60°C	NR
AgO	Acetone, MeCN, H_2O	RT	NR
1)O_3 2) DMS	DCM	-78°C	Decomp.

Table 21

Deprotection of Benzyl-Phosphonates

The deprotection of the dibenzyl protected phosphonate **102** was carried out under the conditions developed by Kundu[65] for the debenzylation N,N-dibnzyluracil using boron tribromide in refluxing xylenes (Scheme 47). The product of this reaction was the parent monophosphonic acid **105** as the deprotection conditions not only cleaved both benzyl groups, but also converted the phosphonate to the phosphonic acid. Attempts to completely deprotect under hydrogenolysis conditions failed to produce the deprotected phosphonate.[66] The inability to remove the benzyl groups via hydrogenolysis is precedented for debenzylation of related pyrimidines, unless very acidic conditions were employed.[67]



102 **108**

Scheme 47

Conclusion

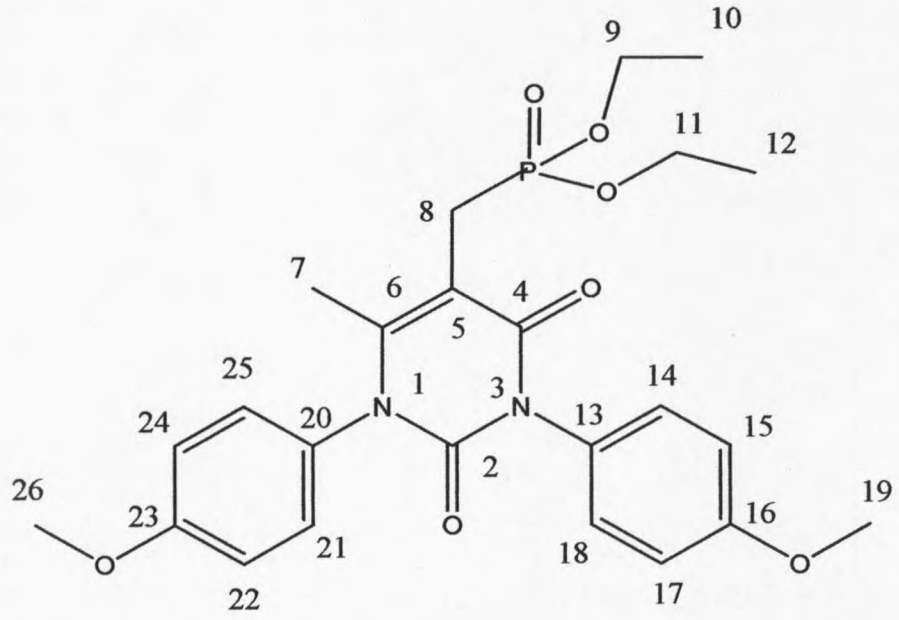
Advances toward the preparation of potential bone anti-resorptive compounds have been made. To this end an N,N-diaryl bisphosphonate (R=PMP) has been prepared in modest yield. This compound will now be submitted for testing to determine its bioactivity against bone-resorption. The N,N-dibenzyl bisphosphonate has also been prepared, but in poor yield. These bisphonate compounds were accessed utilizing the oxaphospholene chemistry developed by McClure, et al.[62,63]

Experimentals

For general experimental information, see the Experimental Section in Chapter 2.

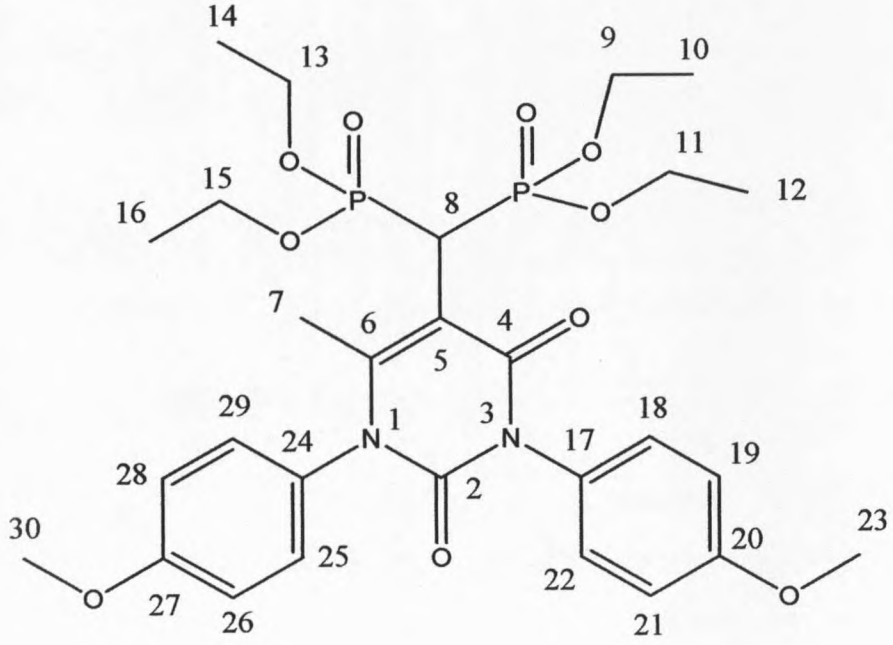
Diethyl [(1,2,3,4-tetrahydro-6-methyl-2,4-dioxo-1,3-bis(4-methoxyphenyl)-5-pyrimidinyl)methyl]phosphonate (97): An oven dried, Argon purged 50 mL round bottom flask was charged with oxaphospholene **12** (2.97 g, 12.6 mmol) and DCM (10 mL). The solution was cooled to ~0°C with an ice bath and 4-methoxyphenylisocyante (4.03 g, 25.3 mmol) was added dropwise. After 3 hours the ice bath was removed, and the reaction stirred at room temperature for 2 days, after which ^{31}P-NMR indicated completion of the reaction. The mixture was poured into a flask containing DI-H_2O (5 mL) and stirred for 0.5 hour. The mixture was separated and the aqueous phase was extracted with DCM (5x20 mL). The combined organic layers were filtered through $MgSO_4$ and conc *in vacuo*. The resulting oil was triturated with ether yielding a white powder. The powder was purified via column chromatography on silica gel eluting with 3% MeOH/DCM yielding the product as a white powder, which was recrystallized in 73% yield (4.5 g, 9.2 mmol), mp 138.9-139.3°C (1:3 DCM/hexanes).

101



^{1}H-NMR: 7.17 (4H, bt, J = 9.1 Hz, H's on C's 14, 18, 21, 25), 6.95 (2H, J = 8.8Hz, H's on C's 15, 17 or C's 22, 24), 6.95 (2H, J = 8.9 Hz, H's on C's 15, 17 or C's 22, 24), 4.13 (4H, app. pent, J = 7.1 Hz, H's on C's 9, 11), 3.81 (3H, bs, H's on C19 or 26), 3.78 (3H, bs, H's on C19 or 26), 3.12 (2H, d, $J_{P\text{-}H}$ = 20.3 Hz, H's on C8), 2.04 (3H, d, $J_{P\text{-}H}$ = 3.2 Hz, H's on C7), 1.29 (6H, t, J = 7.0 Hz, H's on C's 10, 12). ^{13}C-NMR: 162.6 (C4), 159.9 (C16 or 23), 159.4 (C16 or 23), 151.8 (C2), 150.9 (d, $J_{P\text{-}C}$ = 7.2 Hz, C6), 130.1 (C13 or 20), 129.6 (C14 & 18 or C21 & 25), 129.2 (C14 & 18 or C21 & 25), 128.0 (C13 or 20), 114.9 (C15 & 17 or C22 &24), 114.6 (C15 & 17 or C22 & 24), 103.6 (d, $J_{P\text{-}C}$ = 9.9 Hz, C5), 62.3 (d, $J_{P\text{-}C}$ = 6.5 Hz, C9 & 11), 55.6 (C19 or C26), 55.5 (C19 or 26), 23.7 (d, $J_{P\text{-}C}$ = 141.6 Hz, C8), 19.0 (C7), 16.4 (d, $J_{P\text{-}C}$ = 6.3 Hz, C10 & 12). ^{31}P-NMR: 27.0 ppm. IR (cm^{-1}, NaCl): 2980, 1710, 1658, 1511, 1431, 1248, 1026. HRMS calculated for $C_{24}H_{29}N_2O_5P$ (M^+) 488.170441, Found (M^+) 488.171240.

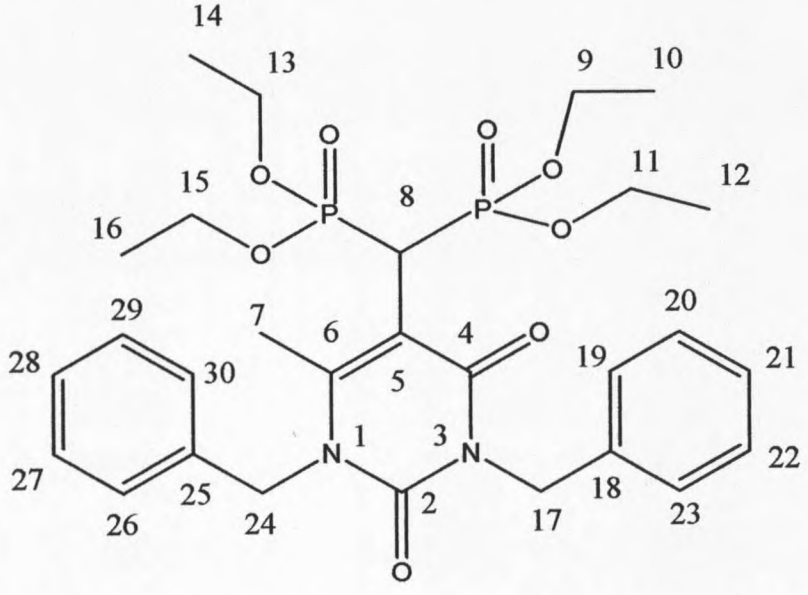
Tetraethyl [(1,2,3,4-tetrahydro-6-methyl-2,4-dioxo-1,3-bis(4-methoxyphenyl)-5-pyrimidinyl)methyl]bisphosphonate (103): An oven dried, Argon purged 50 mL round bottom flask was charged with phosphonate **97** (466 mg, 0.95 mmol) and THF (15 mL). The solution was cooled to -78°C with a dry ice/acetone bath, and a freshly prepared solution of LDA in THF (5 mL, 2.2 mmol, 0.44M) was added dropwise. After stirring at -78°C for 30 minutes chlorodiethyl phosphate was added dropwise. Following the addition the mixture was stirred at -78°C for 2 hours then warmed to -40°C and stirred for 18 hours. The reaction was quenched by pouring the mixture into a saturated ammonium chloride solution (20 mL) and was stirred for 1 hour. Ether (20 mL) was added and the mixture separated. The aqueous phase was extracted with ether (4x20 mL). The combined organic layers were filtered through $MgSO_4$ and conc *in vacuo*. The resulting oil was purified via column chromatography on silica gel eluting with 5% MeOH/DCM giving the product as a yellow oil in 42% yield.



^{1}H-NMR: 7.18 (2H, d, J = 8.4 Hz, H's on C's 18, 22 or C's 25, 29), 7.12 (2H, d, J = 8.4 Hz, H's on C's 18, 22 or C's 25, 29), 6.95 (4H, app. dd, J = 8.9 Hz, J = 2.3 Hz, H's on C's 19, 21, 26, 28), 4.94, (1H, t, $J_{P\text{-}H}$ = 29.4 Hz, H on C8), 4.28-4.04 (8H, m, H's on C' 9, 11, 13, 15), 3.80 (3H, s, H's on C23 or 30), 3.77 (3H, s, H's on C23 or 30), 2.27 (3H, bs, H's on C7), 1.34-1.19 (12H, m, H's on C's 10, 12, 14, 16). ^{13}C-NMR: 162.9 (t, $J_{P\text{-}C}$ = 5.6 Hz, C4), 159.9, (C20 or 27), 159.5 (C20 or 27), 154.3 (C2), 151.4 (C6), 129.9 (C17 or C24), 129.7 (C18 &22 or C25 & 29), 129.0 (C18 &22 or C25 & 29), 128.0 (C17 or C24), 114.8 (C19 & 21 or C26 &28), 114.6 (C19 & 21 or C26 &28), 103.7 (t, $J_{P\text{-}C}$ = 7.4 Hz, C5), 63.1 (d, $J_{P\text{-}C}$ = Hz, C9, 11, 13, 15), 55.5 (C23 or 30), 55.4 (C23 or 30), 33.8 (t, $J_{P\text{-}C}$ = 138.7 Hz, C8), 21.3 (C7), 16.3 (C10, 12, 14, 16). ^{31}P-NMR: 20.1 ppm. IR(cm^{-1}, NaCl): 2980, 2930, 1714, 1651, 1511, 1429, 1297, 1249, 1166, 1026, 970. HRMS calculated for $C_{28}H_{38}N_2O_{10}P_2$ (M^+) 624.199585, Found (M^+) 624.200173.

Tetraethyl [(1,2,3,4-tetrahydro-6-methyl-2,4-dioxo-1,3-dibenzyl-5-pyrimidinyl)methyl]bisphosphonate (106): An oven dried, Argon purged 25 mL round bottom flask was charged with KVP **100** (1.05 g, 5.1 mmol). The solution was cooled to ~0°C with an ice bath and triethyl phosphite (969 mg, 5.8 mmol) was added slowly. After 2 hours of stirring at ~ 0°C the ice bath was removed, and the reaction stirred at room temperature for 25 hours, at which time ^{31}P-NMR indicated formation of the phosphonooxaphospholene **99**. Benzyl isocyanate (1.62 g, 12.1 mmol) was added and the mixture was stirred at room temperature for 16 hours and subsequently refluxed for 25 hours, at which time ^{31}P-NMR indicated that all of the oxaphospholene had been

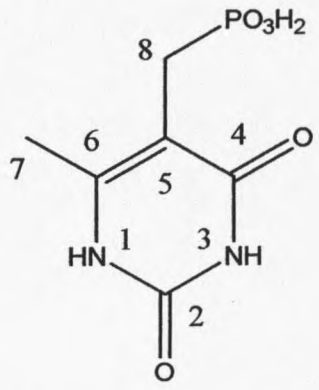
consumed. The reaction was quenched by pouring it into DI-H_2O and the mixture stirred for 1 hour. The mixture was then separated and the aqueous phase was extracted with DCM (5x10 mL). The combined organic layers were filtered through $MgSO_4$ and conc *in vacuo*. The crude product was triturated with water (30 mL) and filtered. The crude product was then taken up in ethanol (25 mL) and treated with ether (10 mL). This solution was filtered and the filtrate was concentrated *in vacuo*. The resulting oil had a ^{31}P-NMR signal at ~20 ppm. The oil was initially purified via column chromatography on silica gel eluting with 3% MeOH/DCM yielding the product as a yellow oil. This material still contained significant contaminants therefore, the oil was further purified via column chromatography on silica gel eluting with 3% MeOH/DCM yielding the product as a pale yellow oil in 3% yield (84 mg, 0.14 mmol).



^{1}H-NMR: 7.40-7.33 (2H, m, H's on C's 19, 23 or C's 26, 30 or C's 20, 22 or 26, 28 or C's 21, 27), 7.29-7.18 (6H, m, H's on C's 19, 23 or C's 26, 30 or C's 20, 22 or 26, 28 or C's 21, 27), 7.08 (2H, bd, J = 6.7 Hz, 5.27 (4H, bs, H's on C's 17, 24), 4.96 (1H, t, $J_{P\text{-}H}$ =

29.5 Hz, H on C8), 4.23-4.05 (8H, m, H's on C's 9, 11, 13,15), 2.54 (3H, bs, H's on C7), 1.31-1.17 (12H, m, H's on C's 10, 12, 14, 16). ^{13}C-NMR: 162.0 (t, J_{P-C} = 5.5 Hz , C4), 153.2 (t, J_{P-C} = 4.6 Hz, C6), 151.6 (C2), 137.9 (C18 or 25), 136.7 (C18 or 25), 129.0 (C21 or 27), 128.7 (C21 or 27), 128.3 (C20 & 22 or C26 & 28), 127.7 (C20 & 22 or C26 & 28), 127.6 (C19 & 23 or C25 & 29), 126.0 (C19 & 23 or C25 & 29), 103.9 (C5), 63.0 (d, J_{P-C} = 26.7 Hz,C9, 11, 13, 15), 48.5 (C17 or 24), 45.7 (C17 or 24), 34.2 (t, J_{P-C} = 137.5 Hz, C8), 19.7 (C7), 16.1 (d, J_{P-C} = Hz, C10, 12, 13, 16). ^{31}P-NMR: 20.1 ppm. HRMS calculated for $C_{28}H_{38}N_2O_8P$ (M+H) 593.219000, Found (M+H) 593.218168.

[(1,2,3,4-tetrahydro-6-methyl-2,4-dioxo--5-pyrimidinyl)methyl]phosphonic acid (108): An oven dried, Argon purged 100 mL round bottom flask was charged with phosphonate **102** (98.3 mg, 0.22 mmol) and dry xylenes (20 mL). The solution was heated to reflux and a solution of boron tribromide (1M, 2 mmol, 2 mL) was added dropwise. The mixture was stirred at reflux for 3 days. The mixture was cooled to room temperature and absolute ethanol (10 mL) was added. The mixture was conc *in vacuo*. Ether (20 mL) and water (20 mL) was added to the residue and stirred for 1 hour. The layers were then separated and the organic layer was extracted with water (2x20 mL). The combined water layers were then conc *in vacuo*. The crude oil was chromatographed on C18-silica gel eluting with 20% acetonitrile/water yielding a white solid, which was recyrstallized from IPA in 89% yield (43 mg, 0.20 mmol), mp 283.4-283.8 °C (Lit mp 282-284 °C).[68]



^{1}H-NMR (DMSO-d6): 10.95 (1H, bs, H on O11), 10.68 (1H, bs, H on O12), 2.65 (2H, d, $J_{P\text{-}H}$ = 20.0 Hz, H's on C8), 2.46 (2H, H's on N1 & N3), 2.05 (3H, d, $J_{P\text{-}H}$ = 2.7 Hz, H's on C7). ^{13}C-NMR (DMSO-d6): 164.3 (C4), 151.1 (C2), 149.8 (d, $J_{P\text{-}C}$ = 7.2 Hz, C6), 102.7 (d, $J_{P\text{-}C}$ = 9.4 Hz, C5), 24.2 (d, $J_{P\text{-}C}$ = 137.1 Hz, C8), 17.2 (C7) Hz,. ^{31}P-NMR (MeOH-d4): 24.9 ppm.

REFERENCES CITED

REFERENCES CITED

. Boger, D. L.; Curran, T. T., *J.Org. Chem.* **1990**, *55*, 5439.

. Serckx-Poncin, B.; Hesbain-Frisque, A.-M.; Ghosez, L., *Tetrahedron Lett.* **1982**, *23*, 261

. Rastogi, R. P., *Indian J. Chem. Sect. A* **1977**, *15*, 941.

. Wittig, G.; Steinhoff, G., *Chem. Ber.* **1962**, *95*, 203.

. (a) Zimmerman, H. E.; Armesto, D, *Chemical Rev.* **1996**, *96*, 3065. (b) Houk, K,, *Chemical Rev.* **1976**, 76, 1. (c) Demuth, M., in "Modern Synthetic Methods". Ed. R. Scheffold, Springer, Berlin, **1986**, *4*, 257. (d) Demuth, M., in "Comprehensive Organic Synthesis Synthesis, Selectivity, Stratagy, & Efficiency in Modern Organic Chemistry", Paquette, L. A. Vol. Ed. Pergamon Press: Oxford. **1991**, 215.

. (a) Singh, V.; Prathap, S; Porinchu, M, *J. Org. Chem.* **1998**, *63*, 4011. (b) Singh, V.; Lahiri, S.; Kane, V. V.; Stey, T.; Stalke, D., *Org. Lett.* **2003**, *5*, 2199. (d) Singh, V., *Acc. Chem. Res.* **1999**, *32*, 324.

. Mehta, G., Sibrahmanyam, D., *J. Chem. Soc. Perkin Trans. 1* **1991**, 395.

. Singh, V.; Samanta, B.; Kane, V. V., *Tetrahedron* **2000**, *56*, 7785.

. Demuth, M.; Hinsken, W., *Helv. Chim. Acta.* **1988**, *71*, 569.

0. McClure, C. K.; Kiessling, A. K.; Link, J. S., *Org. Lett.* **2003**, *5*, 3811.

1. Link, J. S., "Novel Synthetic Methodologies: Radical and Photochemical Approaches Towards Alkaloids. Diels-Alder Methology Towards Inositol Derivatives", *Ph. D. dissertation* Montana State University, **2000**.

24. Private communication with Daniel Comins.

25. Ahond, A.; Cave, A.; Kan-Fan, C.; Husson, J.-P.; De Rostolan, J.; Potier, P., *J. Am. Chem. Soc.* **1968**, *90*, 5622.

26. Comins, D. L.; Hong, H., *J. Org. Chem.* **1993**, *58*, 5035.

27. Comins, D. L.; Dehghani, A., *Tetrahedron Lett.* **1991**, *32*, 5697.

28. Comins, D. L.; Hong, H., *J. Amer. Chem. Soc.* **1993**, *115* 8851.

29. Comins, D. L.; Foley, M. A., *Tetrahedron Lett.* **1988**, *29*, 6711.

30. Raucher, S.; Macdonald, J. E., *Syn. Comm.* **1980**, *10*, 325.

31. Yamada, H,; Aoyagi, S.; Kibayashi, C.; *Tetrahedron Lett*, **1996**, *37*, 8787.

32. Schell, F. M.; Williams, P. R., *Syn. Comm.* **1982**, *12*, 755.

33. Comins, D. L.; Chung, G.; Foley, M. A., *Heterocycles* **1994**, *37*, 1121.

34. Chen, C.; Munoz, B., *Tetrahedron Lett.* **1999**, *40*, 3491.

35. Comins, D. L.; Joseph, S. P.; Goehring, R. R., *J. Am. Chem. Soc.* **1994**, *116*, 4179.

36. Meerwein, H., *Org. Syn. Coll. Vol. 5*, Baumgartenm H. E., Ed.; John Wiley & Sons: New York. **1973**, p 1080.

37. Grieco, P. A.; Nunes, J. J.; Gaul, M. D.; *J. Am. Chem. Soc.* **1990**, *112*, 4595.

38. Streith, J.; Boiron, A.; Paillaud, J.-L; Rodriguez-Perez, E.-M.; Strehler, C.; Tschamber, T.; Zehnder, M., *Helvetica Chimica Acta* **1995**, *78*, 61

39. Chen, C.; McDonald, I. A.; Munoz, B., *Tetrahedron Lett.* **1998**, *39*, 217.

40. Haider et al.; *Helv.Chim.Acta 1975, 58*, 1287.

41. Dauben, W. G.; Kellog, M. S.; Seeman, J. I.; Spitzer, W. A., *J. Am. Chem. Soc.* **1970**, *92*, 1786.

42. Schuster, D. I.; Underwood, G. R.; Knudsen, T. P., *J. Am. Chem. Soc.* **1971**, *93*, 4306.

43. Houk, K. N.; Northington, D. J.; Duke, R. E., *J. Am. Chem. Soc.* **1972**, *94*, 6235.

44. Wilsey, S.; Bearpark, M. J.; Bernardi, F.; Oluvucci, M.; Robb, M. A., *J. Am. Chem. Soc.* **1996**, *118*, 176.

45. Koch, W.; Holthausen, M. C., *A Chemists Guide to Density Functional Theory*; Wiley-VCH: Weinheim, **2000**.

46. Roothan, C. C. H., *Rev. Mod. Phys.* **23**, 69 (1951). (b) Pople, J. A.; Nesbet, R. K., *J. Chem. Phys.* **22**, 571-574 (1954). (c) R. McWeeny and G. Dierksen, *J. Chem. Phys.* **49**, 4852 (1968).

47. Kohn, W.; Sham, L. J., *Physical Review* **1965**, *140*, A1133.

48. Post-SCF methods operate on the HF Wavefunction to add electron correlation, such as in the Moller-Plessett perturbative methods, see reference 64.

49. Szabo, A.; Ostlund, N. S.; "Modern Quantum Chemsitry", Dover Publications Inc., Mineola, NY. **1989**.

50. Becke, A. D., *J. Chem. Phys.* **1993**, *98*, 5648.

51. Ziegler, T.; Rauk, A.; Baerends, E. J., *Theor. Chim. Acta.* **1977**, *43*, 261.

52. Casida, M. E.; Jamorski, C.; Casida, K. C.; Salahub, D. R., *J. Chem. Phys.* **108**, 4439 (1998).

53. Mulliken, R. S., *J. Chem. Phys.* **1955**, *23*, 1833.

54. Foster, J. P.; Weinhold, F., *J. Am. Chem. Soc.* **1980**, *102*, 7218.

55. Frisch, M. J.; Trucks, G. W.; Schlegel, H. B.; Scuseria, G. E.; Robb, M. A.; Cheeseman, J. R.; Zakrezewski, V. G.; Montgomery, J. A. J.; Stratmann, R. E.; Burant, J. C.; Dapprich, S.; Millam, J. M.; Daniels, A. D.; Kudin, K. N.; Strain, M. C.; Farkas, O.; Tomasi, J.; Barone, V.; Cossi, M.; Cammi, R.; Mennucci, B.; Pomelli, C.; Adamo, C.; Clifford, S.; Ochterski, J.; Petersson, G. A.; Ayala, P. Y.; Cui, Q.; Morokuma, K.; Malick, D. K.; Rabuck, A. D.; Raghavachari, K.; Foresman, J. B.; Cioslowski, J.; Ortiz, J. V.; Stefanov, B. B.; Liu, G.; Liashenko, A.; Piskorz, P.; Komaromi, I.; Gumperts, R.; Martin, R. L.; Fox, D. J.; Keith, T.; Al-Laham, M. A.; Peng, C. Y.; Nanayakkara, A.; Gonzalez, C.; Challacombe, M.; Gill, P. M. W.; Johnson, B.; Chen, W.; Wong, M. W.; Andres, J. L.; Head-Gordon, M.; Replogle, E. S.; Pople, J. A., *Gaussian 98; Revision A.1* ed.; Gaussian, Inc.: Pittsburgh, PA. **1998**.

56. Spartan '02, Wavefunction Inc., Irvine, CA.

57. Dunning, T. H., *J. Chem. Phys.* **1989**, *90*, 1007.

58. Turro, N. J., *Modern Molecular Photochemsitry*, University Science Books: Sausilito, CA. **1991**, 557.

59. (a) Moller, C.; Plessett, M.S., *Phys. Rev.* **1934**, *46*, 618. (b) Hehre, W. J.; Radom, L.; Schleyer P. v.R; Pople, J. A. *Ab Initio Molecular Orbital Theory*, Wiley, New York, **1985**.

60. Pople, J.A.; Head-Gordon, M.; Raghavachari,K., *J. Chem. Phys.* **87**, 5968 (1987).

61. (a) Fleisch, H.; Russell, R. G. G.; Bisaz, S.; Casey, P. A.; Mühlbauer, R. C., *Calcif. Tissue. Res.* 2:10–10A, **1968**. (b) Fleisch, H.; Russell, R, G. G.; Straumann, F., *Nature* **1966**, 901.

62. (a) McClure, C. K.; Jung, K.-Y.; Grote, C. W.; Hansen, K., *Phosphorus, Sulfur Silicon Relat.Elem.* **1993**, *75*, 23. (b) Grote, C. W. "Electrophilic Condensation Reactions of Pentacovalent Oxaphospholenes and Pseudorotation Studies of Pentacovalent Spirophospholenes", *Ph. D. dissertation* University of Delaware, **1991**.

63. McClure, C. K.; Grote, C. W., *Tetrahedron Lett.* ***1991,*** *32*, 5313-5316.

64. Easton, C. J.; Love, S. G.; Wang, Peng, *J. Chem. Soc. Perkin Trans.1* **1990**, 2, 277.

65. Kundu, N. G.; Hertzberg, R. P.; Hannon, S. J., *Tetrahedron Lett.* **1980**, *21*, 1109.

66. McClure, C. K.; Cai, B. Z., unpublished results.

67. Shaw, E. *J. Am. Chem. Soc.* **1958**, *80*, 3899.

68. Wasil'ewa, *Zh. Obshch .Khim.* **1958**, *28*; 1063.

APPENDICIES

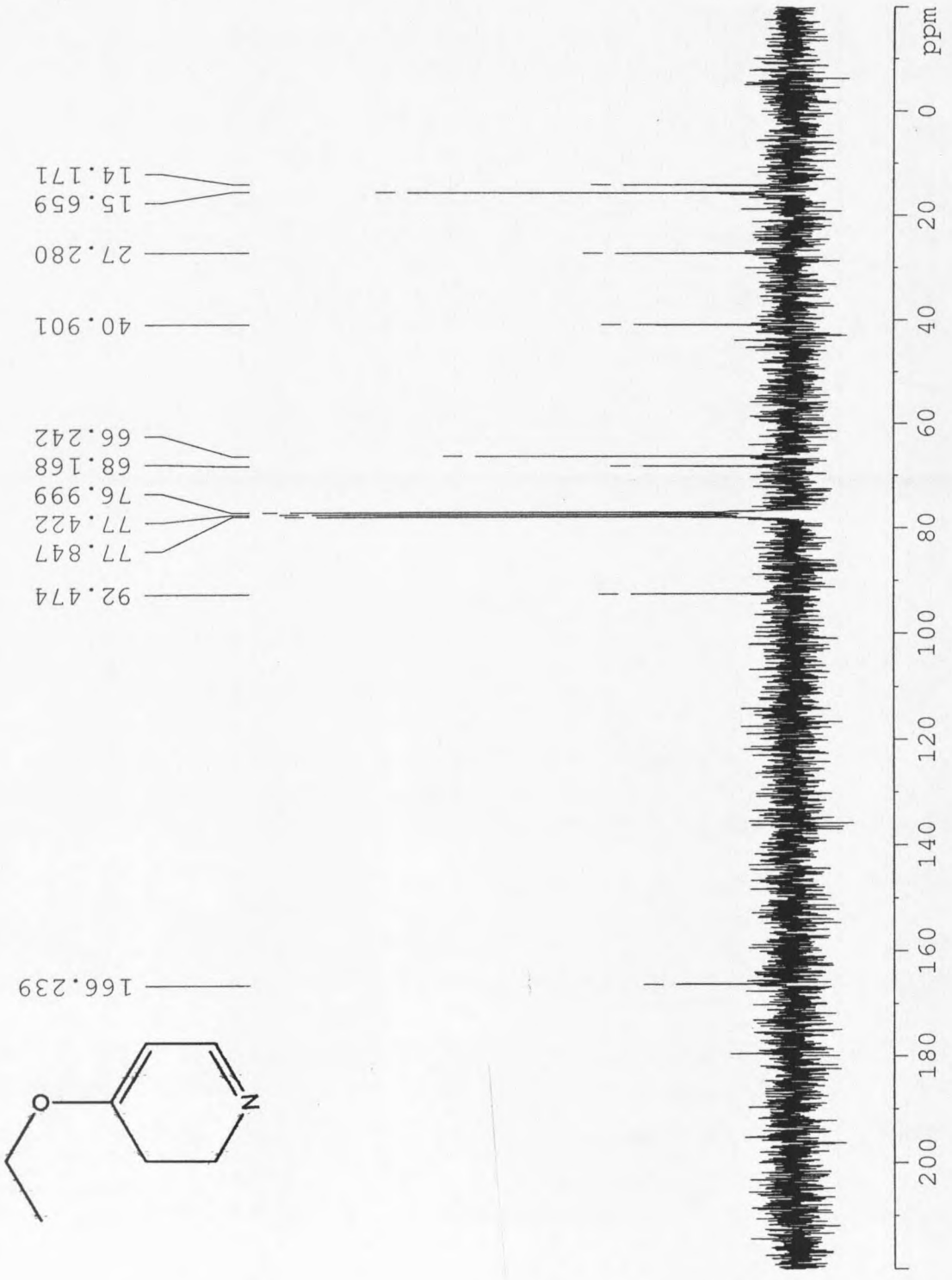
APPENDIX A

NMR Spectra 2,3-Dihydropyridine **1**

^{1}H-NMR Spectrum of 1



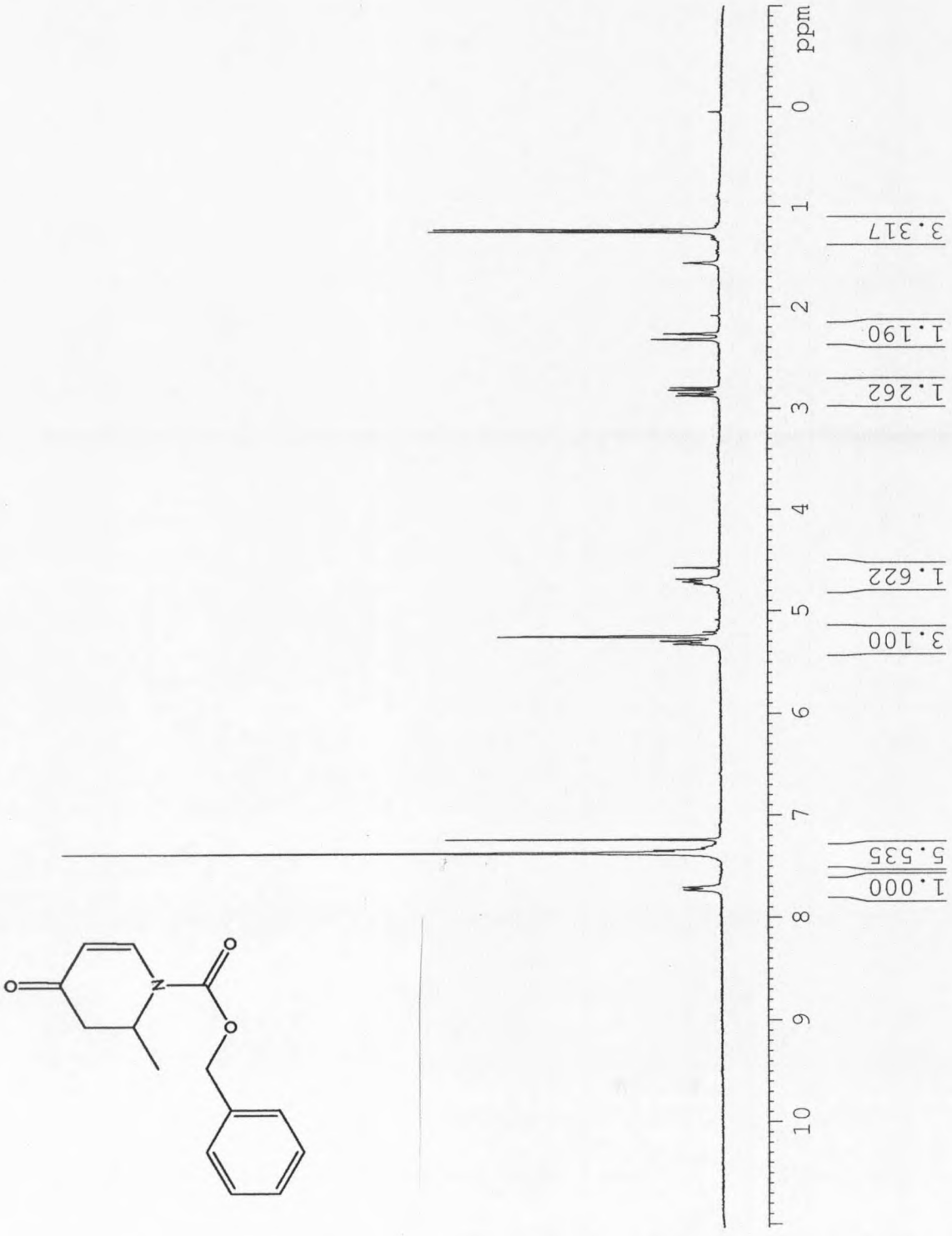
^{13}C-NMR Spectrum of **1**



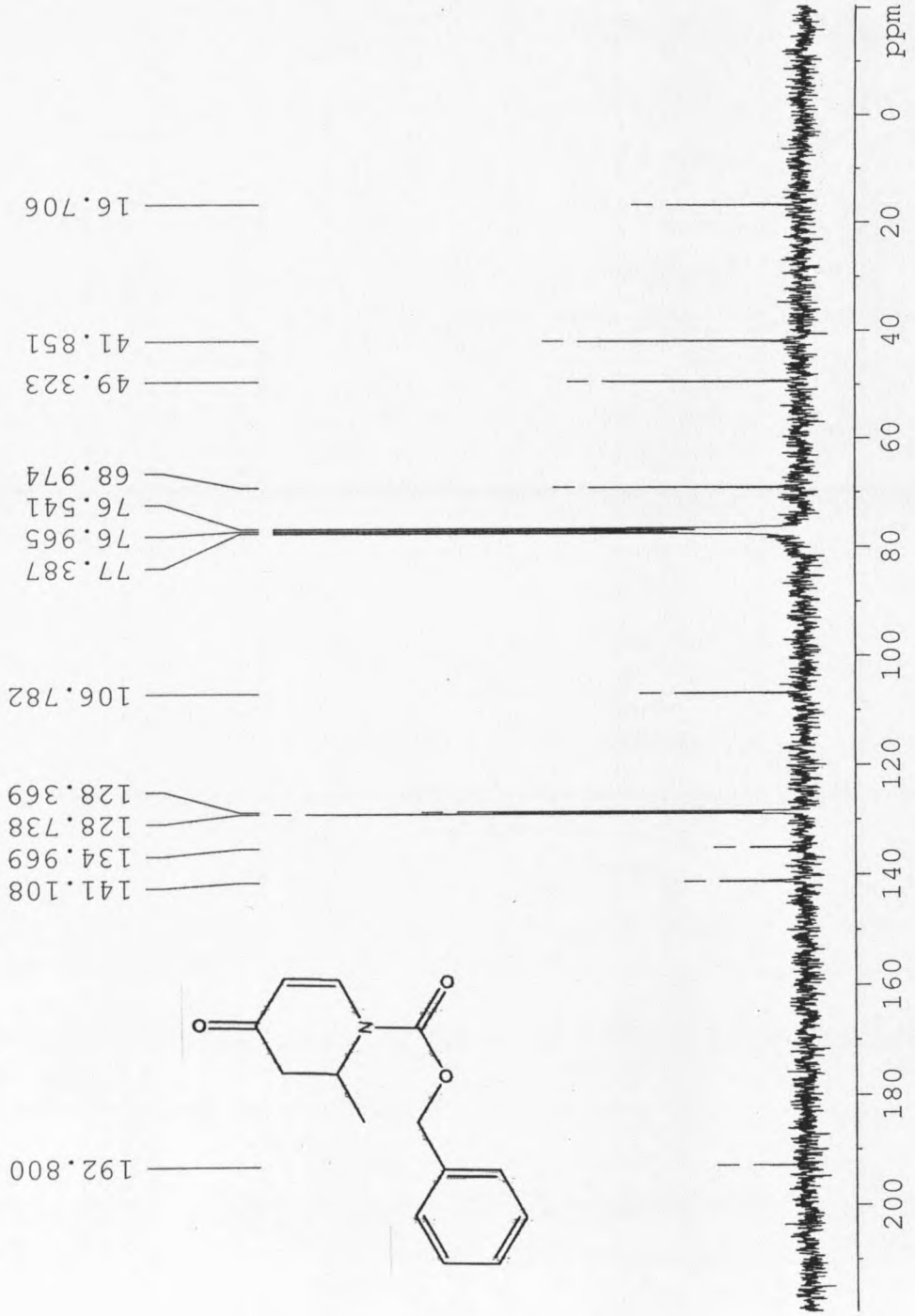
APPENDIX B

NMR Spectra of 2,3-Dihydropyridone **49**

^{1}H-NMR Spectrum of 49



^{13}C-NMR Spectrum of 49



APPENDIX C

NMR Spectra of 2,3-Dihydropyridone **55**

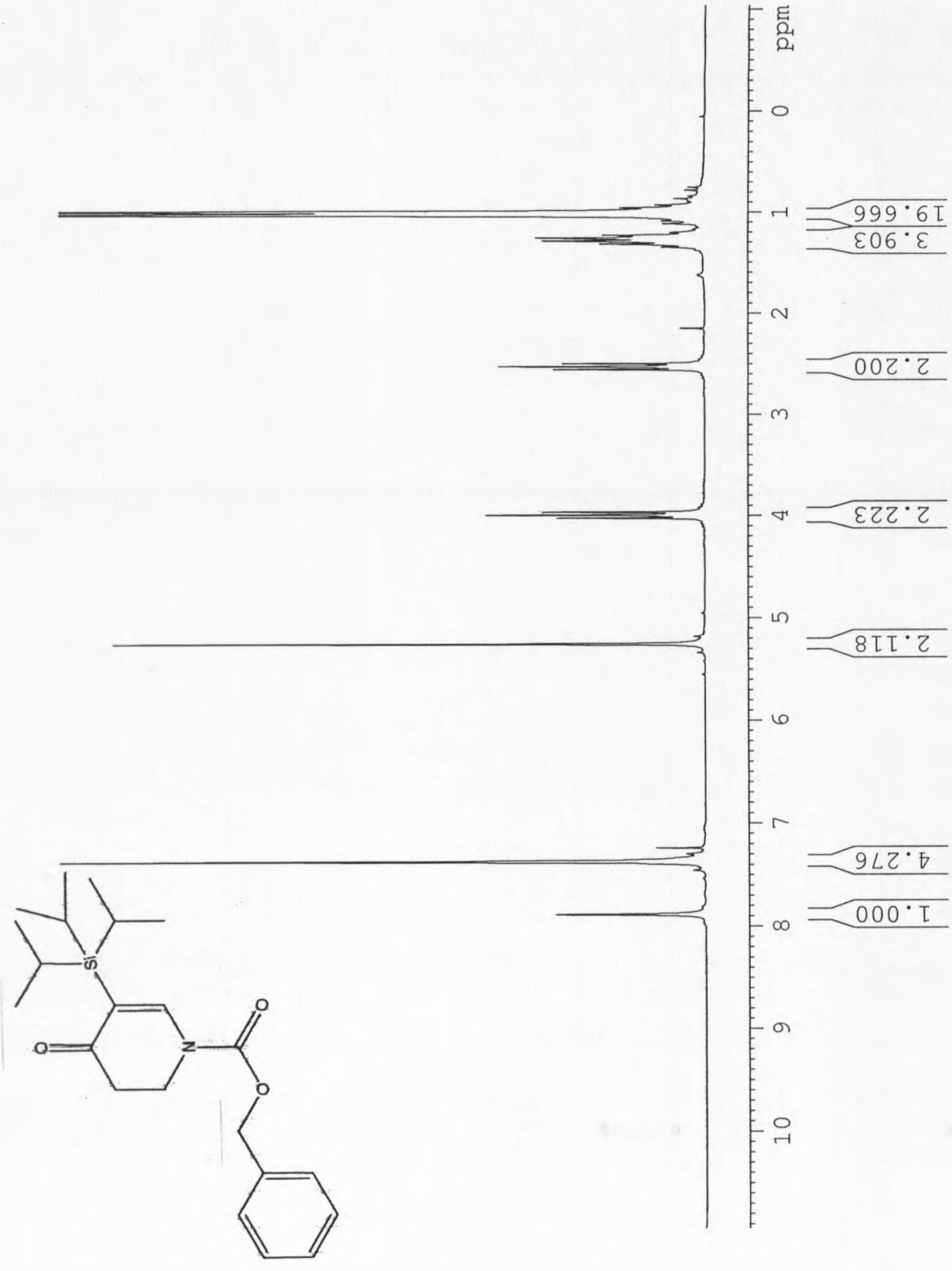
^{1}H-NMR Spectrum of **55**



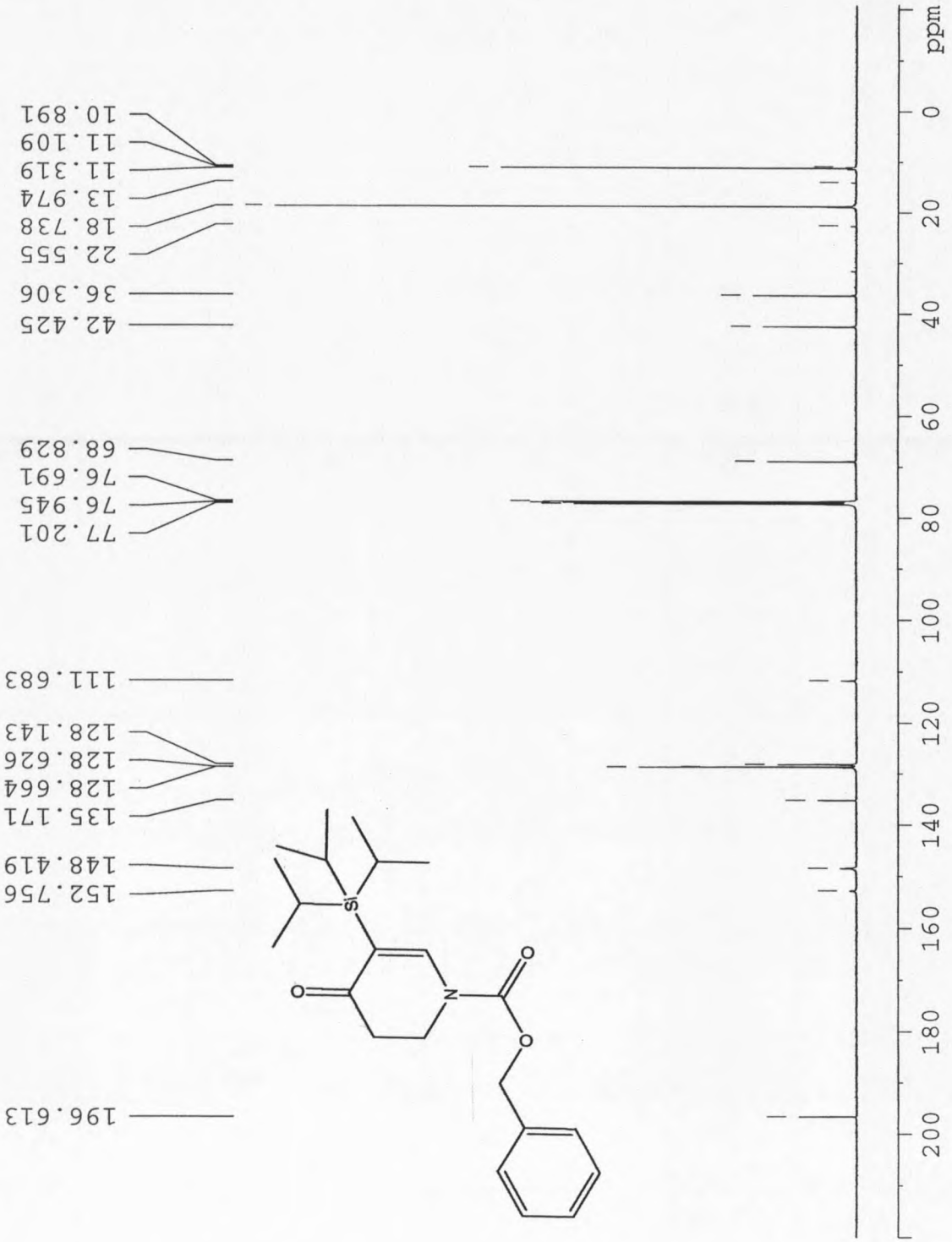
APPENDIX D

NMR Spectra of 2,3-Dihydropyridone **57**

^{1}H-NMR Spectrum of 57



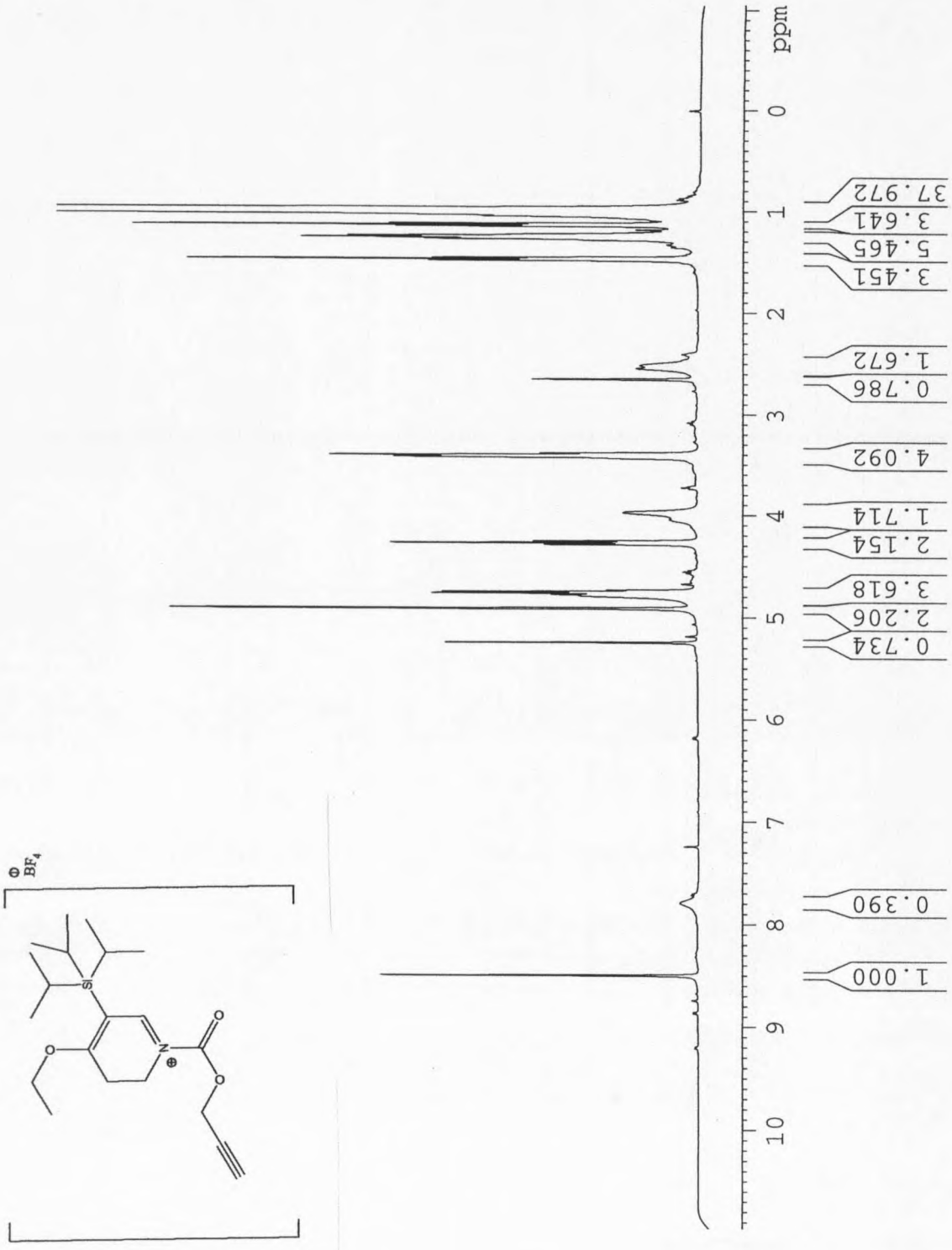
^{13}C-NMR Spectrum of 57



APPENDIX E

^{1}H-NMR Spectrum of 2,3-Dihydropyridinium salt **58**

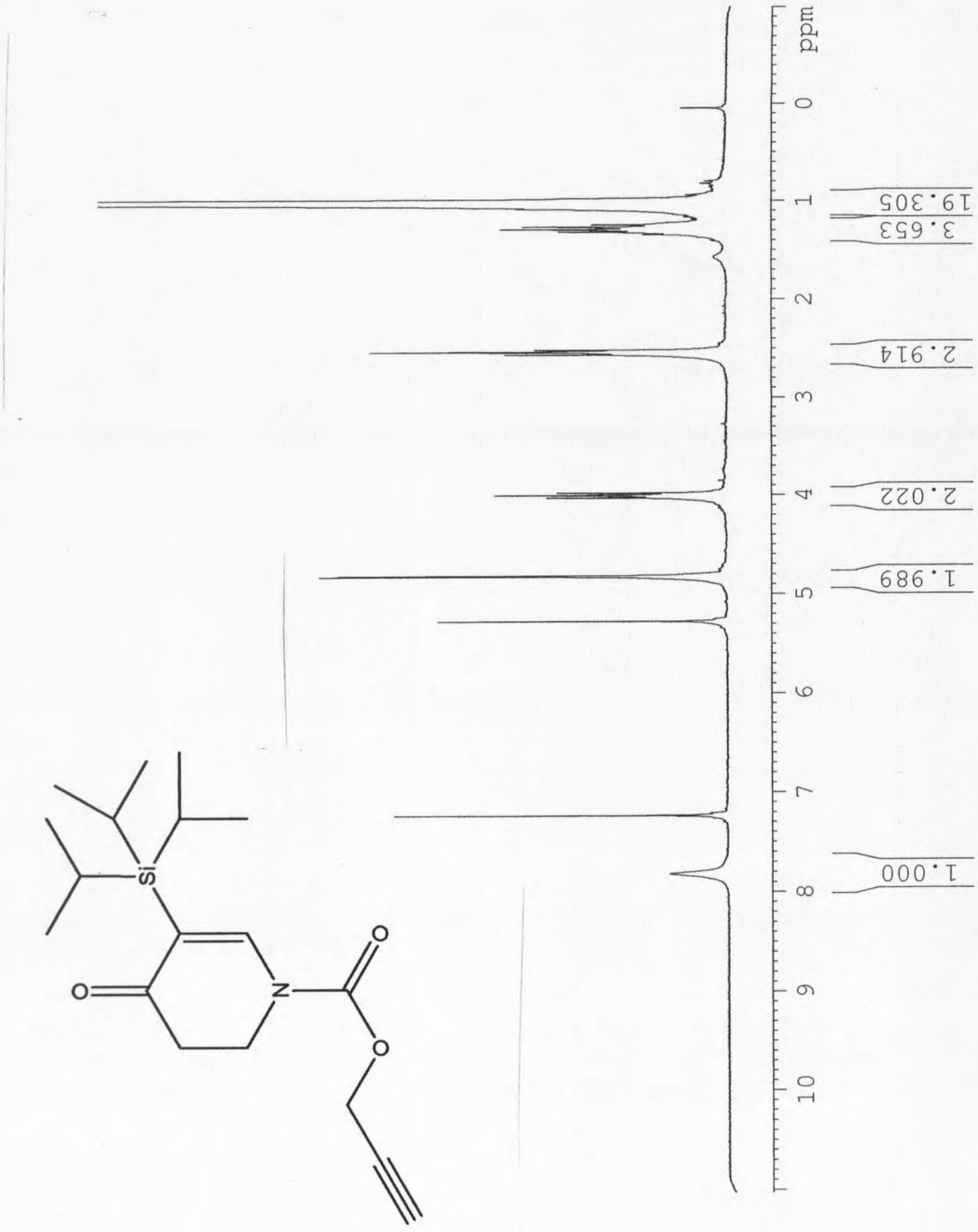
^{1}H-NMR Spectrum of 58



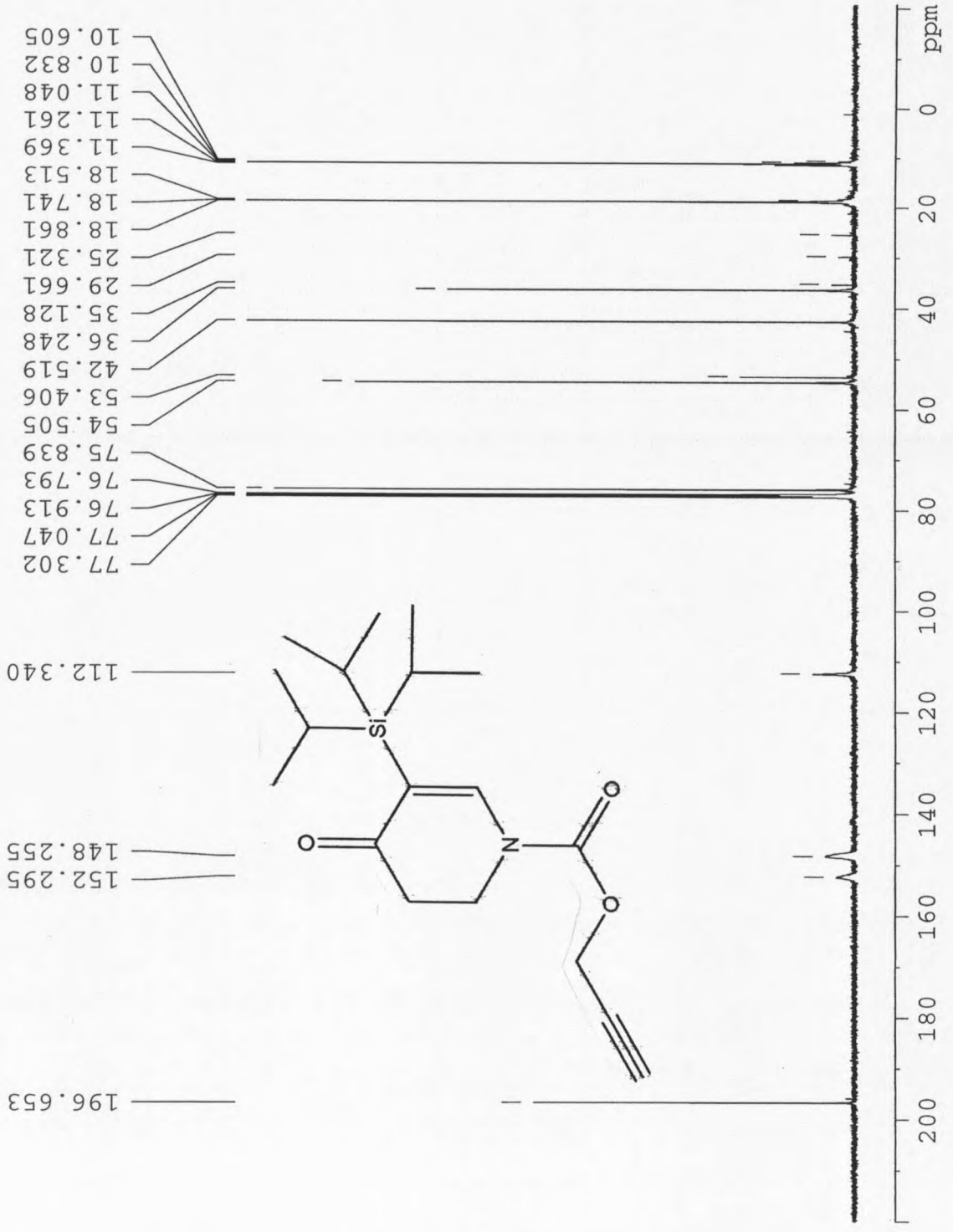
APPENDIX F

NMR Spectra of 2,3-Dihydropyridone **60**

^{1}H-NMR Spectrum of 60



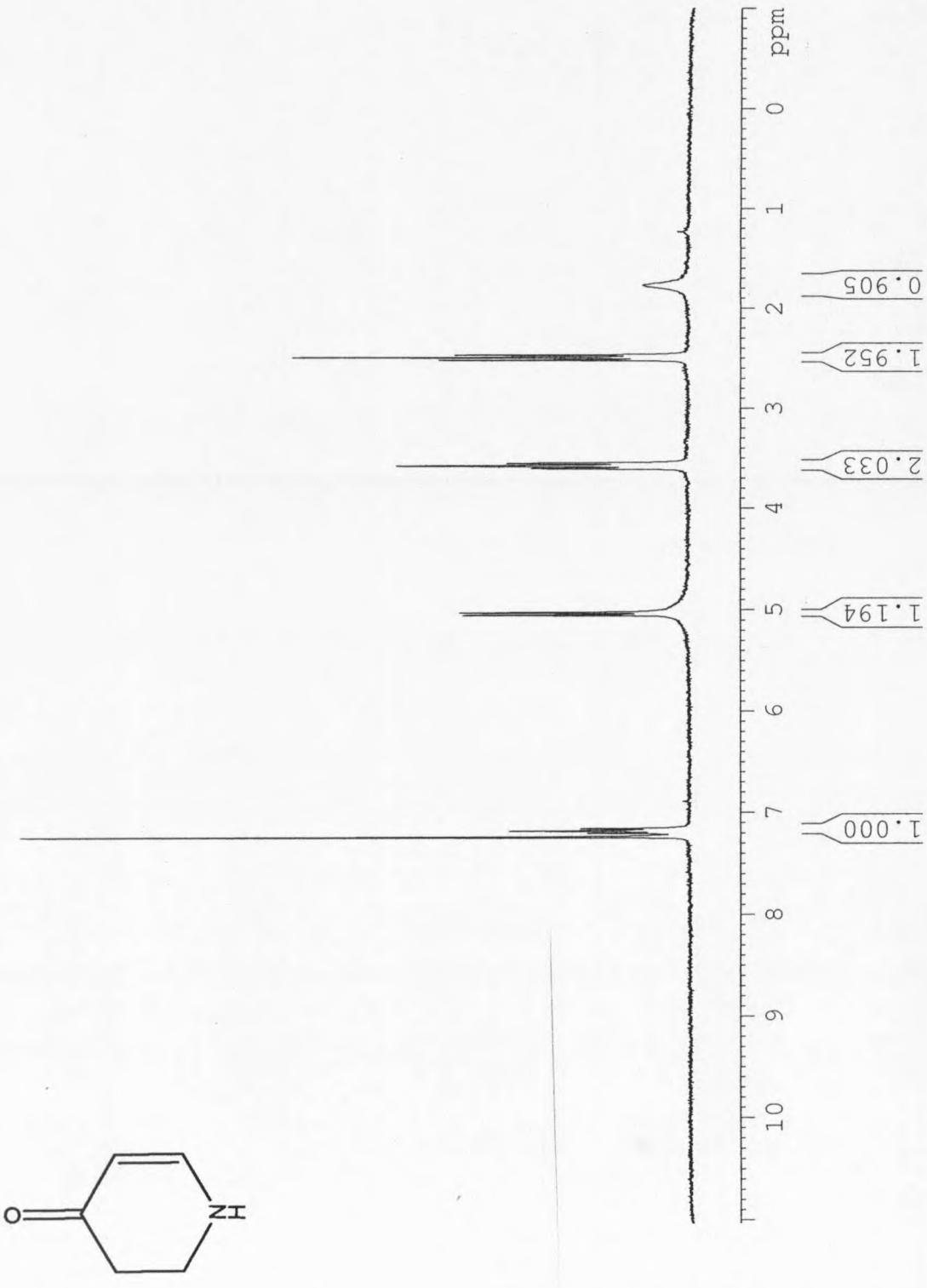
^{13}C-NMR Spectrum of 60



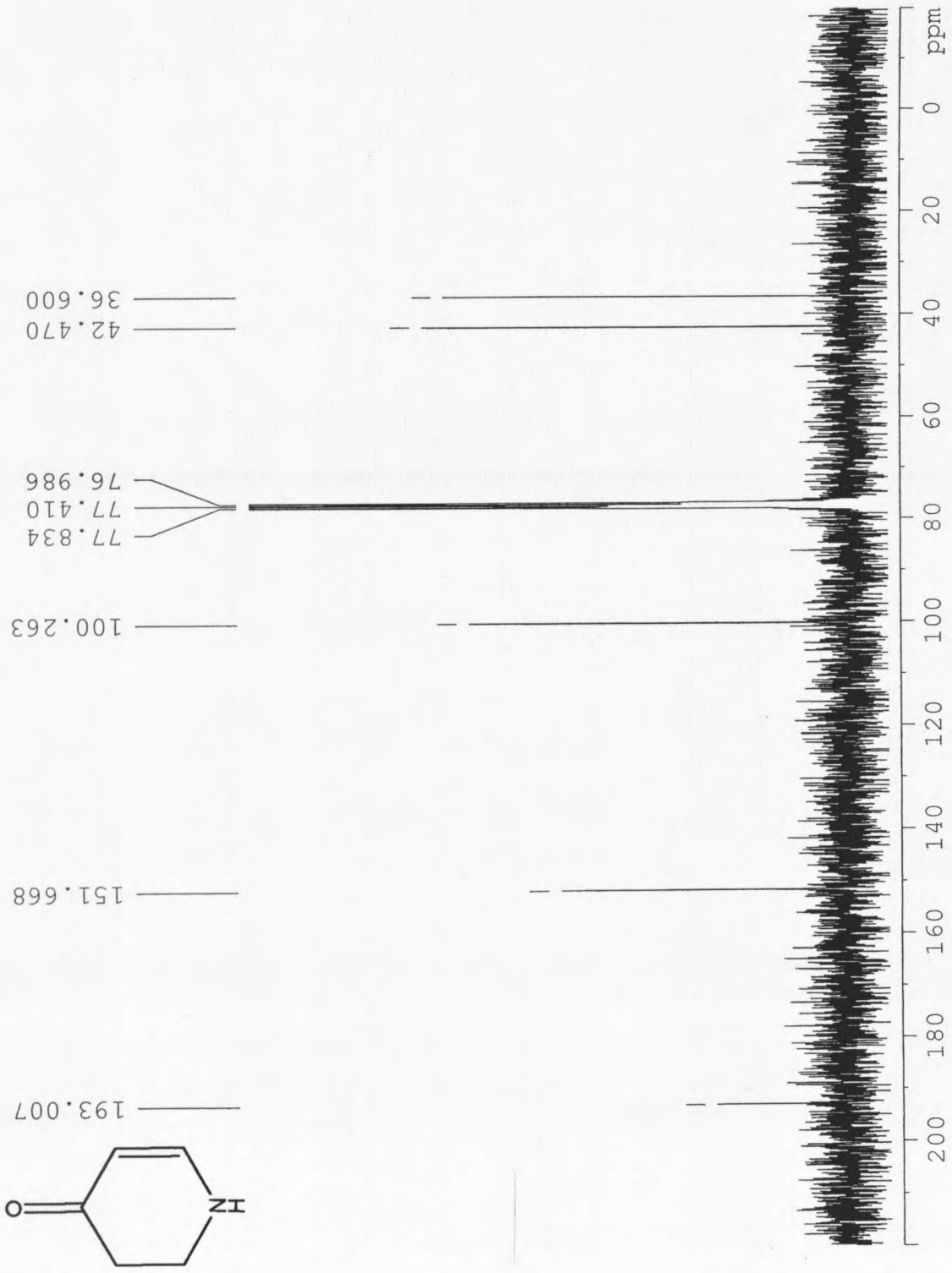
APPENDIX G

NMR Spectra of 2,3-Dihydropyridone **61**

^{1}H-NMR Spectrum of 61



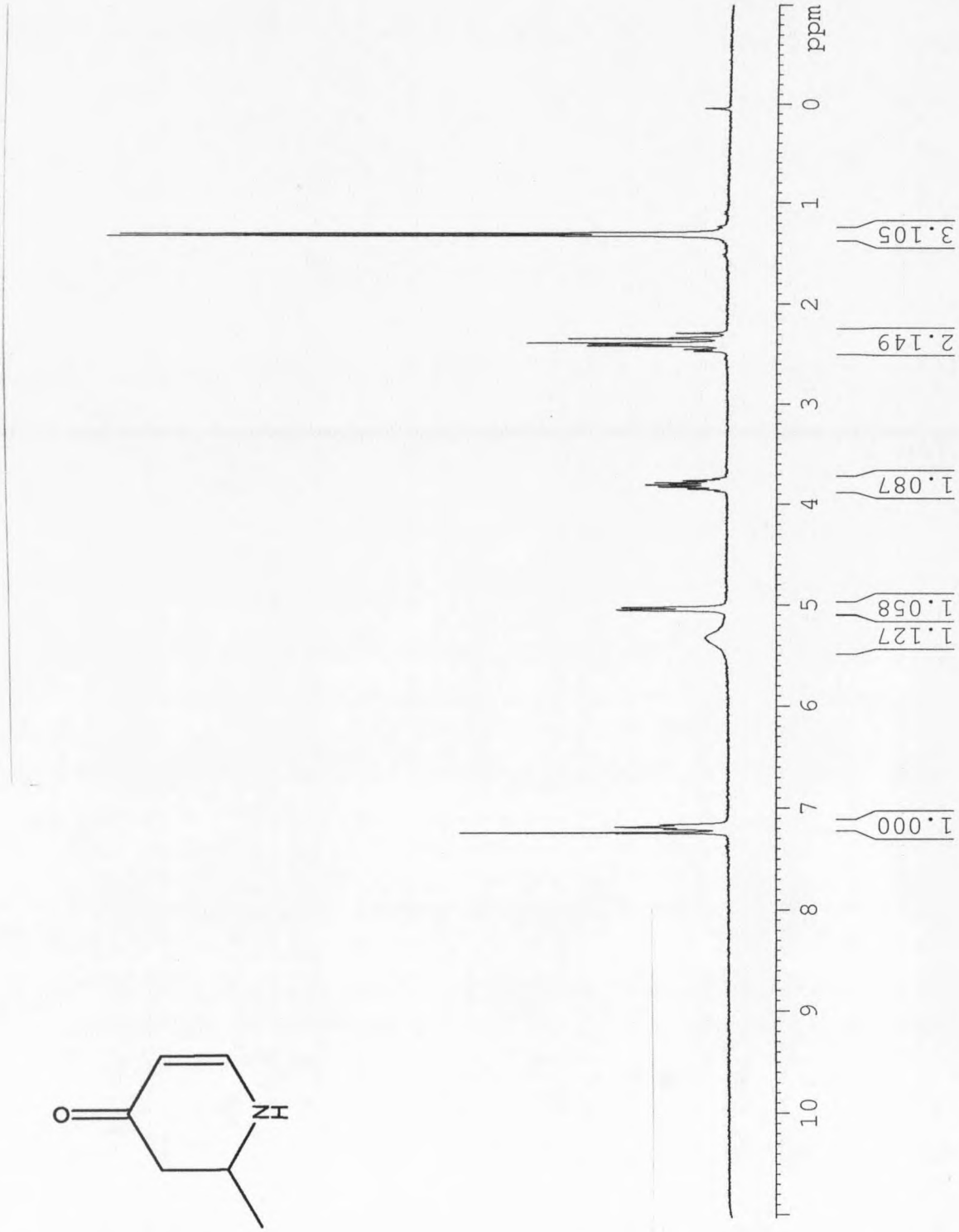
^{13}C-NMR Spectrum of 61



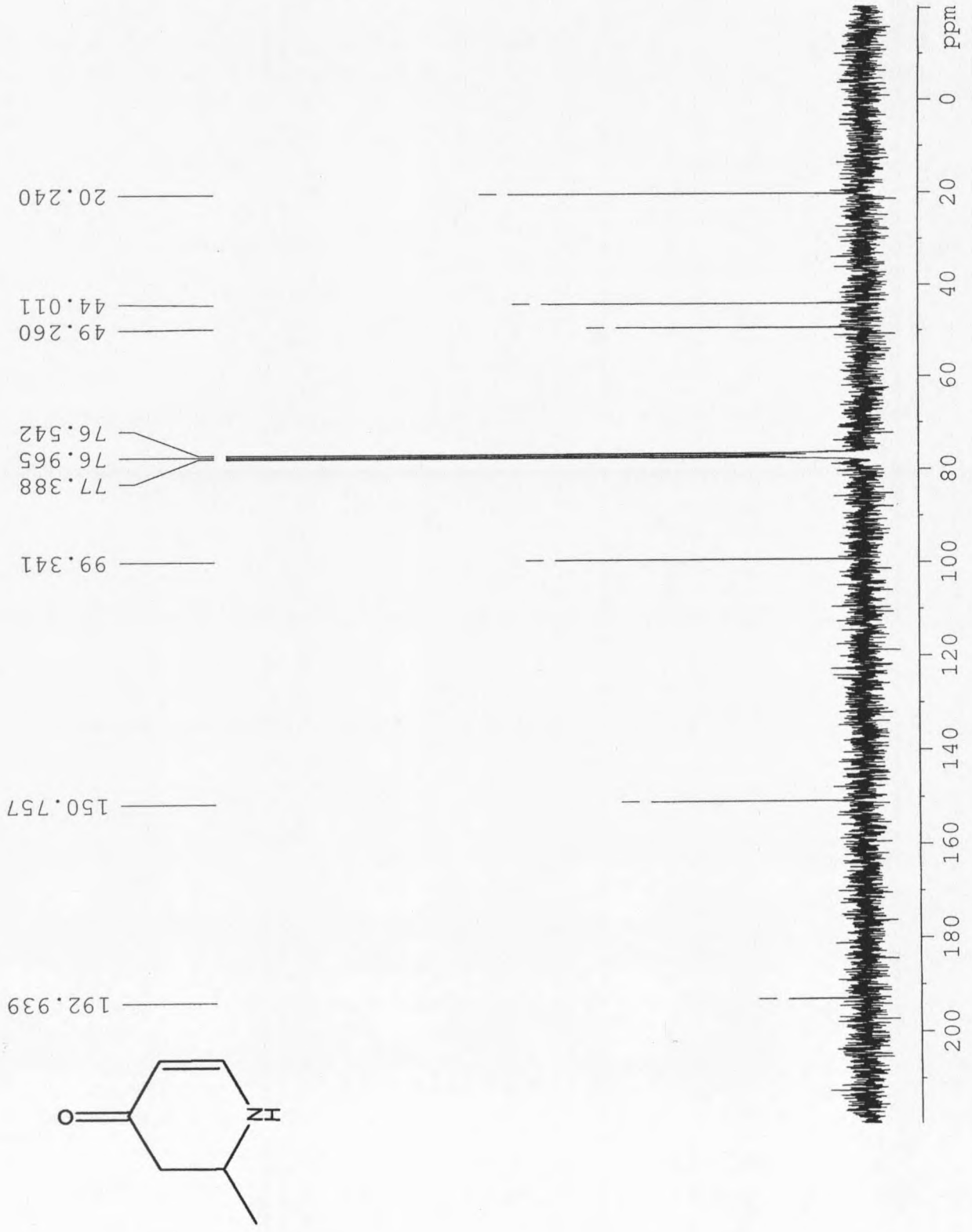
APPENDIX H

NMR Spectra of 2,3-Dihydropyridone **62**

^{1}H-NMR Spectrum of 62



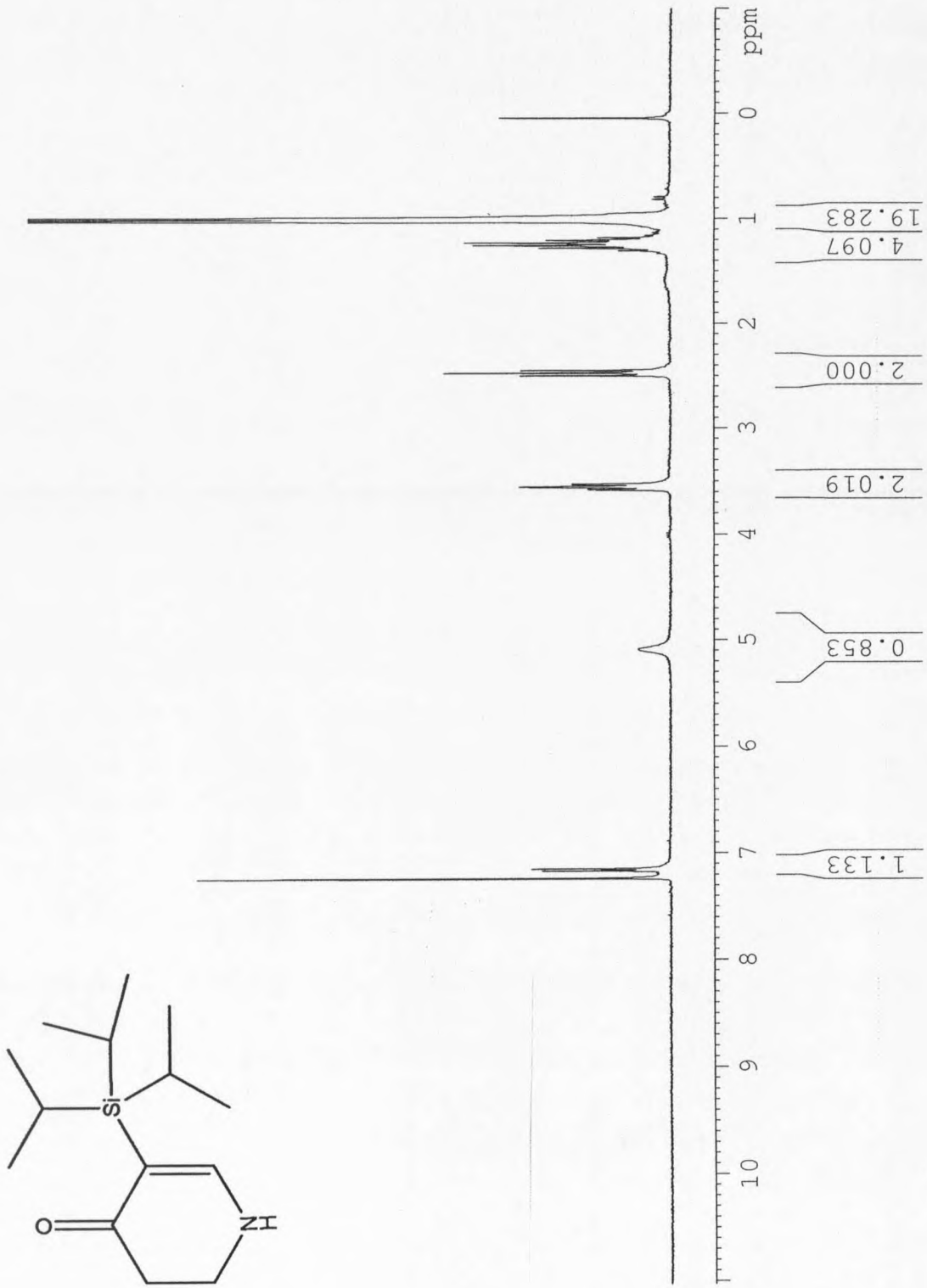
^{13}C-NMR Spectrum of 62



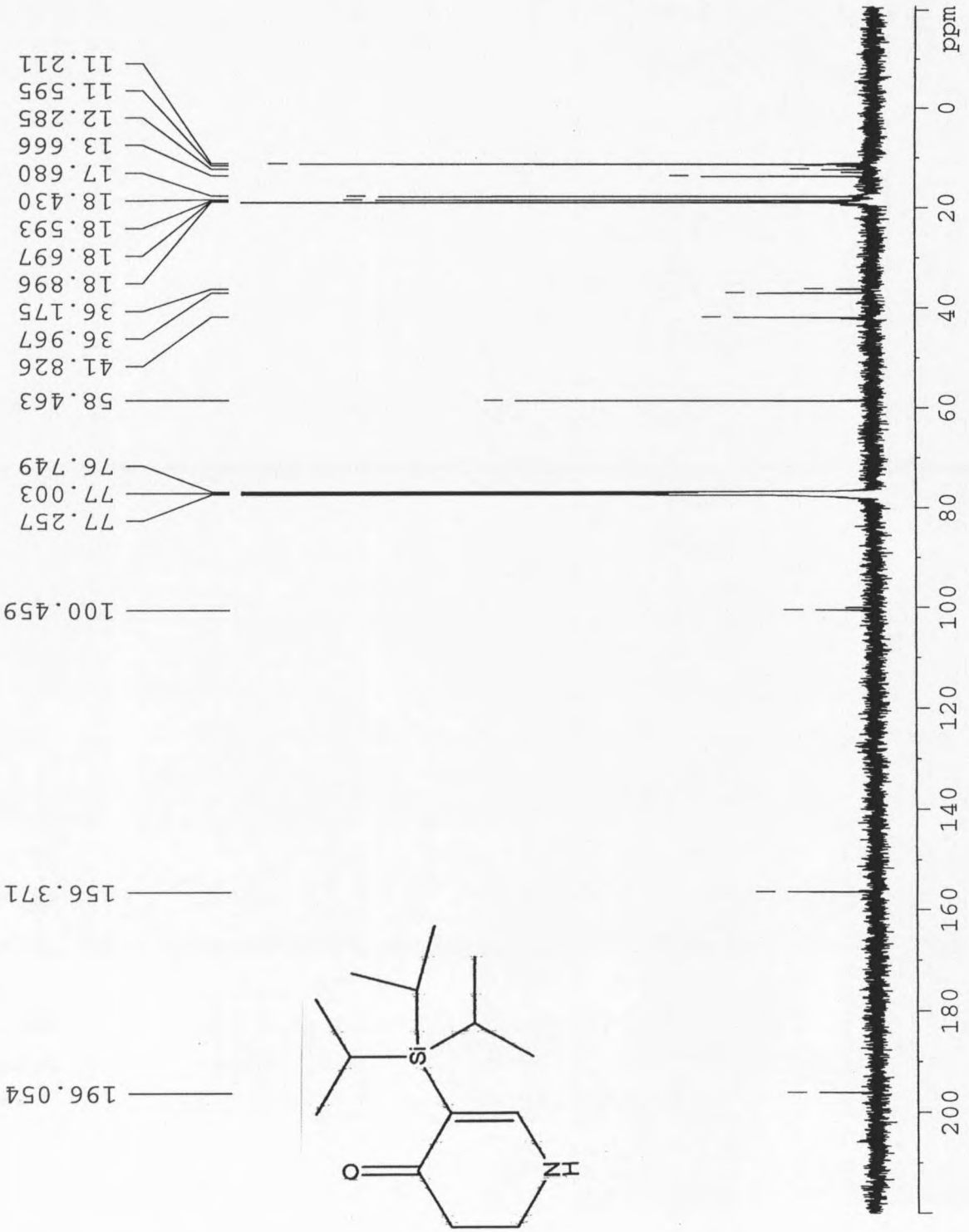
APPENDIX I

NMR Spectra of 2,3-Dihydropyridone **63**

^{1}H-NMR Spectrum of 63



^{13}C-NMR Spectrum of 63



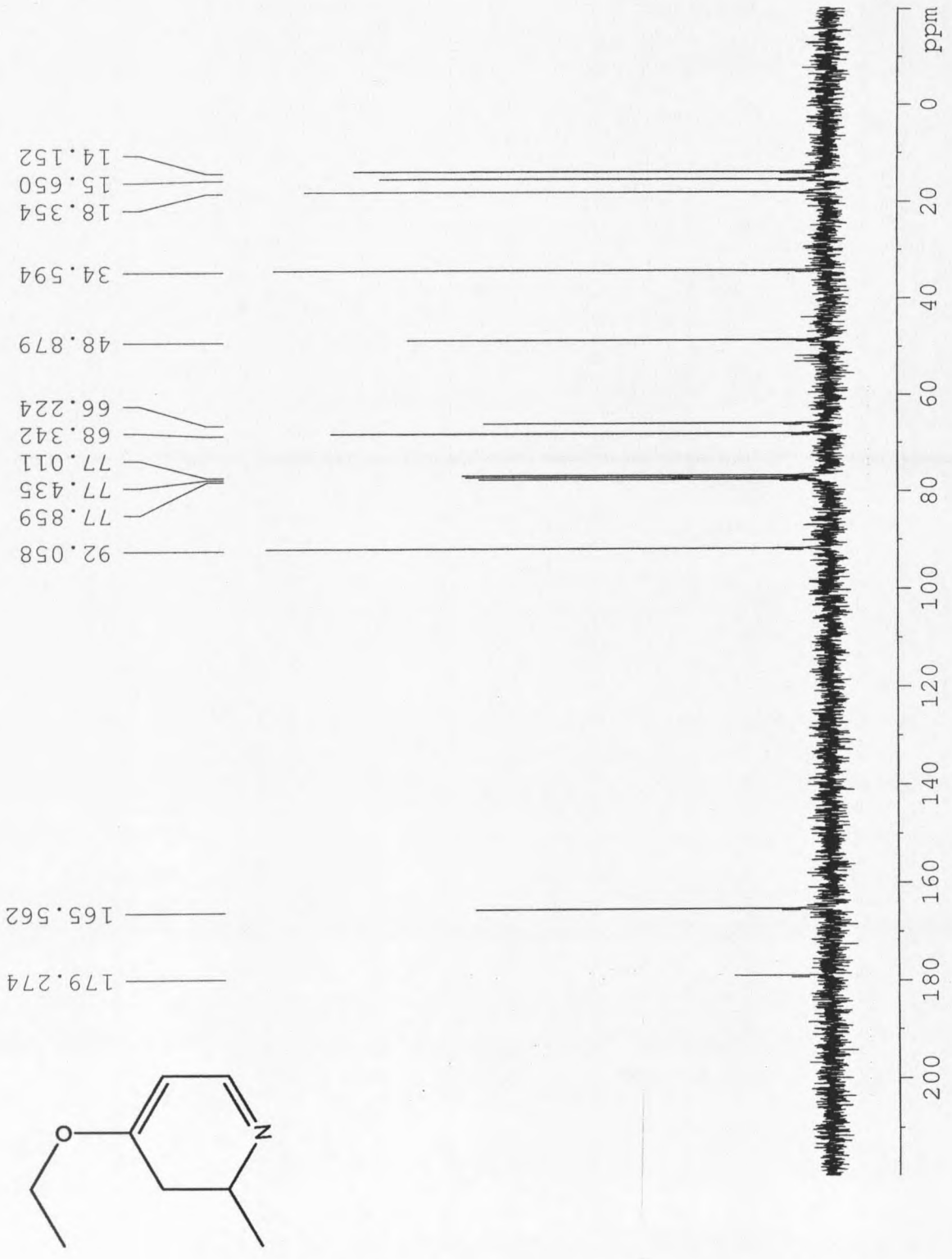
APPENDIX J

NMR Spectra of 2,3-Dihydropyridine **64**

^{1}H-NMR Spectrum of 64



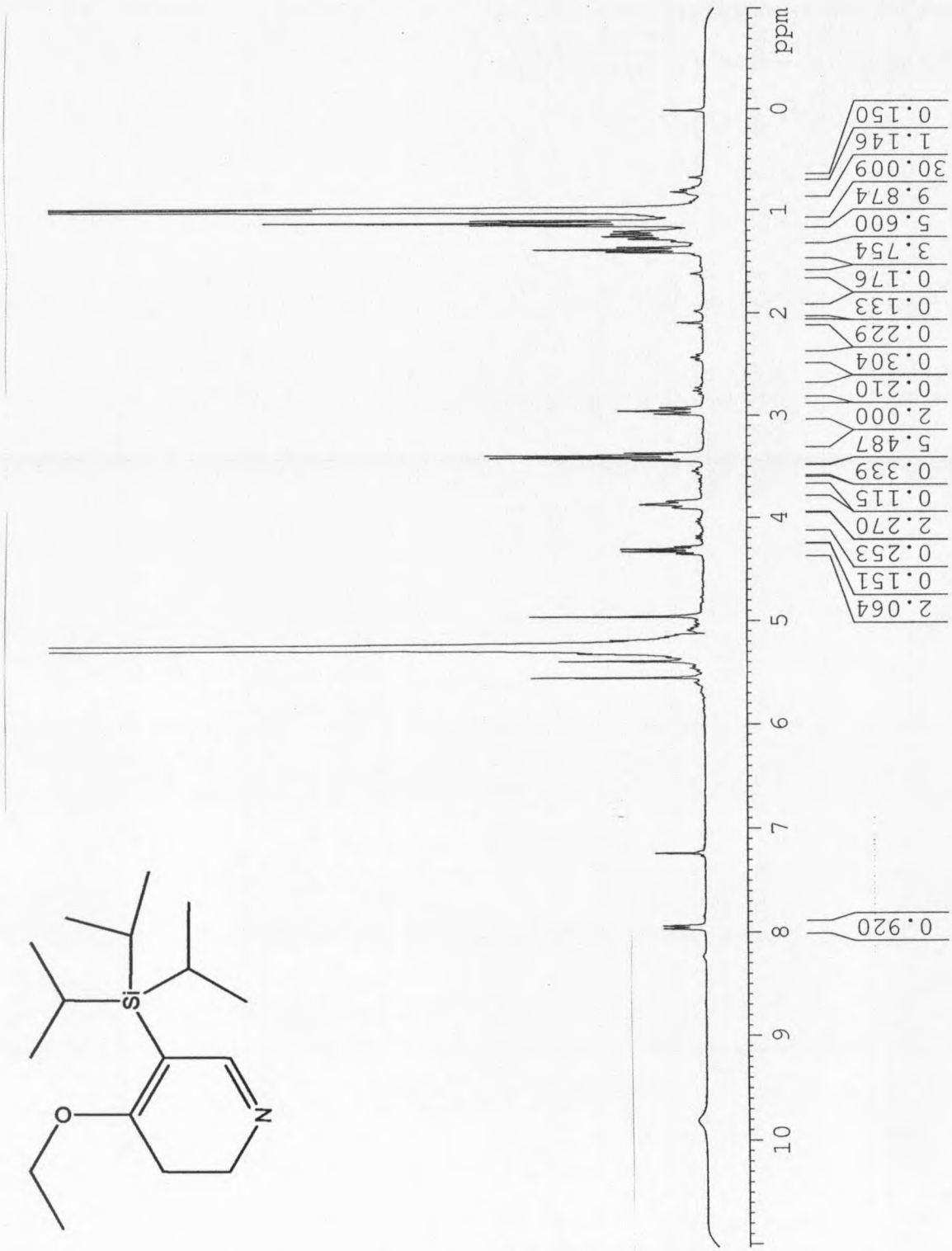
^{13}C-NMR Spectrum of 64



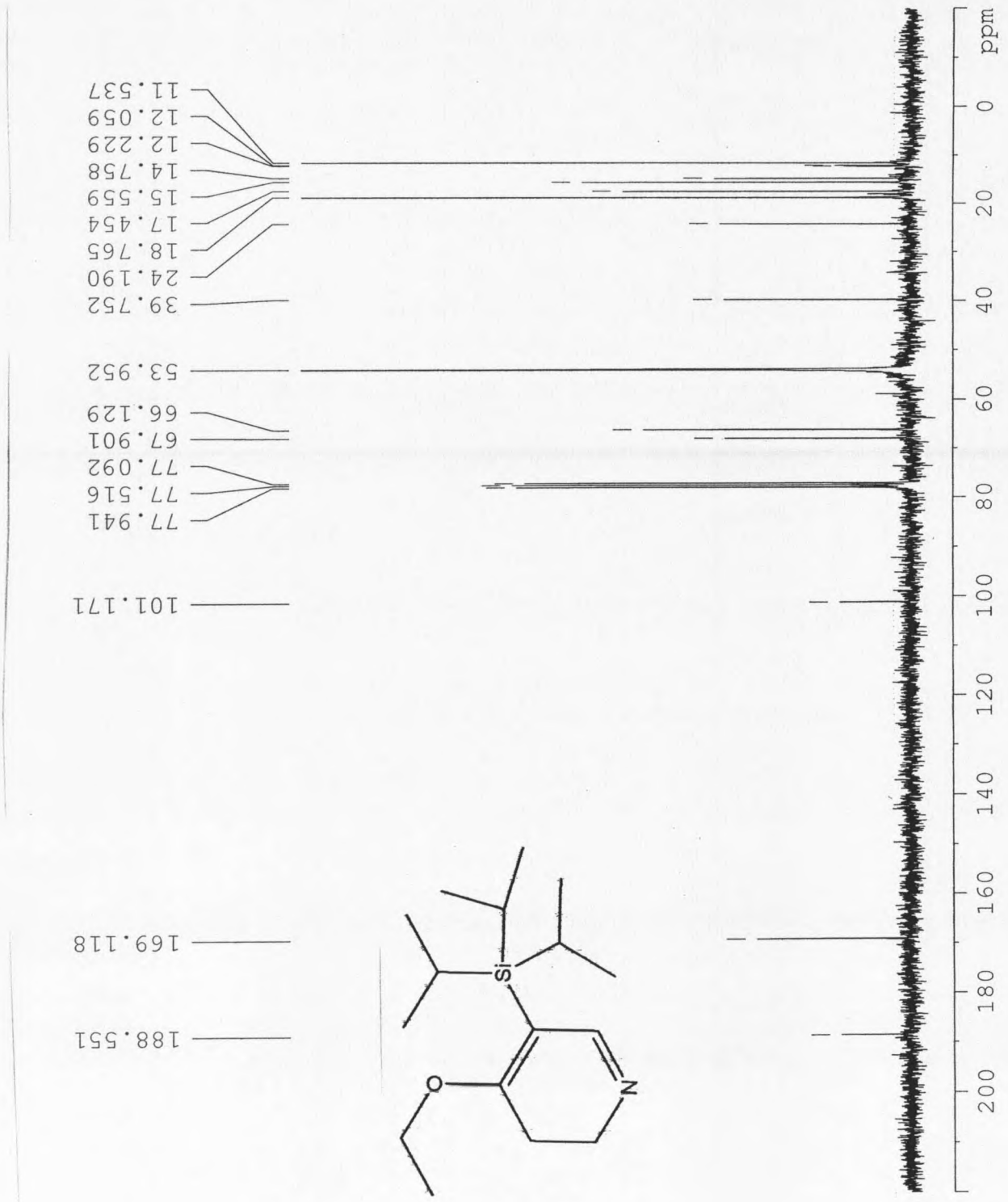
APPENDIX K

NMR Spectra of 2,3-Dihydropyridine **65**

^{1}H-NMR Spectrum of 65



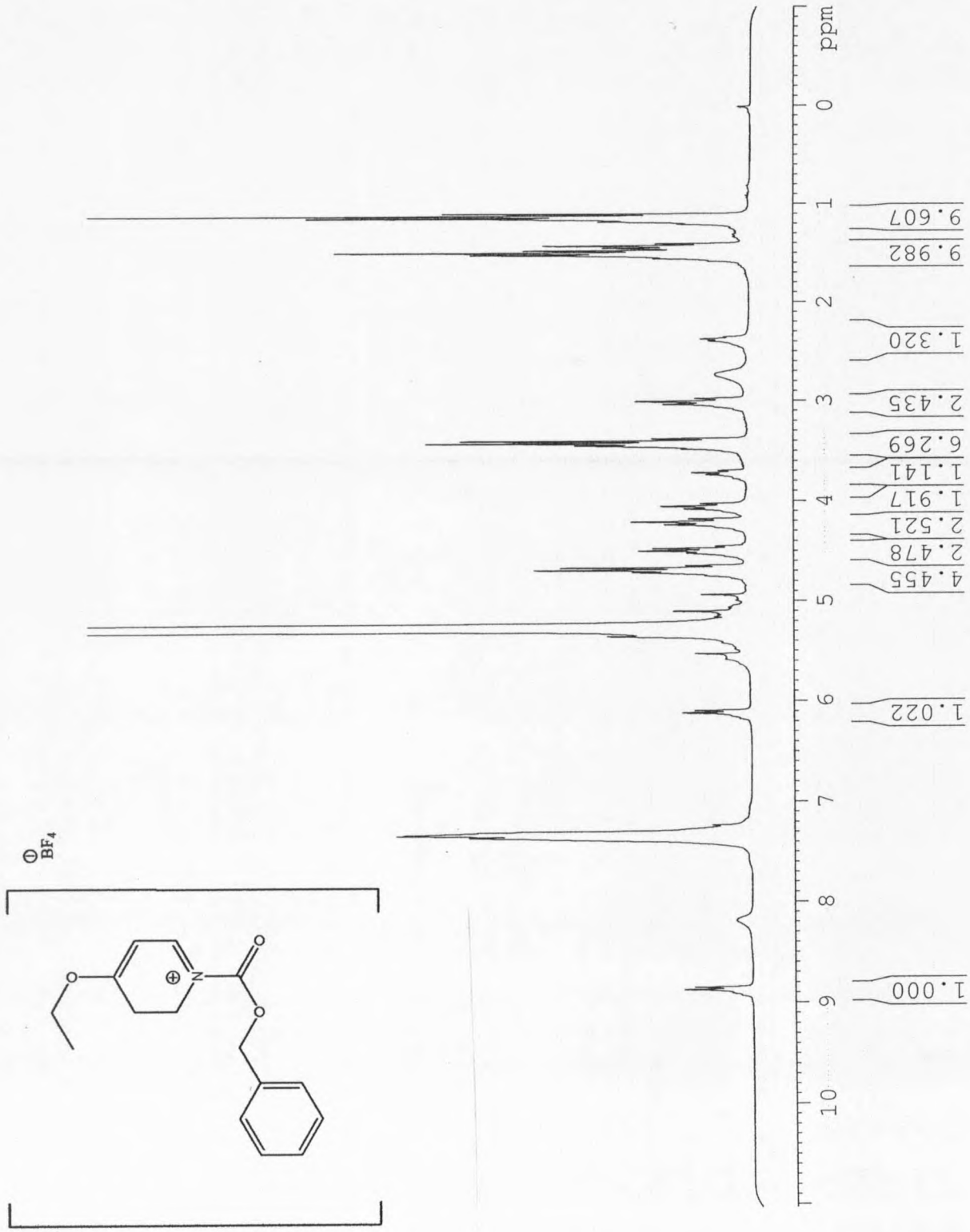
^{13}C-NMR Spectrum of 65



APPENDIX L

^{1}H-NMR Spectrum of 2,3-Dihydropyridinium salt **66**

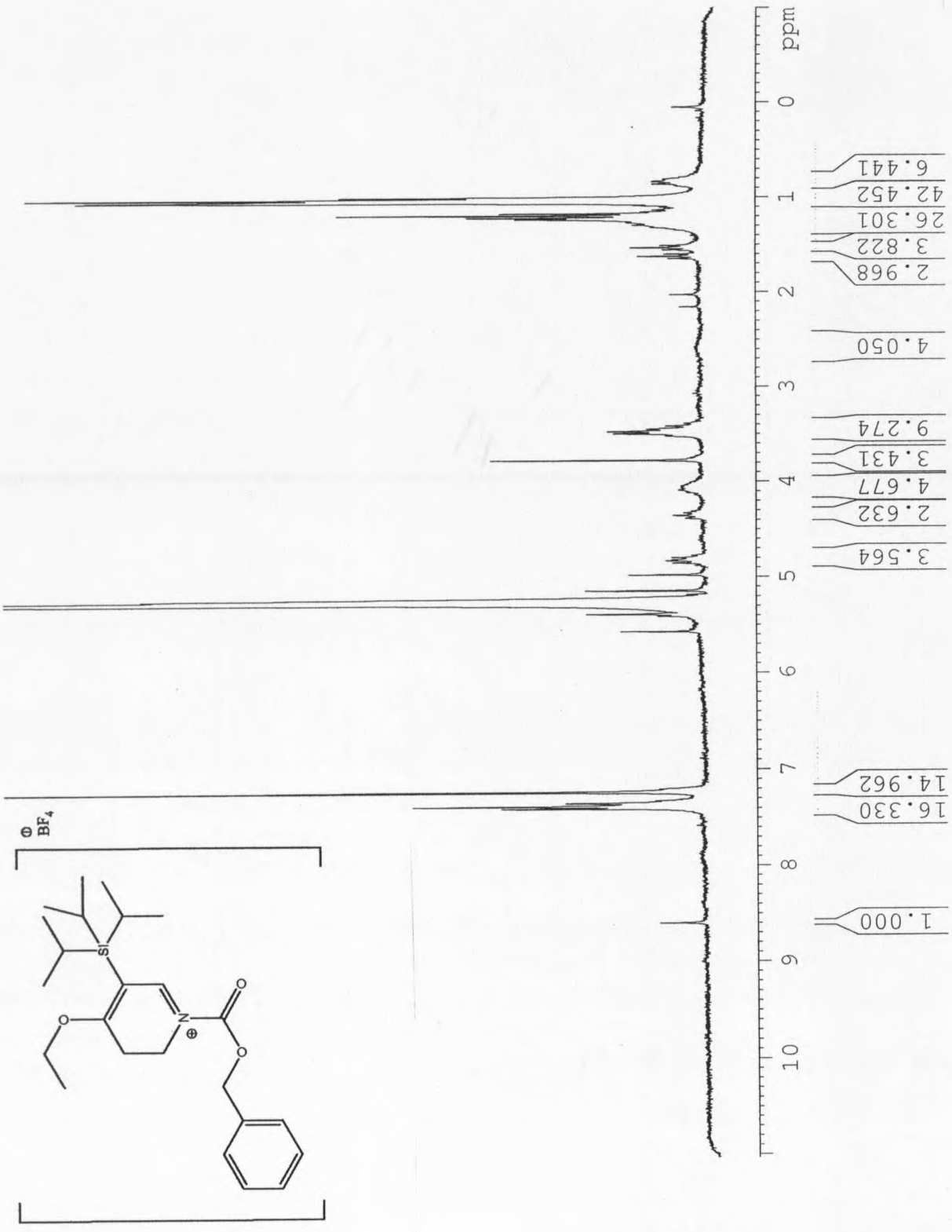
^{1}H-NMR Spectrum of 66



APPENDIX M

^{1}H-NMR Spectrum of 2,3-Dihydropyridinium salt **67**

^{1}H-NMR Spectrum of 67



MONTANA STATE UNIVERSITY - BOZEMAN
3 1762 10399161 6